Final Report

Characterization of Chloride Thresholds in Florida Coastal Concrete Bridge Substructures

(Contract Number BD546, RPWO #05)

submitted to

Florida Department of Transportation Research Center
605 Suwannee Street
Tallahassee, Florida 32399

submitted by

Francisco Presuel-Moreno
Department of Ocean Engineering
Florida Atlantic University – SeaTech Campus
101 North Beach Road
Dania Beach, Florida 33004

William H. Hartt
Hartt and Associates, Inc.
20914 Morada Court
Boca Raton, Florida 33433

Russell Tanner[1]
ExxonMobil Development Company
Houston, Texas

February 11, 2009

[1] Formerly Graduate Research Assistant, Florida Atlantic University

Disclaimer

The opinions, findings, and conclusions expressed in this publication are those of the authors and not necessarily those of the State of Florida Department of Transportation.

SI* (MODERN METRIC) CONVERSION FACTORS

APPROXIMATE CONVERSIONS TO SI UNITS

Symbol	When You Know	Multiply By	To Find	Symbol
		LENGTH		
in	inches	25.4	millimeters	mm
ft	feet	0.305	meters	m
yd	yards	0.914	meters	m
mi	miles	1.61	kilometers	km
		AREA		
in^2	square inches	645.2	square millimeters	mm^2
ft^2	square feet	0.093	square meters	m^2
yd^2	square yard	0.836	square meters	m^2
ac	acres	0.405	hectares	ha
mi^2	square miles	2.59	square kilometers	km^2
		VOLUME		
fl oz	fluid ounces	29.57	milliliters	mL
gal	gallons	3.785	liters	L
ft^3	cubic feet	0.028	cubic meters	m^3
yd^3	cubic yards	0.765	cubic meters	m^3
		NOTE: volumes greater than 1000 L shall be shown in m^3		
		MASS		
oz	ounces	28.35	grams	g
lb	pounds	0.454	kilograms	kg
T	short tons (2000 lb)	0.907	megagrams (or "metric ton")	Mg (or "t")
		TEMPERATURE (exact degrees)		
^oF	Fahrenheit	5 (F-32)/9 or (F-32)/1.8	Celsius	^oC
		ILLUMINATION		
fc	foot-candles	10.76	lux	lx
fl	foot-Lamberts	3.426	$candela/m^2$	cd/m^2
		FORCE and PRESSURE or STRESS		
lbf	poundforce	4.45	newtons	N
lbf/in^2	poundforce per square inch	6.89	kilopascals	kPa

APPROXIMATE CONVERSIONS FROM SI UNITS

Symbol	When You Know	Multiply By	To Find	Symbol
		LENGTH		
mm	millimeters	0.039	inches	in
m	meters	3.28	feet	ft
m	meters	1.09	yards	yd
km	kilometers	0.621	miles	mi
		AREA		
mm^2	square millimeters	0.0016	square inches	in^2
m^2	square meters	10.764	square feet	ft^2
m^2	square meters	1.195	square yards	yd^2
ha	hectares	2.47	acres	ac
km^2	square kilometers	0.386	square miles	mi^2
		VOLUME		
mL	milliliters	0.034	fluid ounces	fl oz
L	liters	0.264	gallons	gal
m^3	cubic meters	35.314	cubic feet	ft^3
m^3	cubic meters	1.307	cubic yards	yd^3
		MASS		
g	grams	0.035	ounces	oz
kg	kilograms	2.202	pounds	lb
Mg (or "t")	megagrams (or "metric ton")	1.103	short tons (2000 lb)	T
		TEMPERATURE (exact degrees)		
^oC	Celsius	1.8C+32	Fahrenheit	^oF
		ILLUMINATION		
lx	lux	0.0929	foot-candles	fc
cd/m^2	$candela/m^2$	0.2919	foot-Lamberts	fl
		FORCE and PRESSURE or STRESS		
N	newtons	0.225	poundforce	lbf
kPa	kilopascals	0.145	poundforce per square inch	lbf/in^2

*SI is the symbol for the International System of Units. Appropriate rounding should be made to comply with Section 4 of ASTM E380.
(Revised March 2003)

Technical Report Documentation Page

1. Report No.	2. Government Accession No.	3. Recipient's Catalog No.
4. Title and Subtitle Characterization of Chloride Thresholds in Florida Coastal Concrete Bridge Substructures		5. Report Date 6. Performing Organization Code
7. Author(s) William H. Hartt, Francisco Presuel-Moreno, Russell Tanner		8. Performing Organization Report No. FAU-OE-CMM-
9. Performing Organization Name and Address Florida Atlantic University – Sea Tech Campus 101 North Beach Road Dania Beach, FL 33004		10. Work Unit No. (TRAIS) 11. Contract or Grant No. BD546, RPWO #05
12. Sponsoring Agency Name and Address Florida Department of Transportation – State Materials Office 5007 NE 39th Street Gainesville, FL 32609		13. Type of Report and Period Covered Final Report 14. Sponsoring Agency Code
15. Supplementary Notes		

16. Abstract

Sea water induced reinforcing steel corrosion often results in high maintenance costs and can be service life limiting for concrete bridge substructure elements in marine environments. In the present research, a novel piling type specimen assembly and test protocol were developed to simulate performance of actual substructure elements undergoing marine exposure. Specimen mix design was based on the mortar component of a FDOT Class V high performance concrete, both with and without fly ash. The relatively low diffusion coefficient for such mixes and the long time that normally would be required for corrosion initiation was offset by employing covers of 12 mm for the non-fly ash mortar and 8 mm for the fly ash one. Exposures involved partial submergence in 15 wt% NaCl and in some cases periodic spraying of the above waterline zone to simulate splash. The rebar of some sprayed specimens was connected to submerged bare steel such that the lower portion of the simulated piling rebar was cathodically polarized, and it is demonstrated that the resultant potential profile was similar to that of actual marine pilings for which reinforcement below the waterline also exhibits a relatively negative potential because of oxygen concentration polarization. Consequently, the above waterline (splash) zone of the present specimens was cathodically polarized similar to what occurs in actual structures. Times to corrosion for the specimens were approximately the same for sprayed and unsprayed specimens but were greater for sprayed and polarized ones. In some cases, corrosion initiated above the waterline for sprayed and sprayed and polarized specimens, as typically occurs in actual bridge substructure elements. Threshold Cl^- concentrations to initiate corrosion, C_T, were measured on the rebar mortar trace subsequent to corrosion initiation and specimen dissection using Energy Dispersive X-Ray Analysis and reported for various test conditions. Values for C_T for corrosion initiation in both the submerged and above waterline zones are projected for both mix designs; however, these were based in some cases on limited data. It is recommended that the specimen design and test protocol investigated here be studied further.

17. Key Word	18. Distribution Statement
Reinforced concrete, bridge substructure, marine, sea water, corrosion, corrosion testing, chloride threshold	No restrictions.

19. Security Classif. (of this report)	20. Security Classif. (of this page)	21. No. of Pages	22. Price
Unclassified	Unclassified		

Form DOT F 1700.7 (8-72) Reproduction of completed page authorized

EXECUTIVE SUMMARY

Sea water induced reinforcing steel corrosion often results in high maintenance costs and can be service life limiting for concrete bridge substructure elements in marine environments. The objective of the present research was to improve upon previously employed piling type specimens and test protocols that simulate exposure and performance of actual substructure elements undergoing marine exposure. Doing this facilitates better defining the critical chloride concentration to initiated reinforcing steel corrosion in substructure elements and thereby provide improved data for life-cycle modeling and maintenance scheduling.

Specimen mix design was based on the mortar component of a FDOT Class V high performance concrete, both with and without fly ash. The relatively low diffusion coefficient for such mixes and the long time that normally would be required for corrosion initiation was offset by employing covers of 12 mm for the non-fly ash mortar and 8 mm for the fly ash one. Exposures involved partial submergence in 15 wt% NaCl and in some cases periodic spraying of the above waterline zone to simulate splash. The rebar of some sprayed specimens was connected to submerged bare steel such that the lower portion of the simulated piling rebar was cathodically polarized, and it is demonstrated that the resultant potential profile was similar to that of actual marine pilings for which reinforcement below the waterline also exhibits a relatively negative potential because of oxygen concentration polarization. Consequently, the above waterline (splash) zone of the present specimens was cathodically polarized similar to what occurs in actual structures. Times to corrosion for the specimens were approximately the same for sprayed and unsprayed specimens but were greater for sprayed and polarized ones. In some cases, corrosion initiated above the waterline for sprayed and sprayed and polarized specimens, as typically occurs in actual bridge substructure elements. Threshold Cl^- concentrations to initiate corrosion, C_T, were measured on the rebar mortar trace subsequent to corrosion initiation and specimen dissection using Energy Dispersive X-Ray Analysis and reported for various test conditions. Values for C_T for corrosion initiation in both the submerged and above waterline zones are projected for both mix designs; however, these were based in some cases on limited data. It is recommended that further evaluation of the specimen design and test protocol that was investigated be studied further.

TABLE OF CONTENTS

TABLE OF CONTENTS (continued)

page no.

LIST OF FIGURES

LIST OF FIGURES (continued)

LIST OF FIGURES (continued)

page no.

LIST OF FIGURES (continued)

page no.

LIST OF FIGURES (continued)

page no.

LIST OF TABLES

LIST OF TABLES

INTRODUCTION

Corrosion of reinforcing steel and resultant concrete former category, it is now generally accepted that the damage process involves the following sequential steps:

1. Penetration of chlorides through the concrete pore structure by either sorption or diffusion (or both).
2. Attainment of a critical chloride concentration, C_T, at the steel surface that irreversibly compromises the otherwise protective passive surface film at local sites,
3. Onset and spread of active corrosion aided by, first, acidification of the relatively confined electrolyte at the active site or sites and, second, a small anode – large cathode active-passive cell,
4. Accumulation of relatively large specific volume solid corrosion products which cause tensile hoop stresses about the reinforcement,
5. Cracking and spalling of the concrete cover, and
6. Direct exposure of reinforcement at spalled locations to chlorides, moisture, and oxygen such that corrosion rate here is enhanced.

Left unaddressed, structural failure can ultimately result.

In past studies, particular attention has focused on identification and characterization of C_T (item 2 above), since corrosion should not initiate as long as chloride concentration, $[Cl^-]$, at the reinforcing steel depth remains below this. Upon knowing C_T, bridge engineers can make materials selection and design choices that best assure structures are not compromised by corrosion induced cracking and spalling during their design life. However, reported values in the literature for C_T extend over more than an order of magnitude from 0.6 to 9.7 kg/m^3 (concrete weight basis assuming 400 kg/m^3 cement content) for concrete test specimens and structures.[1] Variables that contribute to this range include 1) types of raw materials and admixtures, 2) cement composition, 3) mix design, 4) concrete microstructure, 5) rebar surface condition, and 6) type of exposure. Even so, laboratory and test yard experimentations have demonstrated that C_T is variable or distributed over a range for identically designed and exposed specimens.[2] Irrespective of this, the North American concrete community generally accepts a value for C_T of 0.59-0.78 kg/m^3 (1.0-1.3 pounds per cubic yard (pcy)) of concrete based largely upon research and field evaluations in the 1960's and 1970's by the Federal Highway Administration (FHWA) and California Department of Transportation (CalTrans). An alternative approach has been to define a lower limit for $[Cl^-]$, for example 0.1 wt% Cl^- (cement basis).[3]

Regarding a specific definitive value for C_T, Clear[4] projected a corrosion threshold of 0.78 kg/m^3 (1.3 pcy) based on research by Lewis,[5] the rationale being that the latter author was stated to have reported a threshold of 0.3 percent Cl^- per gm of cement for specimens with admixed $CaCl_2$ assuming 50 percent Cl^- solubility. The paper itself, however, simply shows that for reinforcement in concrete specimens a transition from passive to active behavior occurred between admixed $CaCl_2$ concentrations of 0.78 and 1.56 wt% (concrete basis) (0.50-1.00 wt% Cl^-). Because these values are abnormally high compared to others and because Lewis elsewhere always referenced to a cement basis, it may be that the above range (0.78-1.56 wt%) should also have been to a cement rather than concrete basis. Lewis also showed data indicating that about 50 percent of the total NaCl was leached from paste samples upon a two hour water exposure at room temperature. He did not state his mix design; however, if it is assumed that 1) the above [Cl^-] was referenced to a cement basis, 2) 15 percent of his mix was cement, and 3) 50 percent of the chlorides were free, then Lewis's threshold becomes 0.25-0.50 wt% Cl^- (cement basis), which brackets the above 0.3 percent Cl^- per gm of cement choice. However, Clear reasoned that a 0.3 wt% Cl^- (cement basis) threshold translates to 0.2 wt% if Cl^- solubility is 80 percent, the latter being reported by a companion FHWA study that used pastes immersed in boiling water and then left for two days at room temperature (Virmani and Clemena[6] later refer to this FHWA work as indicating a C_T of 0.15 wt% soluble Cl^- (cement basis)).[7] This reasoning is unclear, since if 80 percent of the threshold range quoted by Lewis was free, then the FHWA reported C_T should be 0.4-0.8 wt% Cl^-. However, Clear assumed 0.2 wt% Cl^- for C_T which, for a seven bag mix (cement factor 7), translates to 0.78 kg/m^3 (1.3 pcy). Using this same rationale, the 0.4-0.8 wt% range for [Cl^-] corresponds to 1.5-3.1 kg/m^3 (2.6-5.2 pcy).

An addition problem is that the experiments by Lewis involved galvanostatic anodic polarization of the embedded steel at 10 $\mu A/cm^2$. Such polarization places potential of the steel closer to the pitting potential than for a condition of free corrosion, and C_T should be accordingly lower. Apparently, no experiments that explicitly determined a Cl^- threshold were performed in the classical FHWA studies in the 1970's; but instead the 0.59-0.78 kg/m^3 (1.3 pcy) threshold was assumed based on the above rationale.

Stratfull et al.[8] projected C_T for 22 bridges in California with ages 6-23 years. These authors reported that decks with four percent of potential readings active to -0.35 V_{CSE} and with 0.05 percent delamination had a maximum [Cl^-] at the average rebar depth, as determined from a series of cores taken on each bridge, of 0.59 kg/m^3 (1.0 pcy); and accordingly this was adapted as C_T. A flaw in this rationale, however, is that reinforcement cover was undoubtedly distributed over a range; and it is likely that the active potentials and delaminations occurred at locations where bar cover was least and [Cl^-] higher than

at the average rebar depth. While their conclusion stands as a useful guide for practitioners provided the cover distribution on the California bridges applies in general, it may be misleading as a design tool for two reasons. First, it does not reflect [Cl^-] at actual corrosion initiation sites; and, second, [Cl^-] at the initial locations that become active is likely to be further elevated because of the coarse aggregate volume percentage (CAVP) effect. By this, coarse aggregates serve as obstacles to Cl^- ingress;[9] and because these aggregates are distributed randomly, corrosion is favored at locations with relatively low localized CAVP in the Cl^- ingress path.[2]

While the C_T projected by Stratfull et al.[8] is in good agreement with the value used by Clear, it is considerably below what was reported for laboratory experiments performed by the same authors[10] on partially submerged simulated piling specimens. Here, reinforced concrete prisms that were exposed partially submerged in a 15 wt% NaCl solution were broken open 14 days after potential became active to -0.35 V_{CSE}; and concrete (actually mortar according to the text) was scraped to a depth of approximately 1.5 mm for a length of 76 mm along the portion of the bar that was submerged. The mean [Cl^-] for 20 specimens was 10.6 kg/m^3 (17.9 pcy). Some, but not all, of this difference may be accounted for because the percentage of mortar was probably elevated in local proximity to the reinforcing steel.[9] However, taken as is these results imply that C_T is higher for partially submerged than atmospherically exposed components and, hence, that results from slab type specimens or decks may be overly conservative with regard to substructure elements.

The above distinction in C_T between 1) decks and presumably for ponded slab specimens also and 2) partially submerged prisms may have resulted because exposure is macroscopically uniform for the former but not for the latter. Thus, [Cl^-] is high in the submerged zone of a prism specimen or substructure element and so reinforcement here becomes active; however, corrosion rate and resultant damage are generally nil because of O_2 depletion. On the other hand, in the atmospheric zone well above water, [Cl^-] is relatively low and [O_2] high. Consequently, reinforcement may remain passive here. However, [Cl^-] is generally highest in the zone immediately above the water because of splash and possibly capillary transport from below. Oxygen concentration may be low here; however, proximity to the atmospheric zone above provides a macroscopic active-passive cell between the two with adequate [O_2] in the region above the splash zone to drive the corrosion process. Thus, it is in the splash zone that corrosion rate is highest and cracking and spalling are most severe. Figure 1 shows an example of this damage in the case of a coastal bridge prestressed concrete bridge piling.

Figure 1: Photograph of a coastal bridge spalled piling.

A resistivity gradient from low to high upon proceeding from the submerged to atmospheric zone results from the elevation dependence of moisture saturation. Consequently, macro-cells are likely to be more significant at lower elevations. Also, as noted above, reinforcement in the submerged zone is expected to be active; and because of low $[O_2]$ here, potential is relatively negative (oxygen concentration polarization). The opposite is the case in the atmospheric zone where reinforcement remains passive due to low $[Cl^-]$ and high $[O_2]$, and so potential is relatively positive here. Thus, there is a potential gradient from relatively negative to more positive with increasing elevation. Consequently, reinforcement in the submerged zone tends to cathodically polarize steel in the splash zone. This has implications with regard to defining C_T, since this parameter has been shown to increase with increasing cathodic polarization.[11,12,13]

Experiments intended to simulate marine substructure elements have typically employed partially submerged concrete specimens with a single or several rebars. A shortcoming of this method, however, is that chlorides penetrate the concrete predominantly in the submerged zone; and $[Cl^-]$ is low in the concrete above this; that is, there is no splash zone or, if there is, it is very narrow. Consequently, unlike the case for actual pilings, corrosion initiates in the submerged region without benefit of any cathodic polarization; and C_T projected from such experiments may be lower than what occurs in the splash zone of actual substructure elements. Also, because surface area of the submerged zone steel is relatively small in conventional prism specimens, a small anode-large cathode area ratio results. For actual substructure

elements, however, steel in the submerged zone constitutes a relatively large surface area anode which should lend effectiveness to the cathodic polarization provided to reinforcement in the splash zone, which is where [Cl^-] is expected to be highest and corrosion most significant, as noted above.

The objective of the present research was to develop and test a specimen design that was intended to provide a more realistic simulation of actual bridge substructure elements and thereby result in a more accurate C_T database.

EXPERIMENTAL PROCEDURE

Mix Design

Two mortar mixes, designated MD1 and MD2, were employed to fabricate simulated piling specimens with the materials and proportions for each being listed in Table 1 and cement and fly ash compositions in Table 2. Table 1 also includes a typical mix design for Florida Department of Transportation (FDOT) Type V concrete[14] and reveals that the present mixes are similar to this except that coarse aggregate was excluded and only the MD1 mix contained fly ash. As such, the mixes were intended to replicate the mortar phase (no coarse aggregates) of FDOT Type V concretes by retaining the cement content and water-to-cementiteous material ratio (w/cm) of these.

Table 1: Mix designs.

Material	FDOT Type V		Mix Design 1		Mix Design 2	
	kg/m^3	vol %	kg/m^3	vol %	kg/m^3	vol %
Type I Cement	363	12	389	12.6	530	16.8
Fly Ash	83	4	94	4.25	0	0
Water	163	18	184	18	202	20.2
Fine Aggregate	607	23	1,457	55	1,404	53
Coarse Aggregate	1,047	41	0	0	0	0
Water/Cement	0.37		0.38		0.38	
Sand/Cement	1.36		2.76		2.76	

Table 2: Composition of cement and fly ash.

Material	SiO_2	Al_2O_3	Fe_2O_3	CaO	SO_3	Na_2O	K_2O	EqA
Type I Cement	23.55	6.00	3.88	60.22	2.63	0.09	0.54	0.45
Fly Ash	52.82	21.90	6.06	4.92	0.27	0.28	1.49	1.27

Specimen Geometry

Reinforcement was as-rolled and wire brushed, 9.5 mm diameter (#3) black steel bars. Because the relatively low Cl^- diffusivity that was projected to result for the above mixes as a consequence of the low w/cm (Table 1) should preclude corrosion initiation in a time frame acceptable for most laboratory experimentation utilizing commonly employed standardized specimen designs,[15] clear cover was specified as 8.0 mm for MD1 specimens and 12.0 mm for MD2, these values being selected based upon calculations that assumed diffusion coefficients of 10^{-12} and 10^{-11} m^2/s, respectively, as reported in Appendix A. Exclusion of coarse aggregate from the mixes was a necessary requisite for specifying these relatively low covers.

Specimen molds were fabricated from 13 mm thick polypropylene sheet. Mortar batching employed a 57 liter mixer; and density, air content, and slump were determined for each batch according to ASTM C231.[16] Ten specimens were horizontally cast in three layers for each batch and consolidated by rodding according to ASTM C192.[17] Acceptable ranges for air content and slump were 8-12 percent and 32-64 mm, respectively. Bar positioning in the molds was such that the minimum cover face (the one with concrete cover either 8 or 12 mm) from which chlorides should initially reach the reinforcement was down such that this surface had a form finish. The specimens were covered with plastic wrap at room temperature for the initial 24 hours subsequent to casting, after which they were removed from the molds and cured in sealed plastic containers at 100 percent relative humidity and 38°C. Curing time for MD1 specimens was six months and for MD2 28 days.

A schematic illustration of the simulated piling specimen is shown in Figure 2. This indicates that each specimen consisted of two bars that were aligned and rigidly clamped in the molds prior to casting. Cover was verified subsequent to pouring and curing using a ELE International Model CT-4950A micro-covermeter. A total of ten specimens of each mix design were prepared. Figure 3 shows a photograph of a specimen prior to exposure.

Subsequent to curing, specimens were positioned vertically in groups of four in polyethylene tanks and submerged in 15 wt% NaCl to a depth of 10 cm. Additionally, the minimum cover face of a subset of specimens was sprayed each day for ten minutes every 12 hours to a height of approximately 20 cm above the waterline with the same concentration NaCl solution. Figure 4 shows four specimens positioned in an exposure tank where spraying occurred. After approximately 70 days exposure, rebar of a subset of

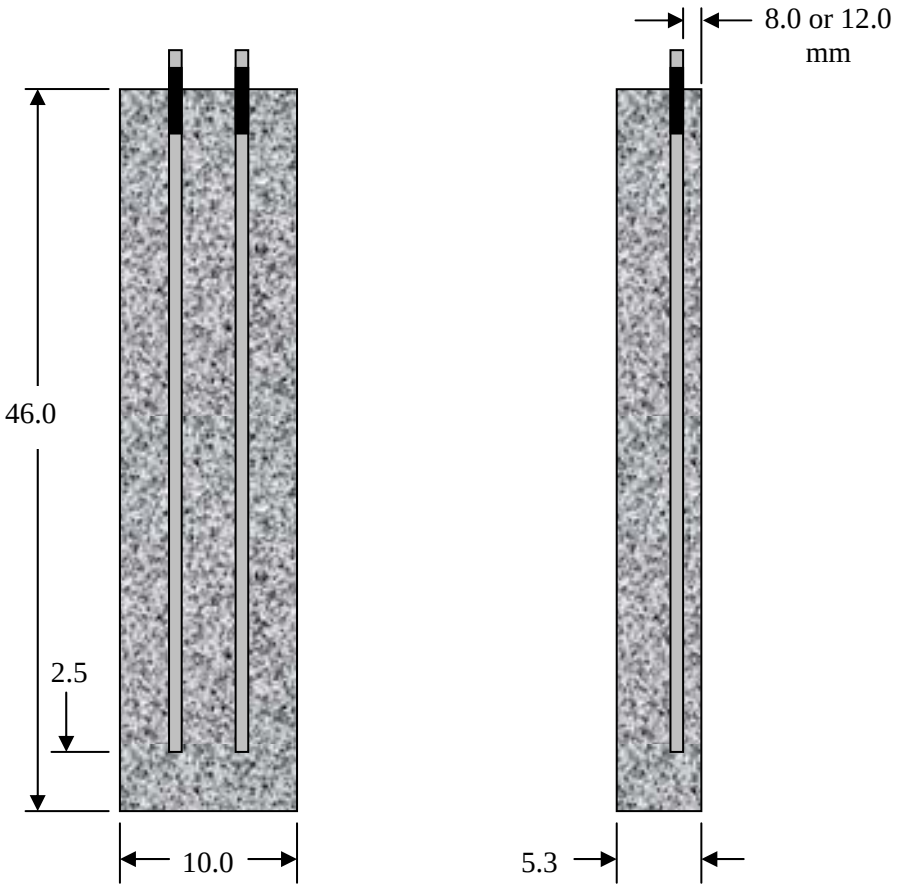

Figure 2: Schematic illustration of the simulated piling specimens (dimensions in cm excepted where noted otherwise).

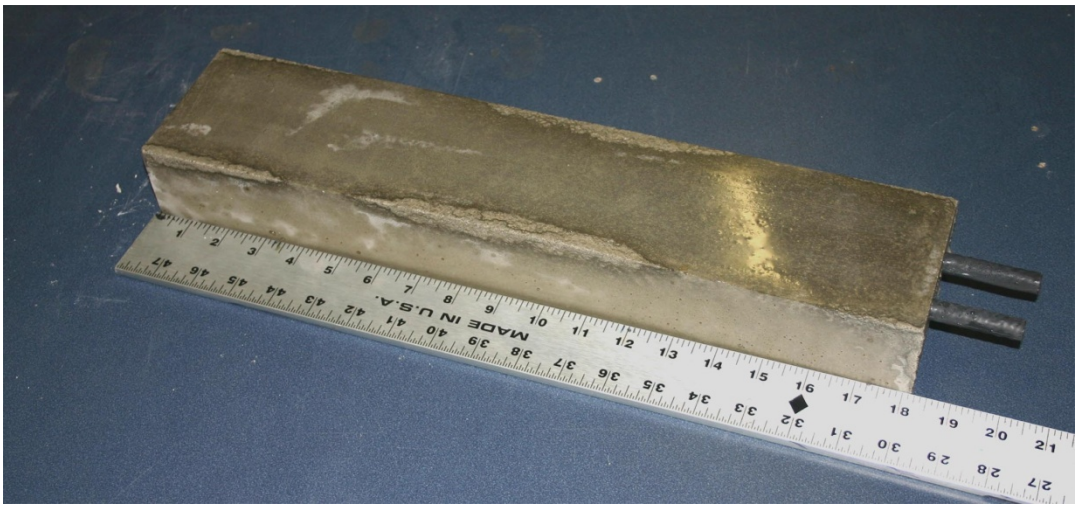

Figure 3: Photograph of an SPS specimen prior to exposure.

Figure 4: Photograph of sprayed specimens under exposure.

sprayed specimens was connected to an individual bare steel rebar submerged in a companion tank that was electrolytically connected to the tank in which the prism specimens were exposed via pvc piping that contained a porous filter. The procedure involved coupling both rebar of a given specimen to the same, dedicated bare submerged bar. The purpose of this was to polarize the lower elevation of the specimen rebar and thereby simulate the potential profile that is expected to occur for actual pilings. Each rebar of simulated piling (SP) specimens that was connected to submerged bare steel (polarized specimens) was independently wired with a 10 Ohm resistor in series. All submerged electrical connections were sealed with a marine epoxy. Figure 5 provides a photograph of this arrangement where the tank with bare submerged steel bars is in the foreground and the one with SP specimens in the back. The pvc piping between the two tanks that contained the filter and provided electrolytic connection is also visible. Potential measurements between reference electrodes in the tanks containing polarized SP specimens and the tanks with submerged bare bar indicated that voltage drop between these was negligible. Table 3 lists the specimen matrix according to exposure variables.

Specimen monitoring involved routine measurement of potential as a function of elevation using a moisten tip reference electrode placed on the concrete surface directly opposite the rebar. Also, current between the submerged bare steel and specimen rebars was calculated from the voltage drop across the resistor in series between the two.

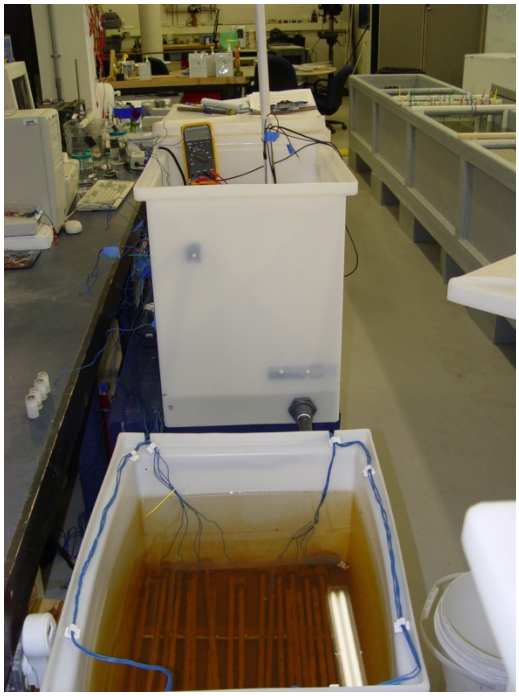

Figure 5: Photograph of the tank assembly for affecting polarization of the lower portion of SPS specimens.

Table 3: Listing of specimens and test condition for each.

Specimen No.	Mix Design	Sprayed	Polarized
1A	MD1	Yes	Yes
1B	MD1	Yes	Yes
2A	MD1	Yes	Yes
2B	MD1	Yes	Yes
3A	MD1	No	No
3B	MD1	Yes	No
4A	MD1	No	No
4B	MD1	Yes	Yes
5A	MD1	No	No
5B	MD1	Yes	No
6A	MD2	Yes	Yes
6B	MD2	Yes	No
7A	MD2	Yes	Yes
7B	MD2	Yes	No
8A	MD2	No	No
8B	MD2	Yes	No
9A	MD2	No	No
9B	MD2	Yes	No
10A	MD2	Yes	Yes
10B	MD2	Yes	No

Once one, but in most cases both, rebars of an individual specimen were judged to have become active, the exposure was terminated. The specimens were then dissected by making a saw cut along the entire length of each of the two side faces opposite both bars to a depth of approximately 20 mm and then splitting open the specimen. The embedded steel was then examined for corrosion. A distinct potential shift to more negative values, in cases where this occurred, served as an indicator that corrosion had initiated for specimens that were not connected to bare submerged steel. This criterion was not an option for specimens connected to bare steel, however, since potential for these was already relatively negative; and it was uncertain if a further potential change would occur once corrosion initiated or, if it did, that its magnitude and sense would be sufficiently distinct and reproducible from one specimen to the next. For this reason, these specimens were periodically disconnected from the bare bar for a 24 hour period; and potential was recorded as depolarization (positive potential shift) occurred. It was considered that specimens that exhibited relatively large depolarization were still passive and that modest depolarization reflected active corrosion. In addition, $[Cl^-]$ was determined at the site on the rebar trace where corrosion had initiated and in some cases at increments along the entire trace as well using energy dispersive x-ray (EDX) spot analysis. This technique was required rather than a more standard wet chemistry one because $[Cl^-]$ varied with elevation on the specimens, and the size of any sample that could be acquired at an acceptable elevation increment would be insufficient for the latter method. The procedure involved breaking the dissected specimen portion that had served as the concrete cover over the reinforcement into approximately 25mm increments along its length. For each analysis location, an image was acquired at 38X; and analyses were conducted using an eight mm working distance, a 0.5 mm aperture, 10 kV acceleration voltage at 0.6 Torr.

RESULTS AND DISCUSSION

Freely Corroding (Non-Polarized) MD2 Mix Specimens

Figure 6 shows an example potential versus time plot for both rebars of Specimen 9A, this trend being typical of all specimens in this category. The data indicate that, for both bars, potential at all elevations was relatively positive and generally in the range -25 to -100 mV_{SCE} during the initial period of exposure but subsequently transitioned abruptly to more negative values. For the left bar, this occurred after 49 days and for the right 66 days. Such a potential shift is indicative of onset of active corrosion, as verified upon specimen dissection which is described below. Once this transition occurred, a more pronounced potential profile along the specimen height resulted, with potential for the lower elevations being relatively negative and the upper portion less so. In these and subsequent plots, elevation is

referenced to the waterline; and the potential labeled as -5 cm corresponds to the reference electrode being positioned in the electrolyte.

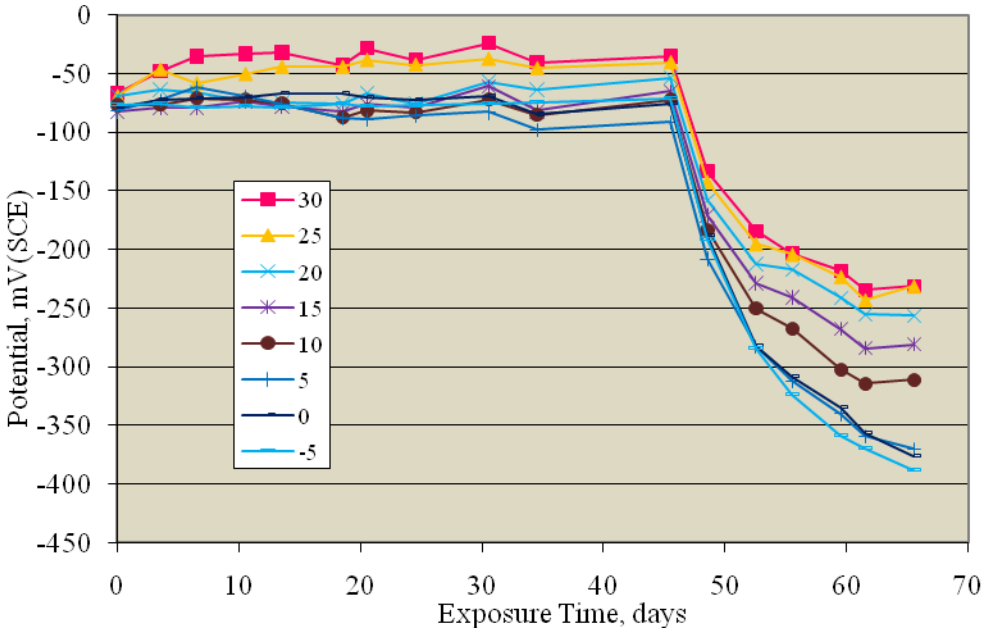

(a)

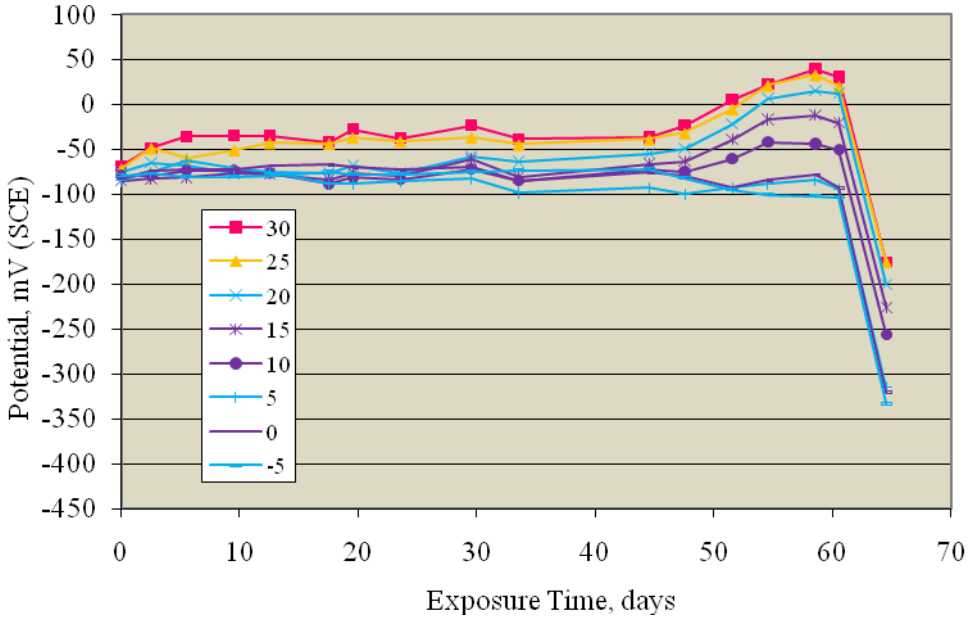

(b)

Figure 6: Potential of the left (a) and right (b) bar of Specimen 9A at different elevations as a function of exposure time (key shows measurement elevations in cm relative to the waterline).

Figure 7 shows a photograph of both Specimen 9A rebars and mortar traces subsequent to exposure termination and dissection. This reveals that corrosion, as evidenced by rust staining on the rebar and on its trace in the mortar at the corresponding elevation, occurred near the bottom end which was below the water line and is greater for the left bar than the right, consistent with the potential data which indicated that the former bar activated first.

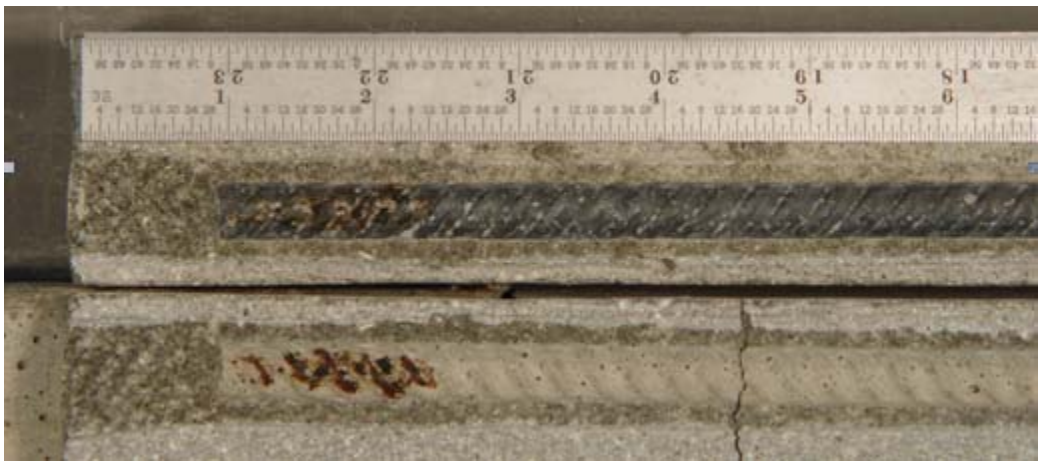

(a)

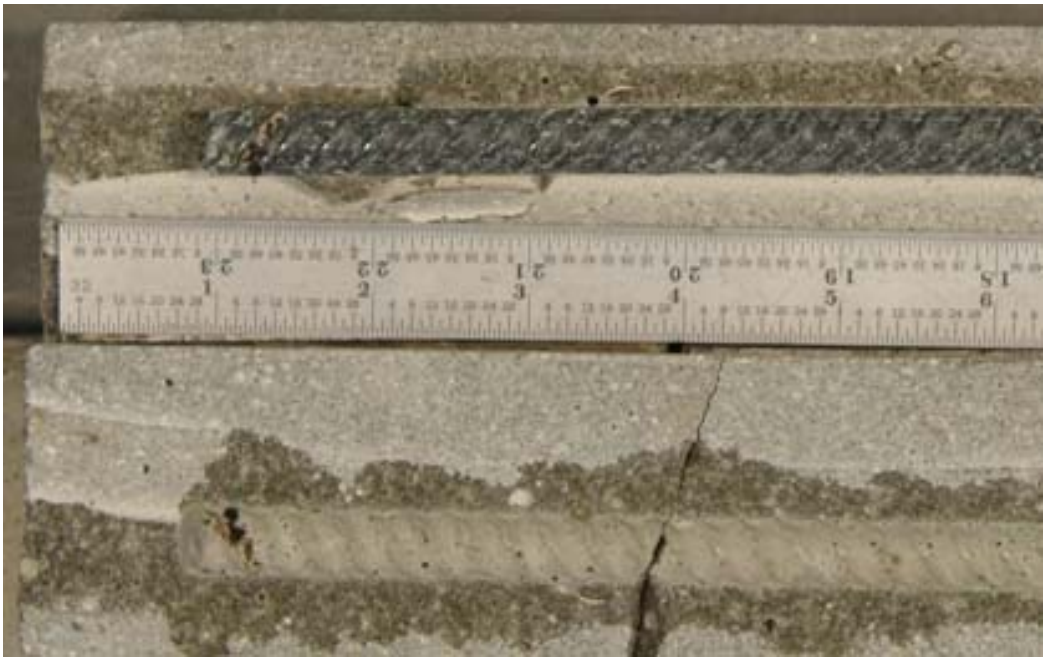

(b)

Figure 7: Photograph of the left (a) and right (b) bars of Specimen 9A and their trace in the mortar subsequent to dissection (cracks in the mortar resulted during the dissection process).

For all specimens in the present category (MD2 mix design and free corrosion (no connection to submerged bare steel)), the potential transition associated with onset of corrosion was relatively abrupt; and corrosion was found to have initiated in the submerged zone, irrespective of whether or not the specimen was sprayed. Apparently, the spray did not concentrate chloride sufficiently at higher specimen elevations for corrosion to initiate here prior to C_T being achieved in the submerged region. Appendix B provides potential versus time plots for other specimens in this category, and Appendix C shows photographs subsequent to exposure termination and dissection. Together, these provide confirmation that the potential shift criterion for defining T_i was appropriate.

A consistent feature of the data for MD2 freely corroding specimens was that, once potential of the first bar to become active shifted to more negative values, potential of the second bar changed also albeit to a lesser extent. In the submerged zone, the potential shift of the still passive bar was in the negative direction; and above this, potential was changes to increasingly more positive values with increasing elevation. This is apparent not only for Specimen 9A (Figure 6), but also for all other specimens in this category (Specimens 6B, 7B, 8A, 8B, 9B, and 10B), as shown by Figures B1-B6 in Appendix B. Table 4 summarizes data relevant to the magnitude of the negative shift that occurred at the lowest measurement elevation for Specimen 9A, and Table 5 does the same for the positive shift at the highest. A similar listing for the positive and negative potential shift of other specimens in this category is provided by the tables in Appendices D and E, respectively. While the magnitude of these potential changes is within the range of expected experimental scatter, still the trends are systematic in that potential in the submerged

Table 4: Summary of data relevant to the negative potential trend near the bottom of the still passive bar subsequent to corrosion initiation of the companion bar (Specimen 9A).

Specimen 9A		
Left Bar	Time of Last Passive Reading, days	46
	Time of First Active Reading, days	49
Right Bar	Time of Last Passive Reading Prior to Activation, days	60
	Potential at 46 days, mV (SCE)	-72
	Potential at 49 days, mV (SCE)	-82
	Average potential 49-60 days, mV (SCE)	-95

Table 5: Summary of data relevant to the positive potential trend near the top of the still passive bar subsequent to corrosion initiation of the companion bar (Specimen 9A).

Specimen 9A		
Left Bar	Time of Last Passive Reading, days	46
	Time of First Active Reading, days	49
Right Bar	Time of Last Passive Reading Prior to Activation, days	60
	Potential at 46 days, mV (SCE)	-39
	Potential at 49 days, mV (SCE)	-24
	Average potential 49-60 days, mV (SCE)	14

region of the still passive bar just after the companion bar activated was always more negative and near the top of the bar more positive than the respective preceding readings at these same elevations. Also, the average potential of the submerged region of the still passive bar in the interim between it and the companion bar activating was more negative in all cases than its potential just prior to companion bar activation. The opposite occurred at the highest elevation for which readings were acquired. These trends are thought to have resulted from there being parallel paths for macro-cell current between the anodic site near the base and higher elevation cathodic sites of the active rebar, one through the mortar alone and the second via a mortar-adjacent rebar-mortar (alternatively, mortar-NaCl solution-mortar-adjacent rebar-mortar) path, as illustrated schematically in Figure 8.

Table 6 lists time-to-corrosion, T_i, values for the above specimens, where this parameter has been defined according to time of last recorded potential at the lowest elevation that was positive to -200 mV_{SCE}. A sole exception to this is the left bar of Specimen 10B where activation occurred during an 11 day data acquisition gap. Here, T_i was taken as the mid point between the two times that spanned initiation. Based upon the explanation for the potential shifts discussed above, it should be considered that the lower elevation of the second bar of a given specimen to activate was cathodically polarized by current from the macro-cell established by the first, as explained above. As such, test conditions for the second bar of each specimen to activate differed from those of the first in that C_T for the second bar may have been greater than for the latter.[11,12,13] In this regard, the average T_i for the initial bar of each specimen to activate was 52 days and for the second 74 days. These averages are essentially the same irrespective of whether or not the specimen was sprayed (average T_i for the first bar of a sprayed specimen is 54 days and for non-sprayed 53 days, whereas for the second bar these averages are 73 and 72 days, respectively) and are consistent with the finding that corrosion initiated in the submerged zone in

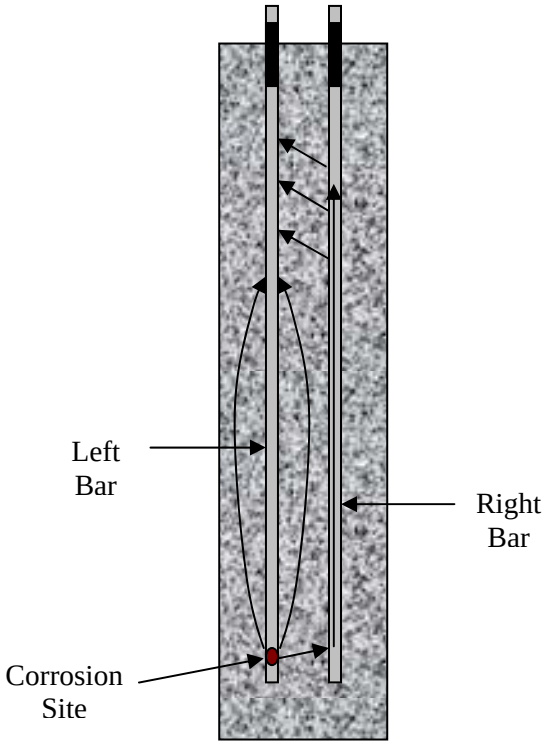

Figure 8: Schematic illustration of current flow between anodic and cathodic sites of an active bar and stray current from this bar onto the adjacent bar.

Table 6: Listing of T_i data for free corrosion MD2 specimens.

Specimen Number	Test Condition	Bar	Ti, days
6B	Spray	L	49
		R	70
7B	Spray	L	77
		R	56
8A	No Spray	L	81
		R	60
8B	Spray	L	66
		R	81
9A	No Spray	L	46
		R	62
9B	Spray	L	60
		R	84
10B	Spray	L	41
		R	53

all cases for both types of exposure. Thus, data for sprayed and non-sprayed specimens were treated as belonging to a common population. Figure 9 provides a cumulative distribution plot of the first and second bar activation T_i assuming that the times are normally distributed. While it can be reasoned based on the above findings that specimen designs with multiple bars is not the best choice, at the same time, such specimens may better represent an actual substructure element than do single bar specimens in that second bar activation relates to the C_T required for corrosion to initiate on bars adjacent to the initial one to activate and, hence, to the rate at which corrosion induced damage spreads.

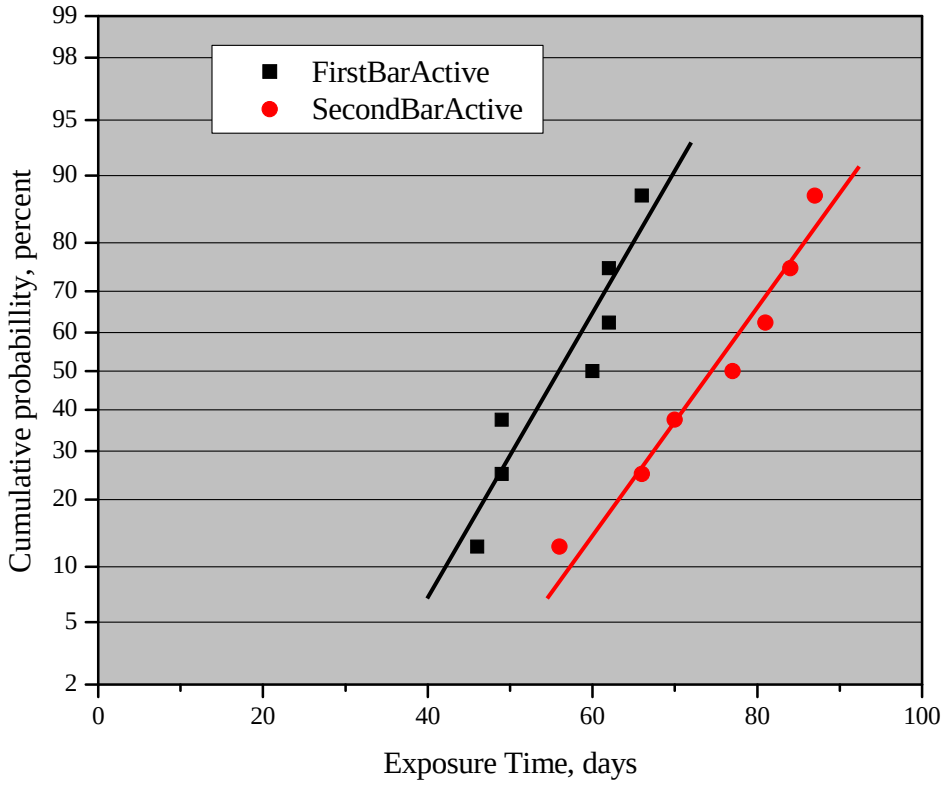

Figure 9: Cumulative distribution plot of T_i for free corrosion MD2 specimens.

Freely Corroding (Non-Polarized) MD1 Mix Specimens

Table 3 indicates that there were five freely corroding MD1 specimens (3A, 3B, 4A, 5A, and 5B). In one case (Specimen 4A), a relatively sharp potential shift to more negative values occurred (similar to freely corroding MD2 specimens as discussed above), presumably indicating corrosion initiation; however, for the other four the potential transition, once it began, was more gradual. Figure 10 shows potential versus time data for Specimen 4A. Here, T_i for the left bar was defined according to the

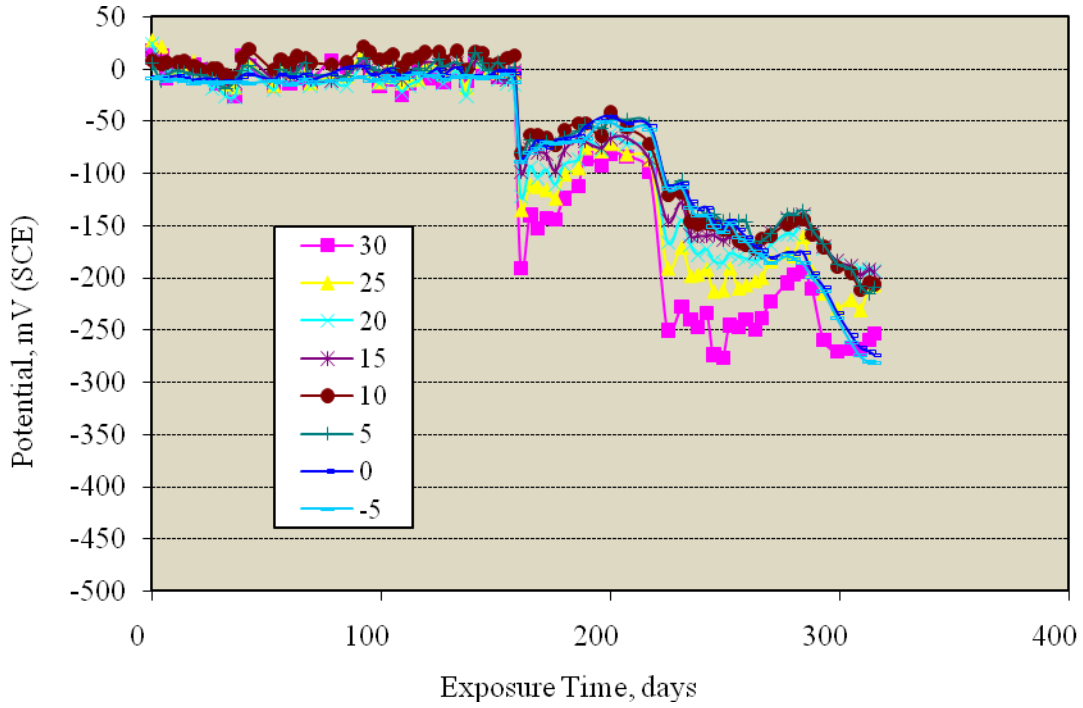

(a)

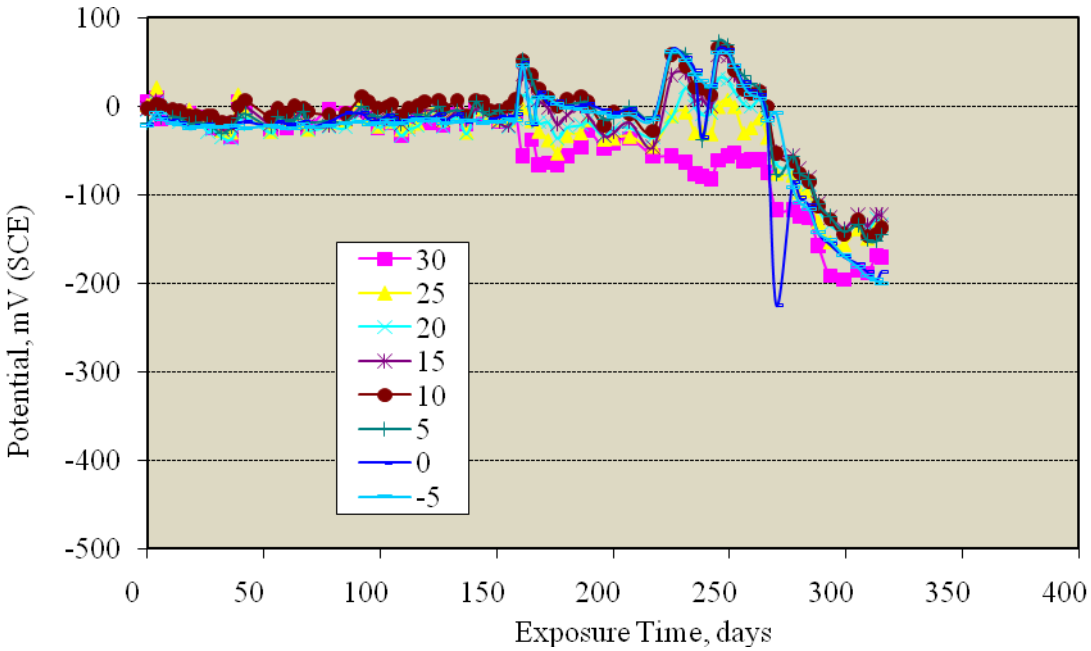

(b)

Figure 10: Potential of the left (a) and right (b) bars of Specimen 4A at different elevations as a function of exposure time (key shows measurement elevations in cm relative to the waterline).

initial negative potential shift at 158 days irrespective of the subsequent positive drift that suggests repassivation or partial repassivation. This activation of the left bar was accompanied by a positive potential shift at the upper portion of the right bar and a negative shift of the lower, which is the same trend noted above for freely corroding MD2 specimens. Corrosion initiation is less defined for the right bar; however, T_i was assumed to correspond to the relatively small but definitive negative potential shift at 263 days. Figure 11 shows a photograph of the two bars of this specimen subsequent to dissection, where corrosion products are apparent in both cases about six to seven cm above the base (submerged zone). The products are more developed on the left bar than the right, consistent with corrosion having initiated here first. This specimen was removed from testing after 315 days exposure (154 days after the sharp potential decrease for the left bar), suggesting that corrosion had been ongoing for some time prior to terminating the exposure. However, the relatively modest dimensions of the products suggests a lesser corrosion rate subsequent to initiation than for the MD2 mix, consistent with what should be a high mortar resistivity for MD1.

Figure 12 plots potential versus exposure time for Specimen 5B and provides an example of the cases where there was a gradual potential change to more negative values in lieu of a sharp transition, and Figure 13 shows a photograph of both bars from this specimen after dissection. The latter figure reveals that corrosion initiated at various locations along both bars and was most advanced above the waterline. Corrosion initiation was defined for both bars, albeit with uncertainty, as corresponding to the inflection in the potential-time trace at 186 days.

Figure 14 shows the potential versus time behavior for Specimen 3A. These data show a trend somewhat similar to that of Specimen 5B but with a more gradual potential decay which began after 85 days for the left bar and 141 days for the right. Figure 15 provides photographs of these bars and reveals that corrosion was modest and limited to above waterline locations. This is in spite of the fact that this specimen was not sprayed. Corrosion initiation was defined as having initiated, again with uncertainty, in conjunction with the minor potential decay inflection at 326 days for the left bar and 343 days for the right.

Figure 16 shows the potential versus time history for Specimen 5A, which was also not sprayed, and reveals that a gradual rather than sharp transition occurred here also. Photographs of bars subsequent to dissection for this specimen are provided in Figure 17. These show that the most advanced corrosion occurred in the submerged zone of the right bar, although instances of lesser corrosion are also apparent at above waterline locations despite the fact that this specimen was not sprayed. The -72 mV potential

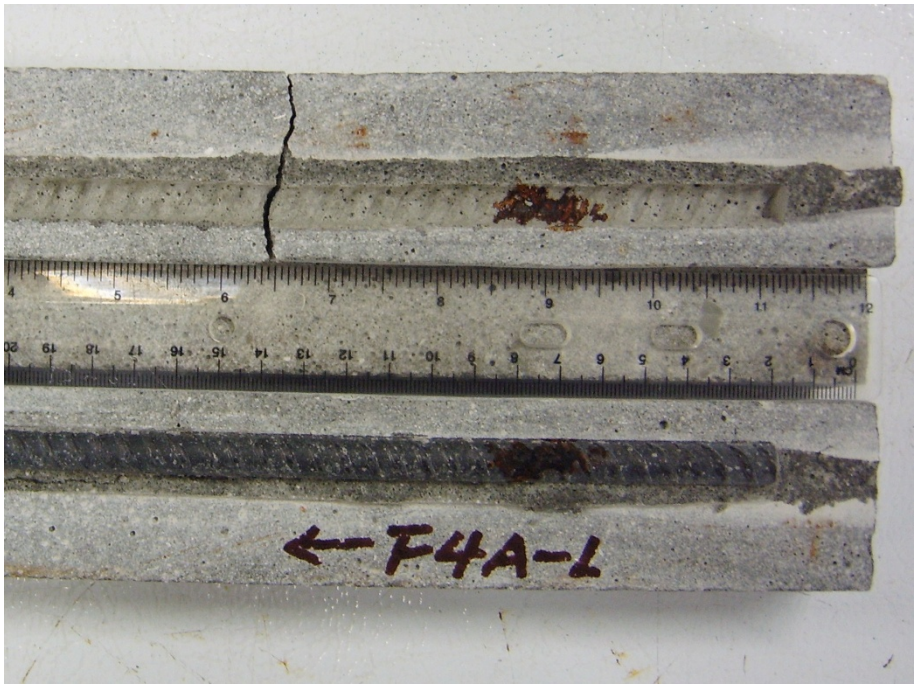

(a)

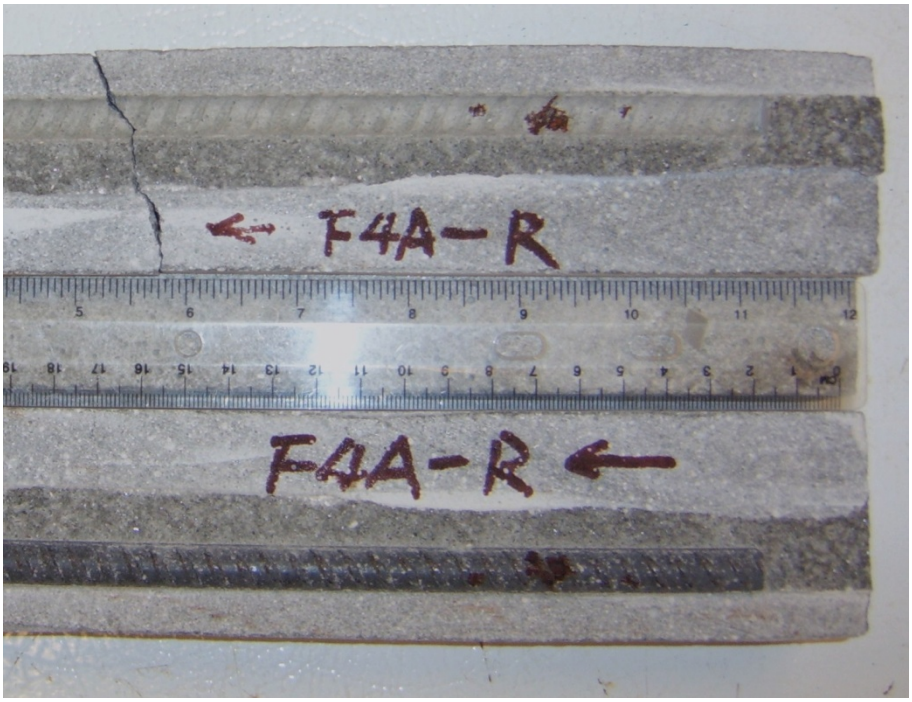

(b)

Figure 11: Photograph of the left (a) and right (b) bars of Specimen 4A subsequent to dissection.

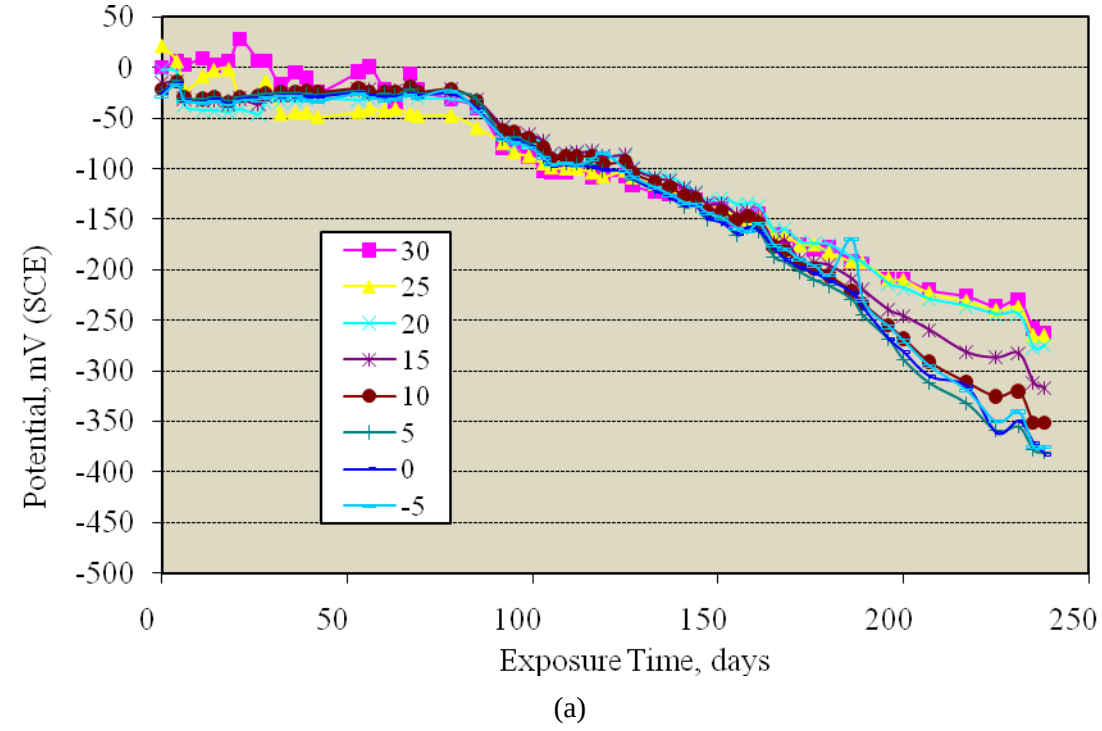

(a)

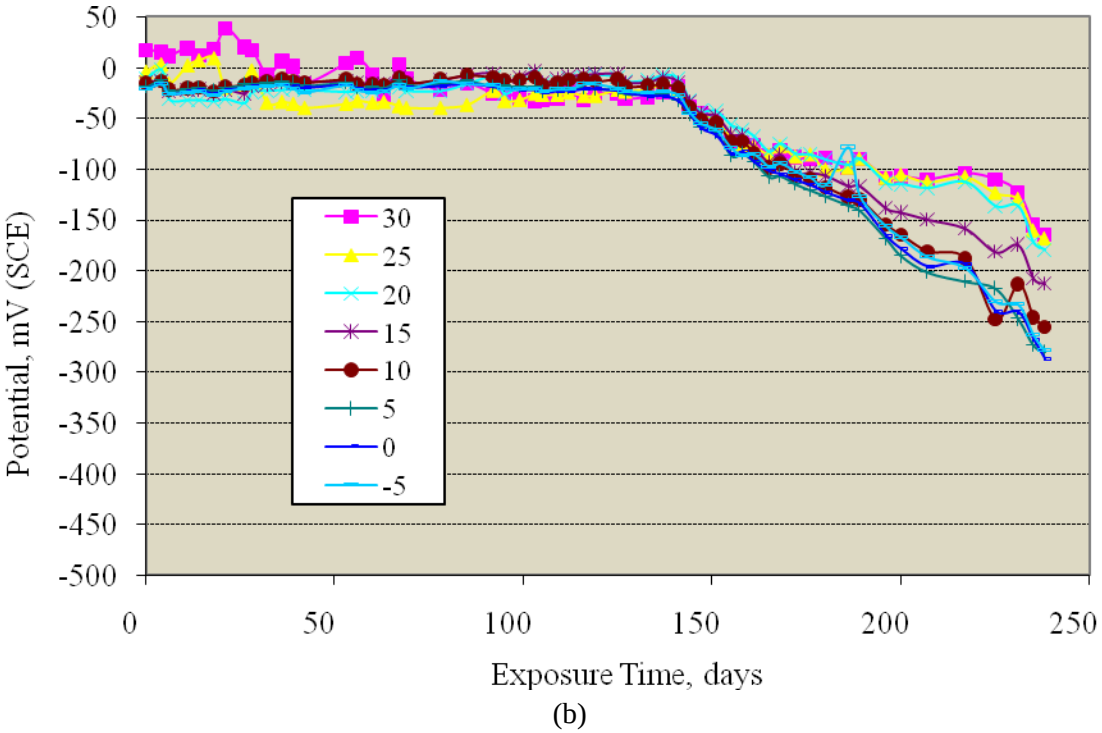

(b)

Figure 12: Potential of the left (a) and right (b) bars of Specimen 5B at different elevations as a function of exposure time (key shows measurement elevations in cm relative to the waterline).

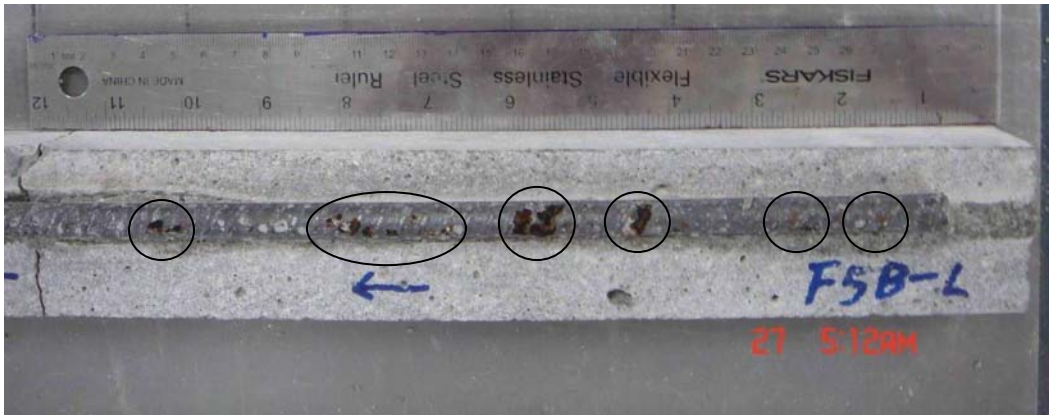

(a)

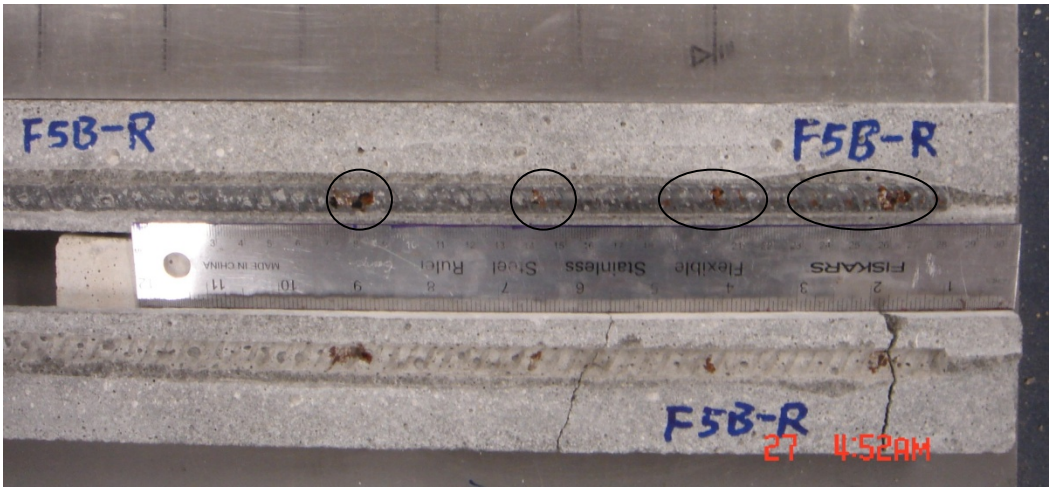

(b)

Figure 13: Photograph of the left (a) and right (b) bars of Specimen 5B subsequent to dissection where locations of corrosion are indicated at circles/ellipses.

change for the right bar between days 78 and 85 was assumed to constitute a potential shift corresponding to corrosion initiation. This specimen was exposed for an additional 153 days subsequent to this potential shift, and the most advanced corrosion is approximately the same as for Specimen 4A which had essentially the same propagation period. For the left bar, corrosion initiation was taken as the potential inflection at 168 days, which also corresponds to the time at which the potential gradient along this bar began to increase.

Figure 18 provides the potential versus time trend for Specimen 3B, and Figure 19 shows photographs of these bars. Corrosion of the left bar initiated below the waterline, whereas for the right

this occurred at an entrapped air void with corrosion products that extended through the cover to the exposed surface 26 cm above the specimen base. This latter corrosion was disregarded, and T_i was taken as >137 days, which is when testing was terminated and the specimen dissected.

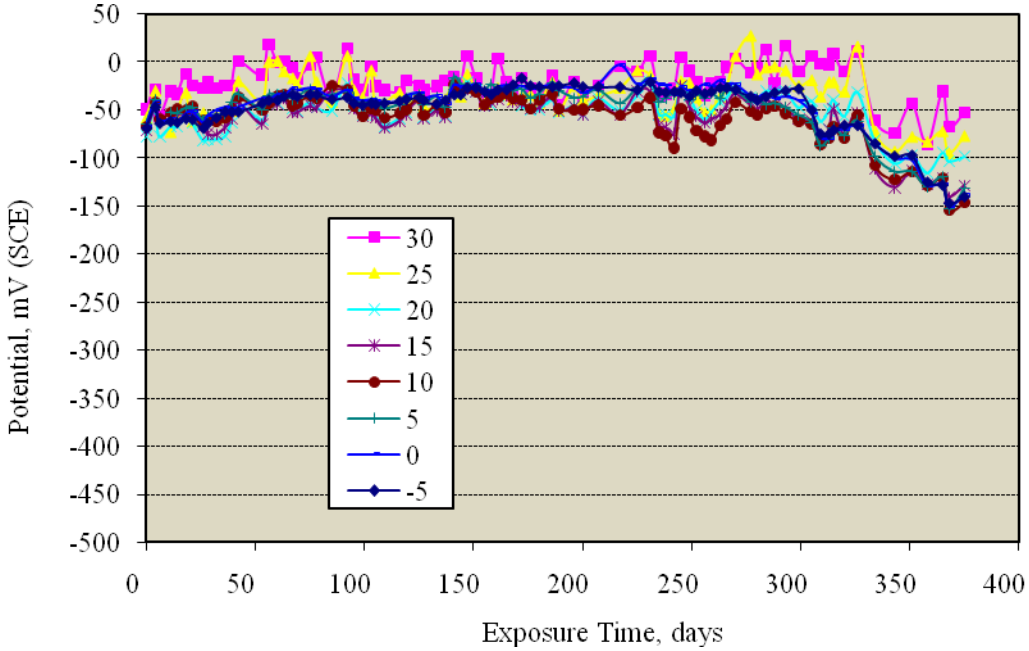

(a)

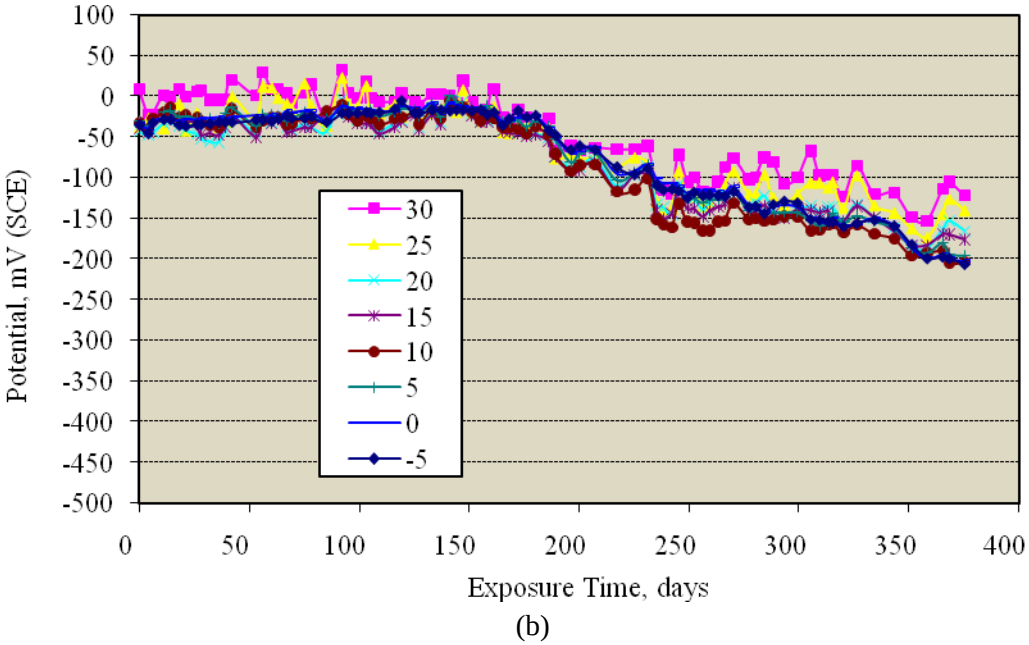

(b)

Figure 14: Potential of the left (a) and right (b) bars of Specimen 3A at different elevations as a function of exposure time (key shows measurement elevations in cm relative to the waterline).

(a)

(b)

Figure 15: Photograph of minor corrosion approximately 20 cm from the specimen base on the left (a) and right (b) bars of Specimen 3A subsequent to dissection.

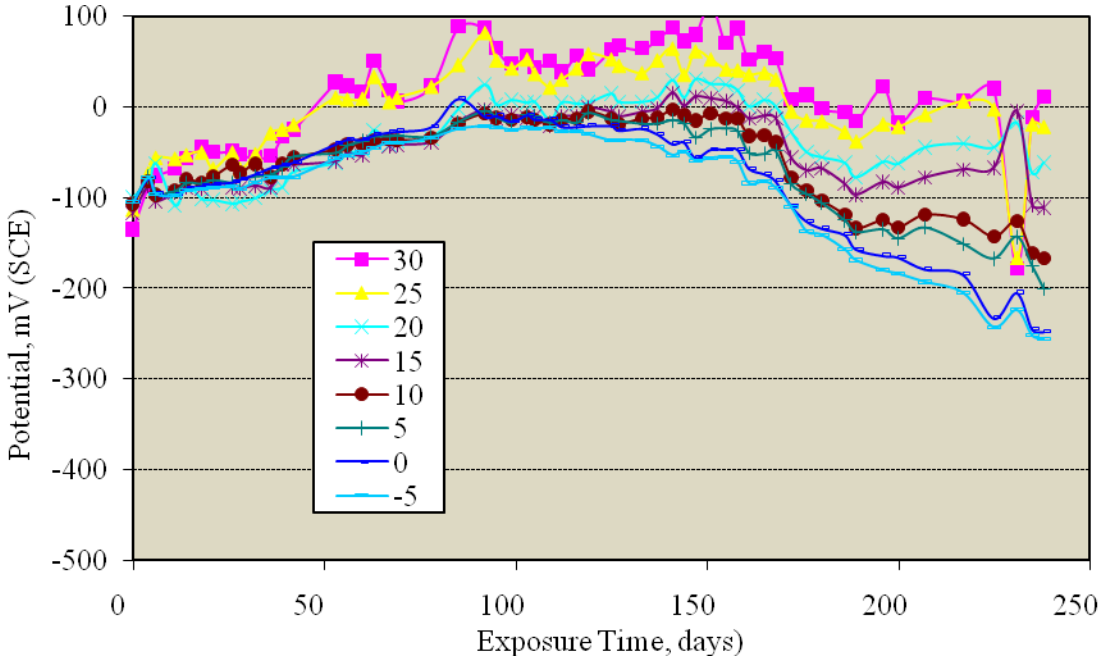

(a)

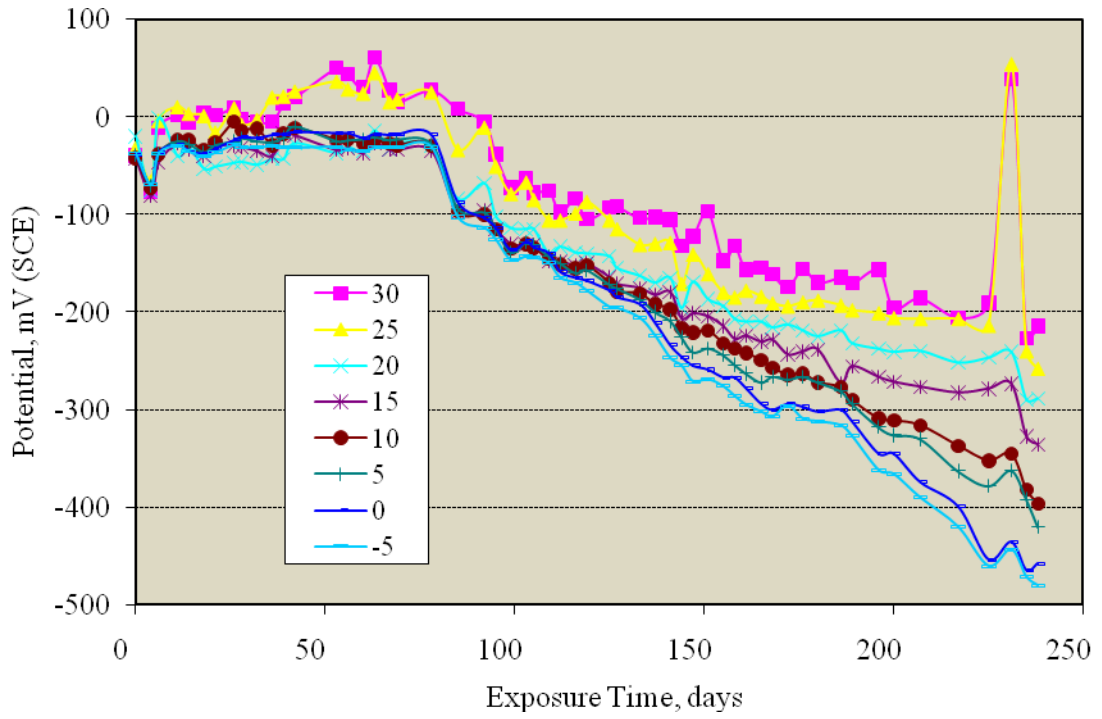

(b)

Figure 16: Potential of the left (a) and right (b) bars of Specimen 5A at different elevations as a function of exposure time (key shows measurement elevations in cm relative to the waterline).

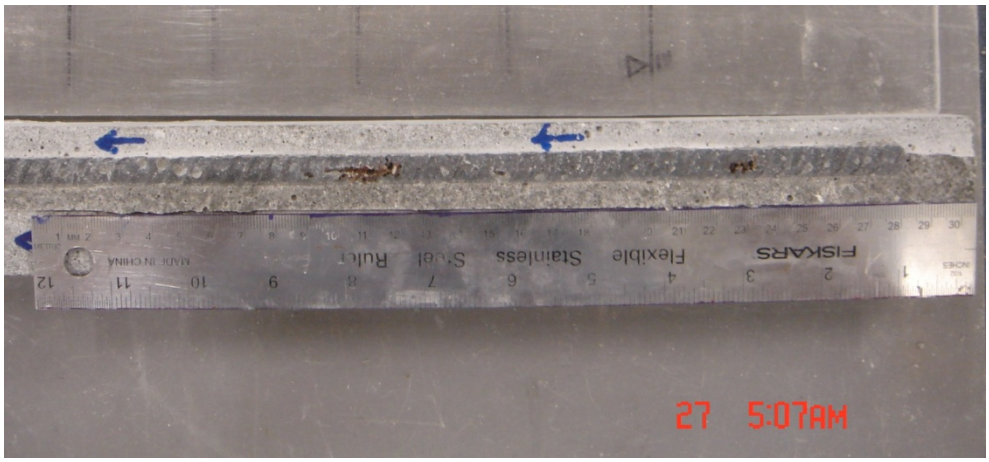

(a)

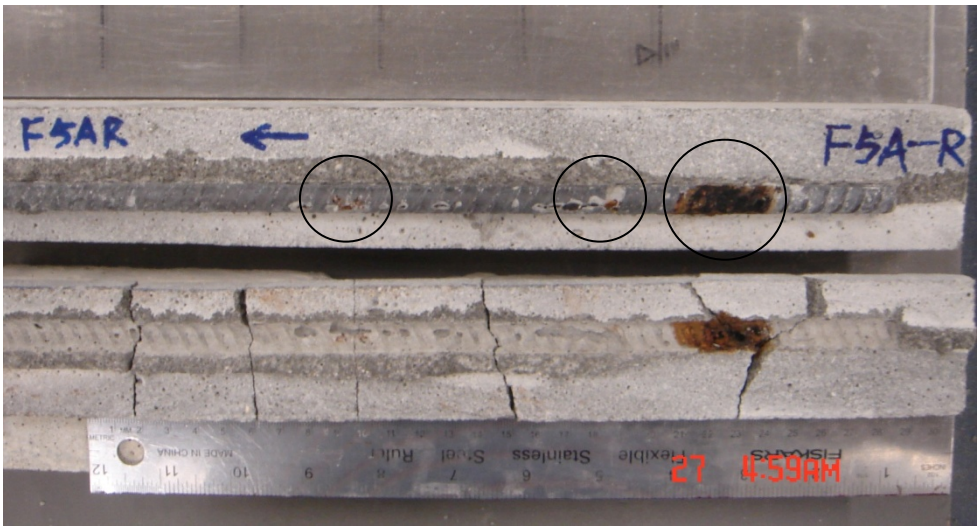

(b)

Figure 17: Photograph of the left (a) and right (b) bars of Specimen 5A subsequent to dissection where locations of corrosion are indicated at circles.

Table 7 lists T_i for specimens in the present category, and Figure 20 provides a cumulative distribution function plot of these data. In this representation, the right bar of Specimen 3B, which had not initiated corrosion, was assumed to have activated at the time of exposure termination (data point with arrow in Figure 20). With the exception of Specimen 4A, there is no definitive indication from the potential data that corrosion initiation on the initial bar of a specimen to become active affected potential of the other, as was the case for freely corroding MD2 specimens as discussed above; and so data for all bars of MD1 mix specimens were considered to conform to a common population. Also shown in Figure

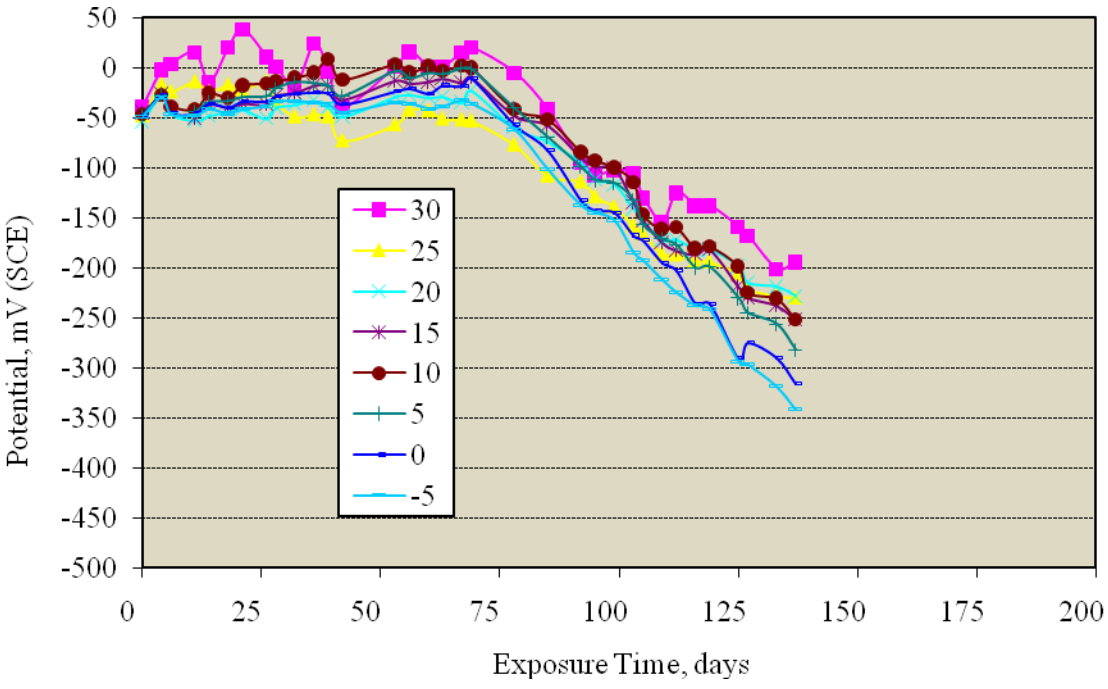

(a)

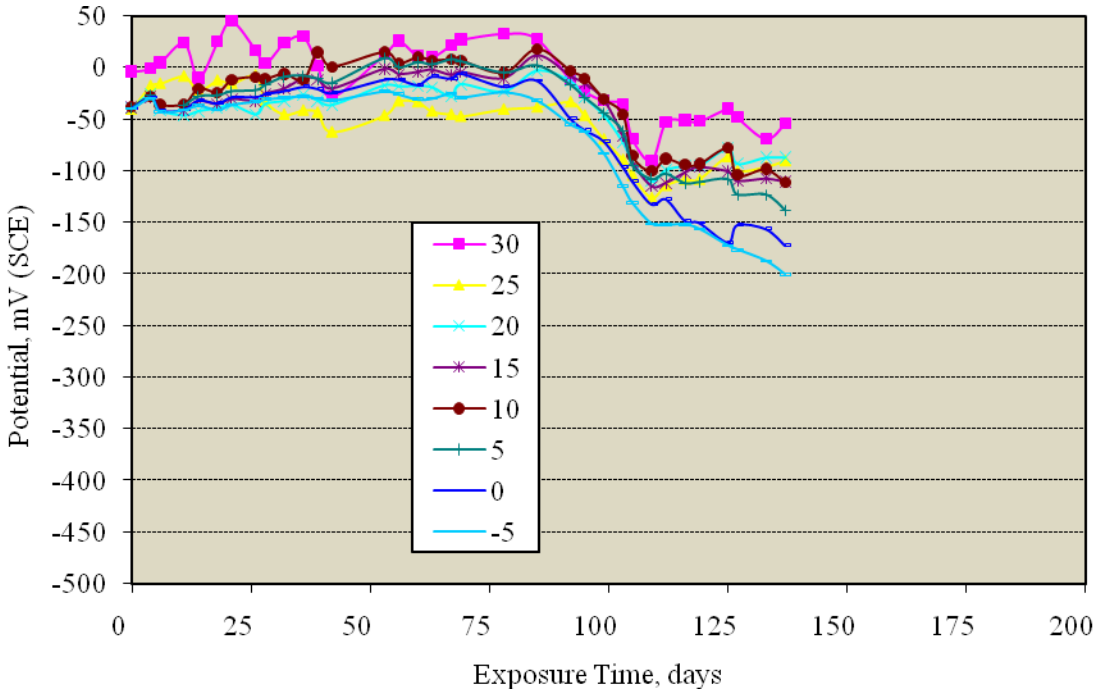

(b)

Figure 18: Potential of the left (a) and right (b) bars of Specimen 3B at different elevations as a function of exposure time (key shows measurement elevations in cm relative to the waterline).

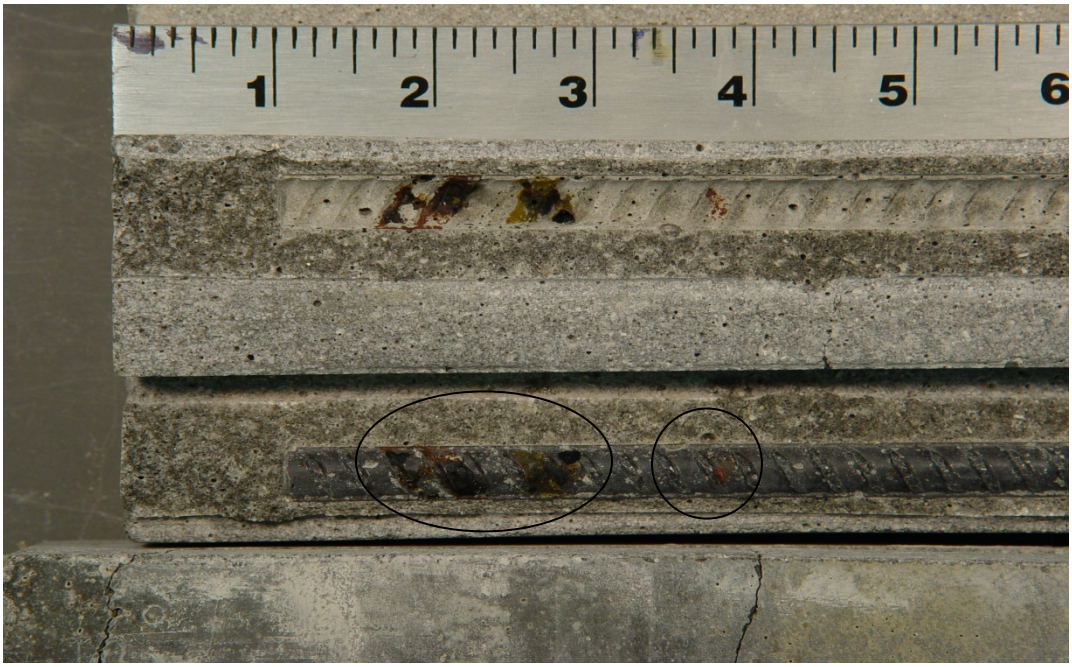

(a)

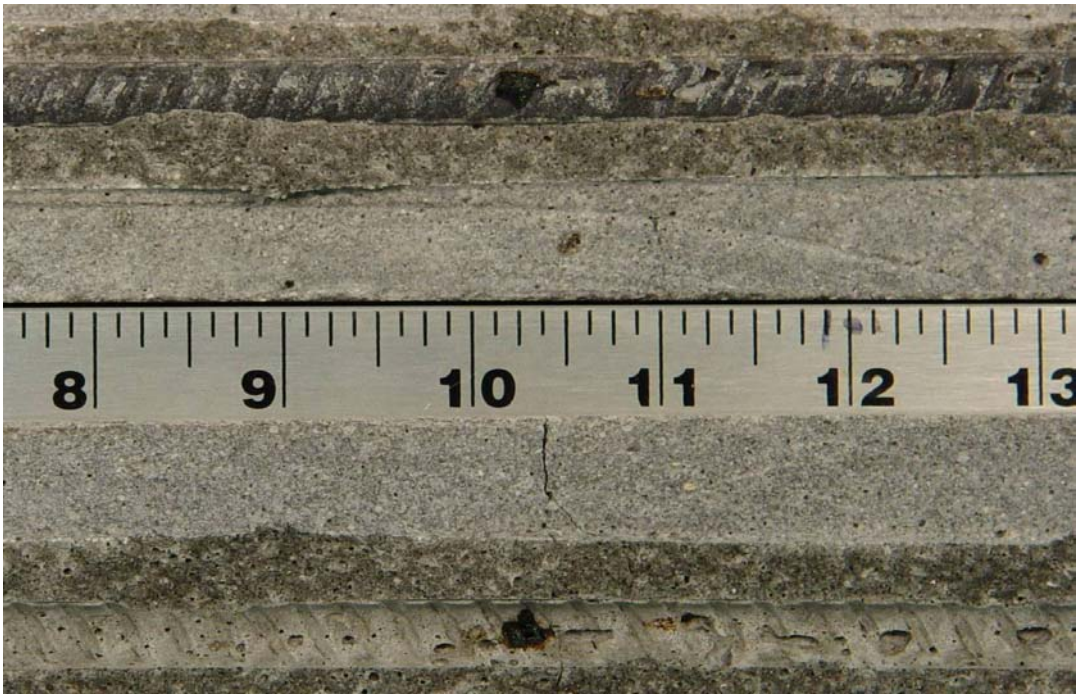

(b)

Figure 19: Photograph of corrosion approximately on the left (a) and right (b) bars of Specimen 3B subsequent to dissection. On the right bar the corrosion was at an air void in the mortar approximately 26 cm from the specimen base.

Table 7: Listing of T_i data for free corrosion MD1 specimens.

Specimen Number	Test Condition	Bar	T_i, days
3A	No Spray	L	326
		R	343
3B	Spray	L	109
		R	>137
4A	No Spray	L	158
		R	263
5A	No Spray	L	168
		R	125
5B	Spray	L	186
		R	186

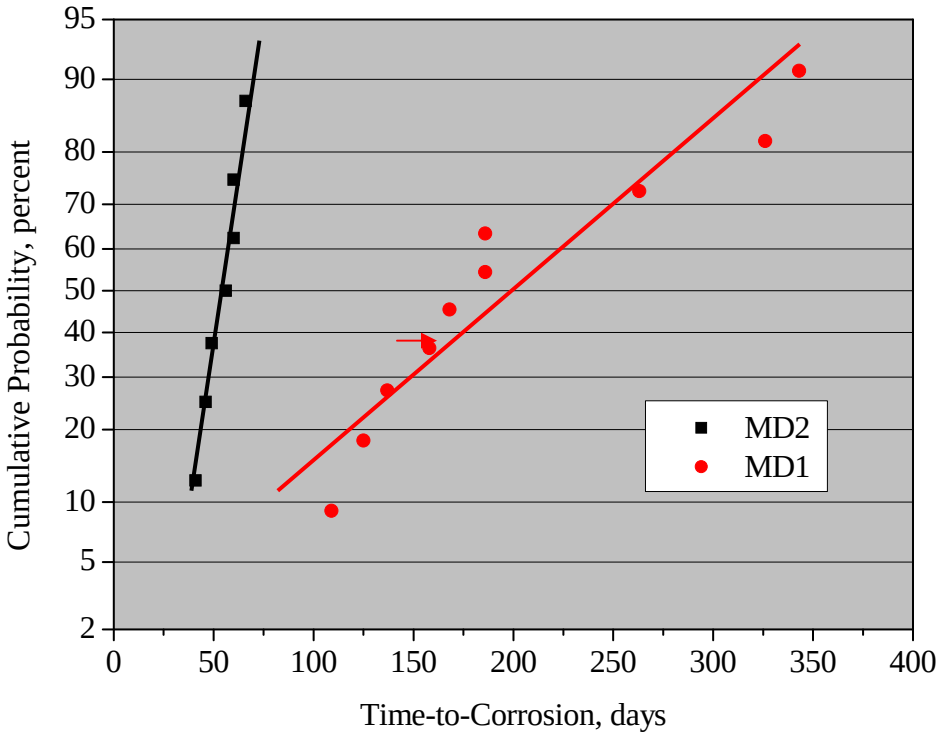

Figure 20: Cumulative distribution function plot of T_i for MD1 and MD2 free corrosion specimens.

20 for comparison are data for the initial bar of MD2 mix design specimens that became active. The data indicate that the mean T_i for bars in MD1 specimens is almost four times greater than for the MD2 ones. Reduced Cl^- diffusivity for the MD1 mix compared to the MD2 apparently more than offset a possibly lower C_T and lesser cover for the fly ash mix (MD1) specimens.

An attempt was made to improve upon the uncertainty associated with identifying T_i for some of the above bars based upon the extent to which corrosion had progressed. The approach considered that size of the corrosion increased linearly with time of corrosion propagation, $T_d - T_i$, where T_d is the time of test termination and dissection. Table 8 lists the minor (smallest) dimension of corrosion products as measured on the bar/bar trace of these specimens. This minor dimension rather that the major (largest) one was chosen because in some cases it appeared that there were multiple initiation sites that grew together, and so measuring this would underestimate time of corrosion. Other parameters that are listed in Table 8 are T_i, T_d, and T_d-T_i. In doing this, the right bar of Specimen 3B was assumed to have initiated corrosion at the time testing was terminated. Figure 21 plots the corrosion spread dimension for these specimens versus T_d-T_i. A best fit line through the origin has an R^2 of 0.82, which is essentially the same as the best fit line otherwise (not shown). Given that the above method for characterizing duration of ongoing corrosion is approximate, the results are taken as generally supportive of the T_i values listed in Table 7.

Table 8: Listing of corrosion size and other measured parameters for freely corroding MD1 specimens.

Specimen Number	Bar	Exposure	T_i, days	T_d, days	T_d-T_i, days	Corrosion Size, mm
3A	L	No Spray	326	375	49	5
	R		343	375	32	3
3B	L	Spray	109	137	28	9
	R		>137	137	0	0
4A	L	No Spray	158	315	157	24
	R		263	315	52	8
5A	L	No Spray	168	238	70	6
	R		125	238	113	25
5B	L	Spray	186	238	52	9
	R		186	238	52	8

Polarized MD2 Mix Specimens

Table 3 indicates that rebar pairs from three MD2 specimens (6A, 7A, and 10A) were connected to a common bare submerged steel bar. In all three cases, this was done after specimens had been freely corroding for 66 days. Figure 22 shows potential versus time data for Specimen 6A. Connection to the bare steel resulted in an abrupt polarization of the embedded steel to more negative potentials, the effect being more pronounced at lower elevations. Also, the polarization became greater as exposure continued. Figure 23 shows data that illustrate this for the above specimen. Likewise, Figure 24 provides a

photograph of each of the bars from this specimen upon dissection. In both cases, localized corrosion is apparent in the submerged zone. Appendix F provides potential versus time plots for the other two specimens in this category.

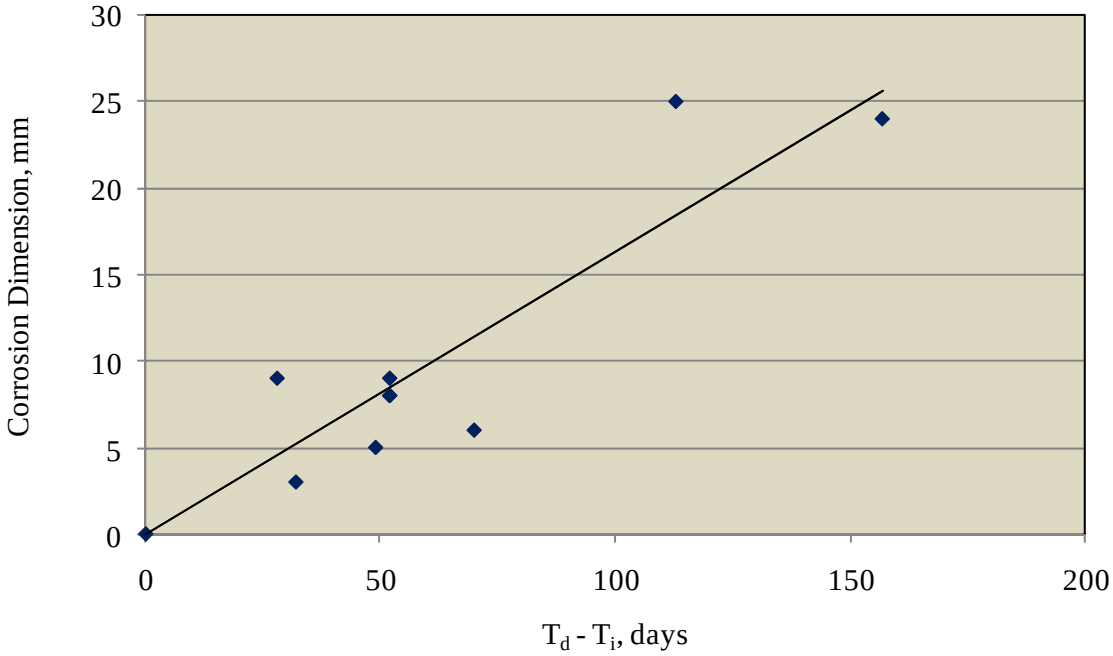

Figure 21: Plot of corrosion size versus propagation time (T_d-T_i) for freely corroding MD1 specimens.

A difficulty associated with this test method is that identification of T_i from the potential – time trend is less certain than for the non-polarized counterpart specimens or not even possible. However, potential of the left bar of Specimen 6A exhibited a post-connection potential arrest or quasi-plateau before subsequently polarizing further. The end of this potential pause at 104 days may have resulted from corrosion initiation. In support of this, a small positive potential shift occurred at this same time on the upper portion of the right bar and a negative shift on the lower portion as observed for free corrosion MD2 specimens. No post-connection potential plateau occurred for the right bar, however; and it is uncertain when corrosion initiated in this case.

Figure 25 provides potential versus time data for Specimen 7A; and Figure 26 shows photographs of the two bars after this specimen was opened. This indicates that corrosion initiated in both cases in the submerged zone. No post-connection potential plateau is apparent from the data for either of these bars.

Results for Specimen 10A are shown in Figure 27 (potential versus time) and Figure 28 (photographs of bars). For both bars, a post connection potential plateau and subsequent second negative

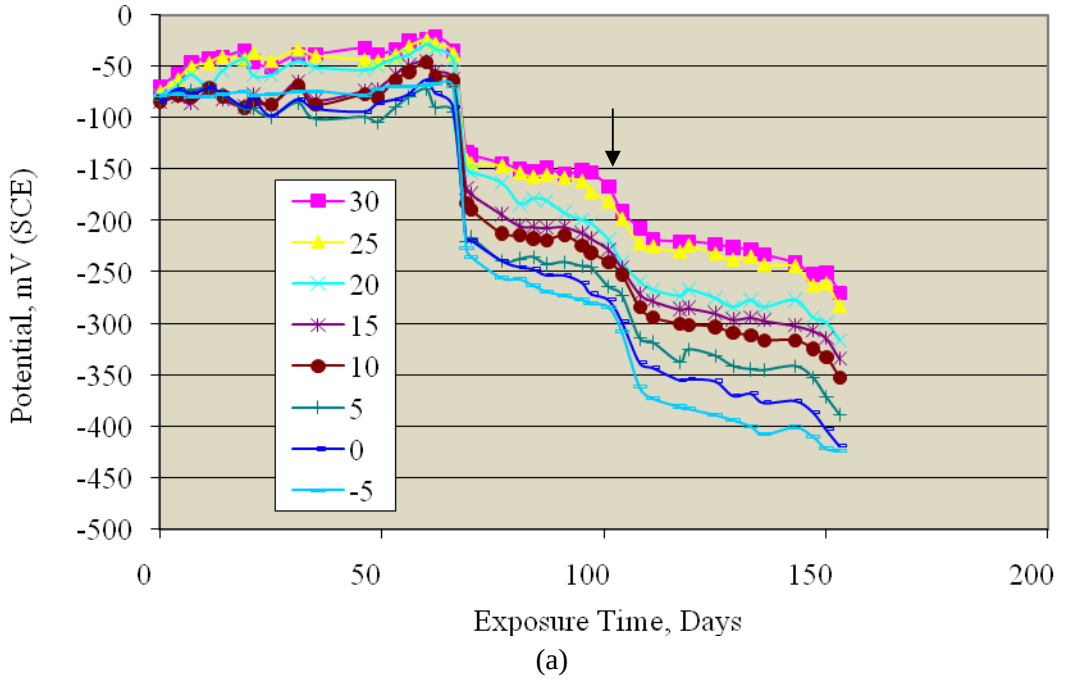

(a)

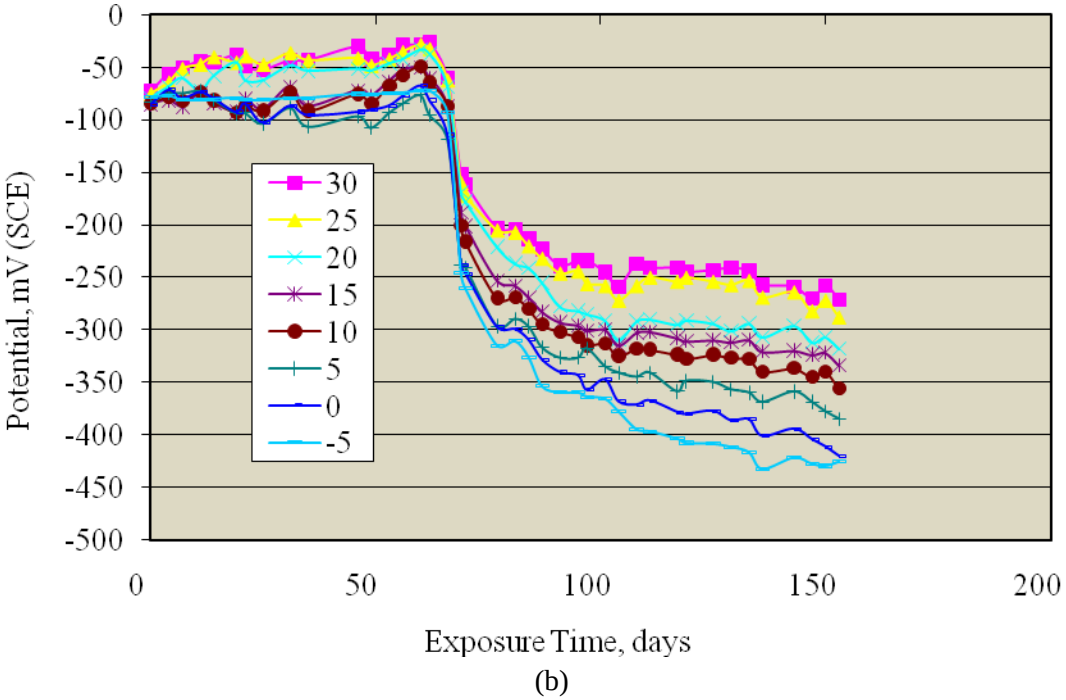

(b)

Figure 22: Potential of the left (a) and right (b) bars of Specimen 6A at different elevations as a function of exposure time (key shows measurement elevations in cm relative to the waterline). Arrow in graph (a) indicates the assumed T_i.

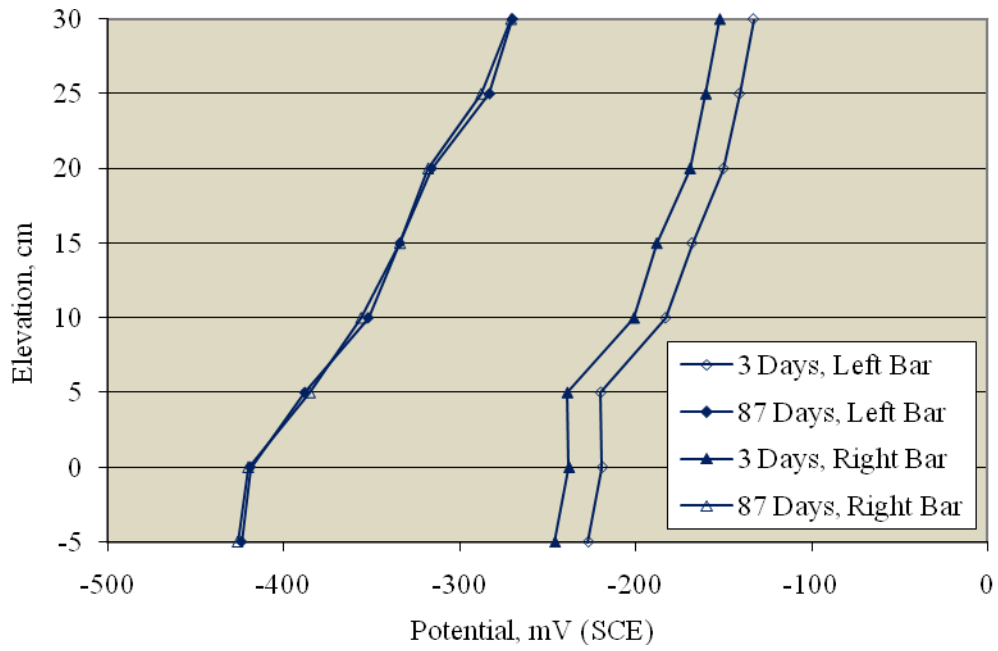

Figure 23: Potential of Specimen 6A as a function of elevation three days and 87 days after polarization.

potential shift are apparent: for the left bar after 108 days and for the right 91 days. The photographs indicated that, as for the other two specimens, corrosion initiated in the submerged zone. Table 9 lists the exposure time of the second negative potential shift as T_i in the case of bars for which this occurred.

In order to possibly identify T_i for bars where this parameter was not apparent from the potential-time record, corrosion size was measured and correlated with time of propagation, $T_d - T_i$, for freely corroding MD2 specimens, as was done above for freely corroding MD1 specimens (Table 8 and Figure 21). Table 10 lists the minor (smallest) dimension of corrosion products as measured on the MD2 bar/bar trace. Other parameters listed are T_i, T_d, and T_d-T_i. Likewise, Figure 29 plots corrosion size versus $T_d - T_i$ for these specimens. A best fit line through the origin has an R^2 of 0.50, whereas the best fit line otherwise (not shown) has an R^2 of 0.62. Next, the corrosion spread dimension for polarized MD2 bars was measured with the results being as shown in Table 11 along with other relevant parameters; and Figure 30 plots corrosion size versus $T_d - T_i$ for the three bars for which T_i was projected. A best fit line forced through the origin (R^2 in this case is 0.94) is also shown. Considering the data scatter for the similar freely corroding MD2 data (Figure 29), this goodness of fit was probably fortuitous. Irrespective of this, from the equation of this line,

$$\text{Corrosion Size} = 0.20 \cdot (T_d - T_i), \qquad (1$$

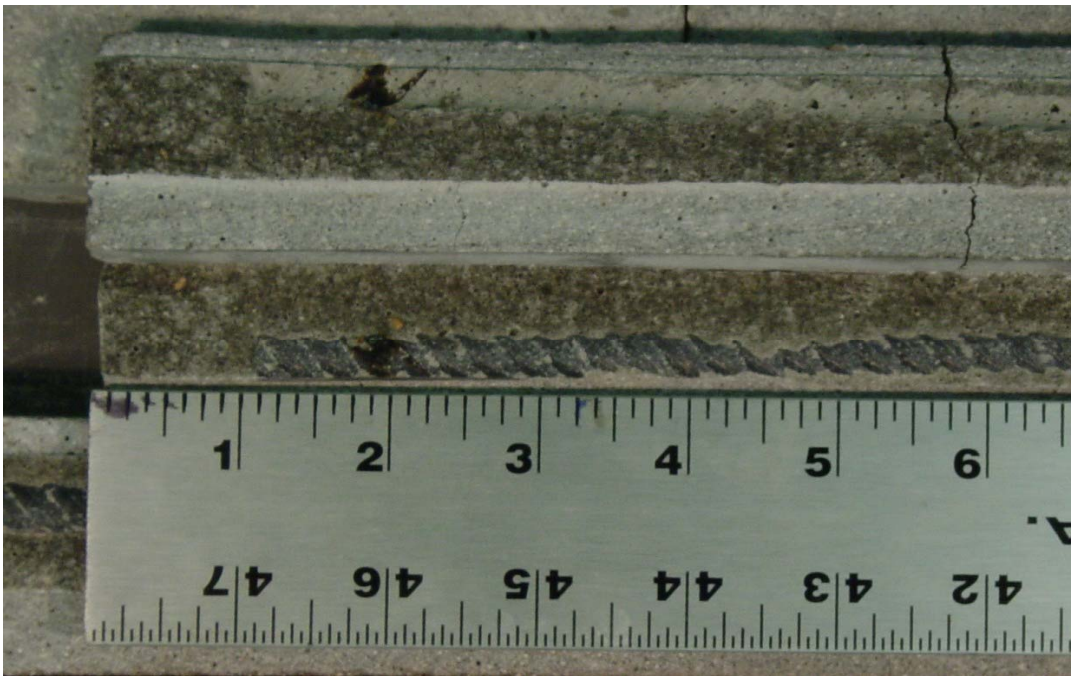

(a)

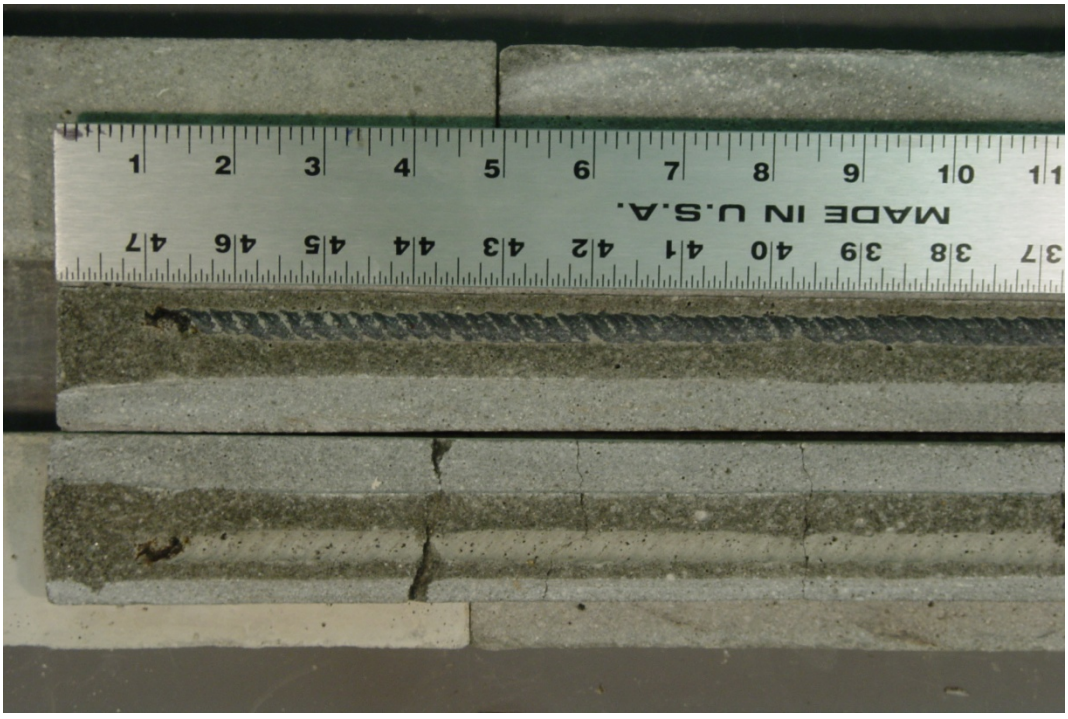

(b)

Figure 24: Photograph of corrosion on the left (a) and right (b) bars of Specimen 6A subsequent to dissection (mortar cracks resulted from the dissection process).

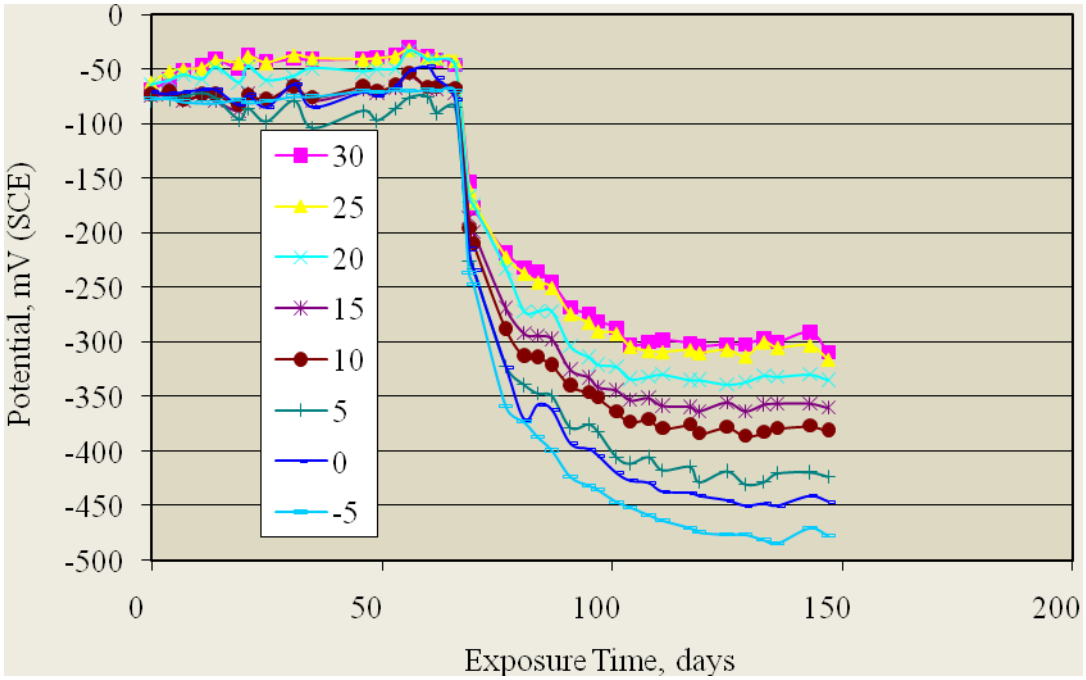

(a)

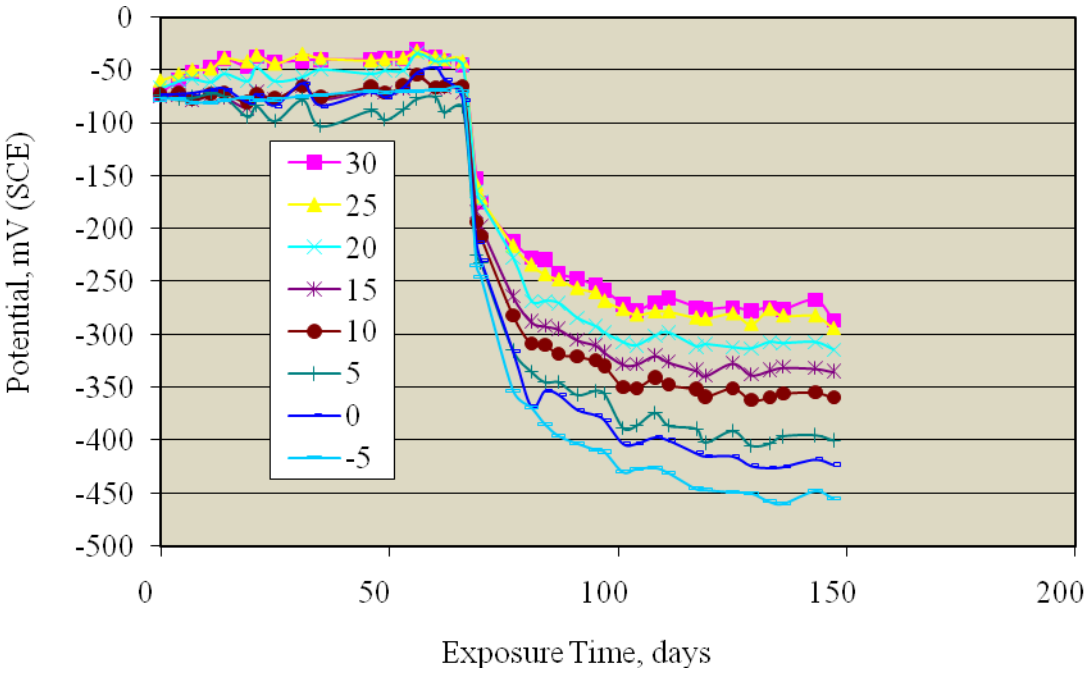

(b)

Figure 25: Potential of the left (a) and right (b) bars of Specimen 7A at different elevations as a function of exposure time (key shows measurement elevations in cm relative to the waterline).

(a)

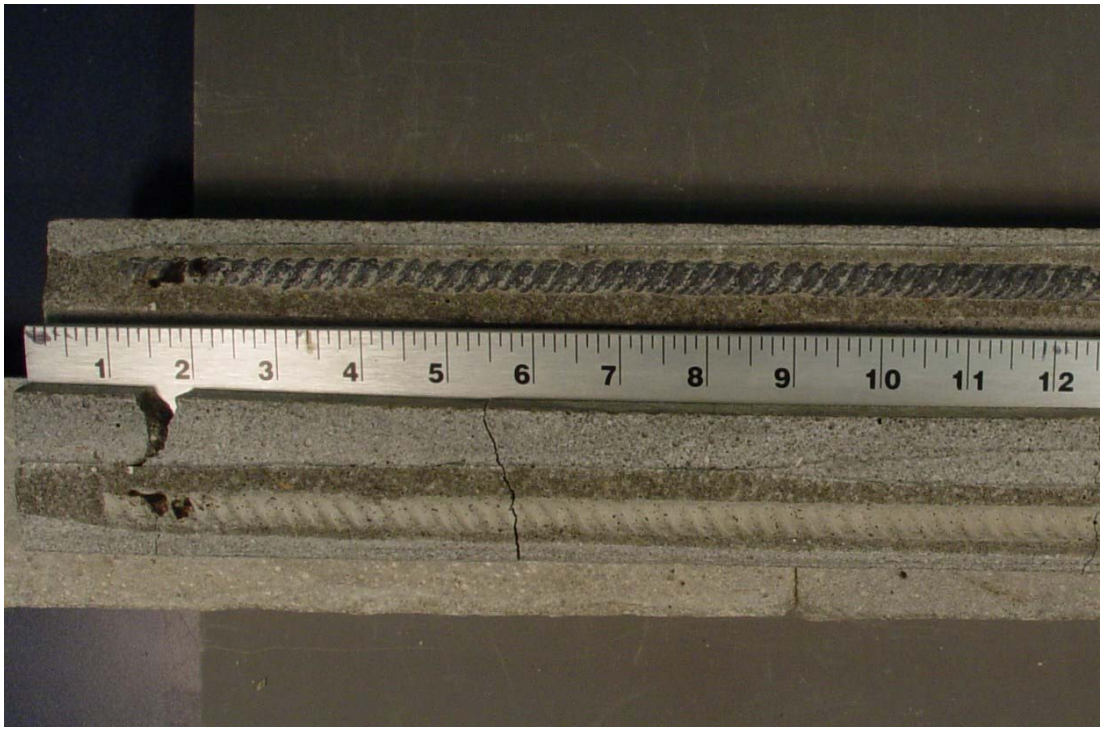

(b)

Figure 26: Photograph of corrosion on the left (a) and right (b) bars of Specimen 7A subsequent to dissection (mortar cracks resulted from the dissection process).

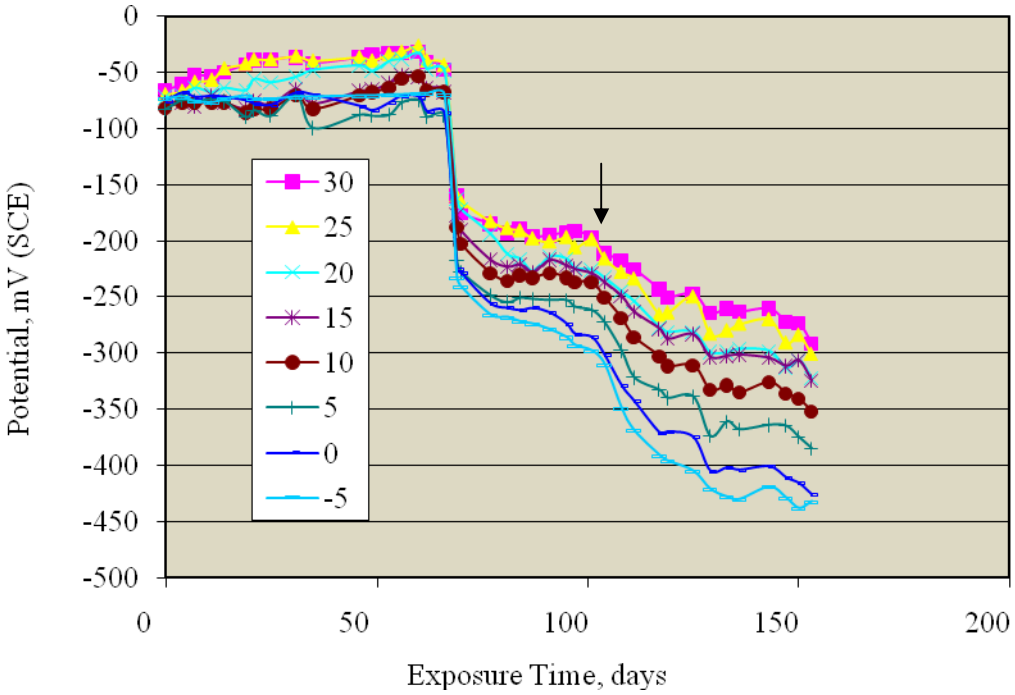

(a)

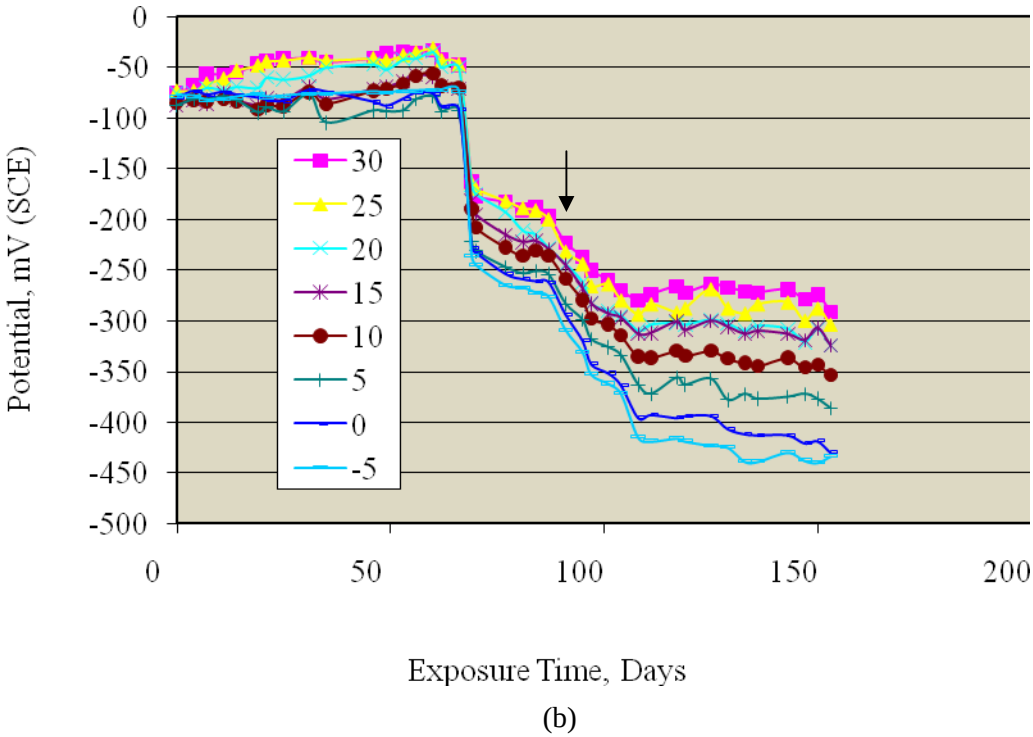

(b)

Figure 27: Potential of the left (a) and right (b) bars of Specimen 10A at different elevations as a function of exposure time (key shows measurement elevations in cm relative to the waterline). Arrow in both graphs indicates the assumed T_i.

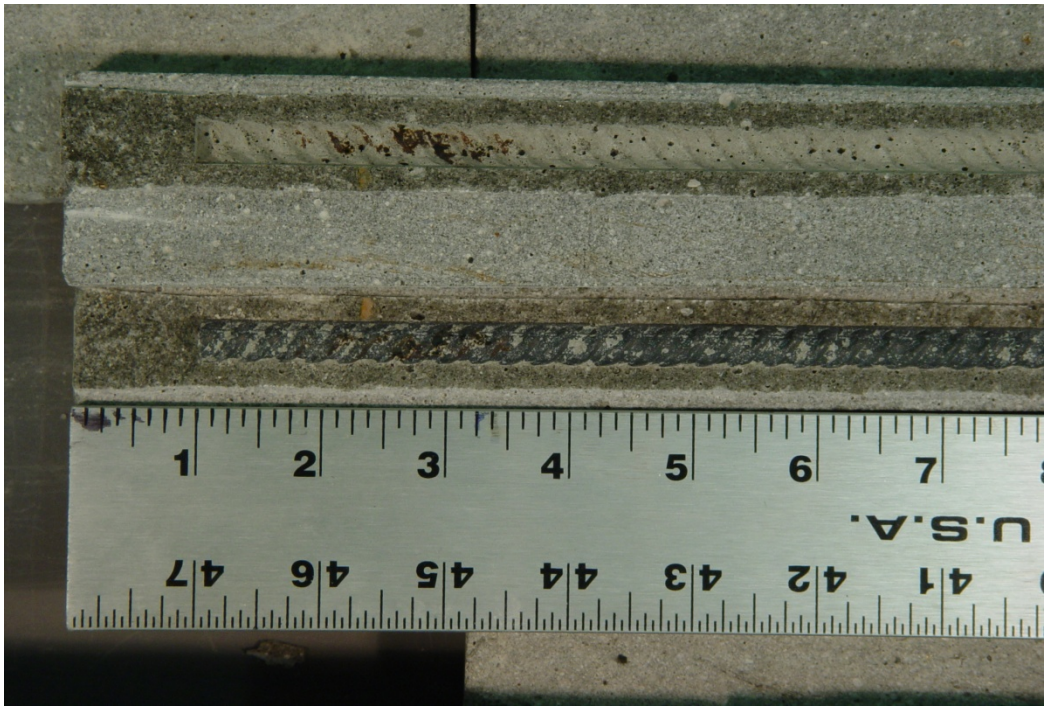

(a)

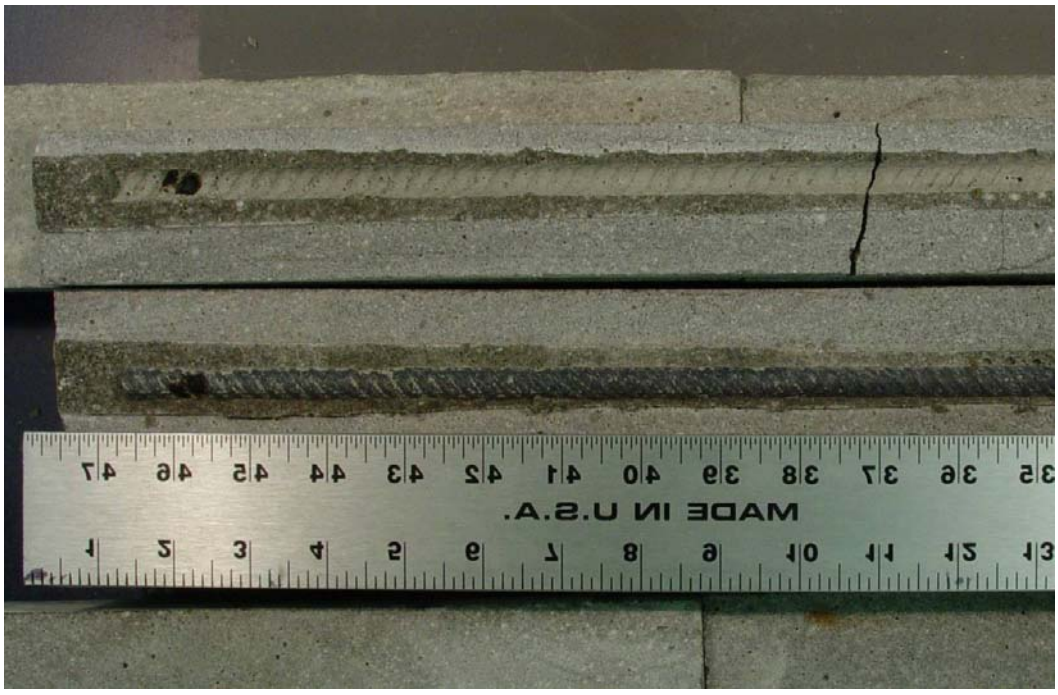

(b)

Figure 28: Photograph of corrosion on the left (a) and right (b) bars of Specimen 10A subsequent to dissection (mortar cracks resulted from the dissection process).

Table 9: Listing of T_i data for polarized MD2 specimens.

Specimen Number	Bar	Ti, days
6A	L	104
	R	-
7A	L	-
	R	-
10A	L	108
	R	91

Table 10: Listing of corrosion size and other parameters for freely corroding MD2 specimens.

Specimen Number	Bar	T_i, days	T_d, days	T_d-T_i	Corrosion Spread, mm
6B	L	53	81	28	10
	R	70	81	11	2
7B	L	77	81	4	2
	R	60	81	21	6
8A	L	81	94	13	2
	R	60	94	34	6
8B	L	66	94	28	6
	R	81	94	13	4
9A	L	49	66	17	8
	R	65	66	1	2
9B	L	62	94	32	7
	R	87	94	7	3
10B	L	46	59	13	5
	R	56	59	3	2

T_i was calculated for bars for which this parameter was indeterminate from the potential-time data. Table 12 lists the results from this calculation, and Figure 31 reproduces Figure 30 with these data added. However, there is no means to independently evaluate the accuracy of these calculations. More confidence in this procedure can be gained by developing a larger T_i database for specimens for which T_i is directly measureable. Also, attention should be focused upon defining that aspect or parameter(s) of corrosion on dissected specimen bars that best correlates with propagation time.

Slope of the best fit line through the free corrosion data (Figure 29), although not indicated above, is 0.26, which is 24 percent less than for the polarized specimens (Figure 30). This difference may reflect measurement scatter; however, it is also consistent with cathodic polarization from the bare submerged bar slowing the rate of attack, once initiated.

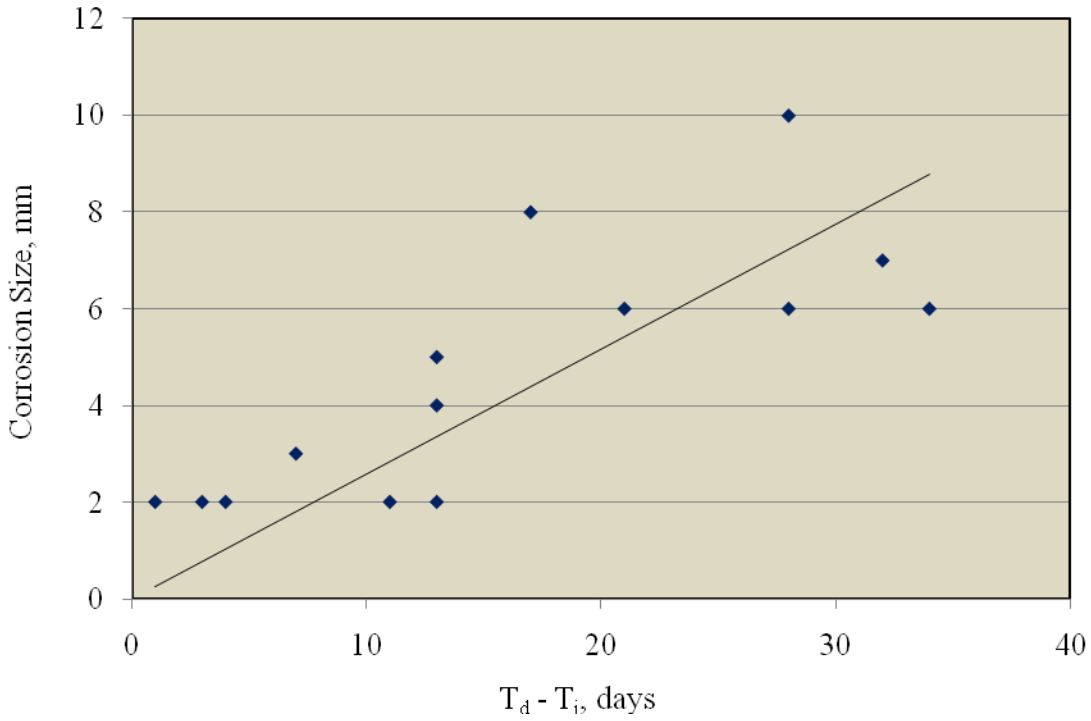

Figure 29: Plot of corrosion size versus propagation time (T_d-T_i) for freely corroding MD2 specimens.

Table 11: Listing of corrosion size and other measured parameters for polarized MD2 specimens.

Specimen Number	Bar	T_i	T_d	T_d-T_i	Corrosion Size, mm
6A	L	104	153	49	10
	R	-	153	-	8
7A	L	-	147	-	19
	R	-	147	-	8
10A	L	104	153	49	9
	R	87	153	66	13

Current between the individual bars of the above specimens and the submerged bare bar to which each pair of embedded bars was connected was measured as a function of time. Figures 32 and 33 illustrate the two types of behavior that were encountered; one where current was constant initially for some period but then decreased to a steady-state value (left bar of Specimen 6A (Figure 32)) and the second for which current decreased with time from the outset to a steady-state value (right bar of this same specimen (Figure 33)). Table 13 summarizes the current-time trend for the six bars in these three specimens and provides companion information regarding the post-connection potential plateau in cases where one occurred and the final potential. Figure 34 is a schematic drawing that illustrates and defines

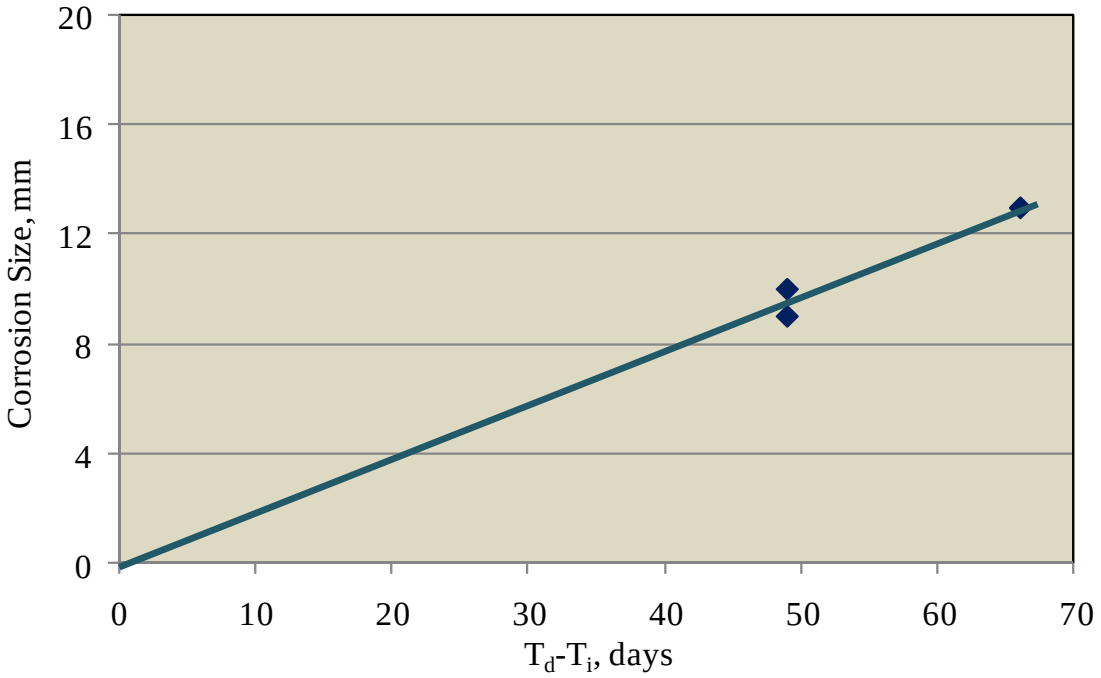

Figure 30: Plot of corrosion size versus propagation time (T_d-T_i) for polarized MD2 specimens for which T_i could be measured.

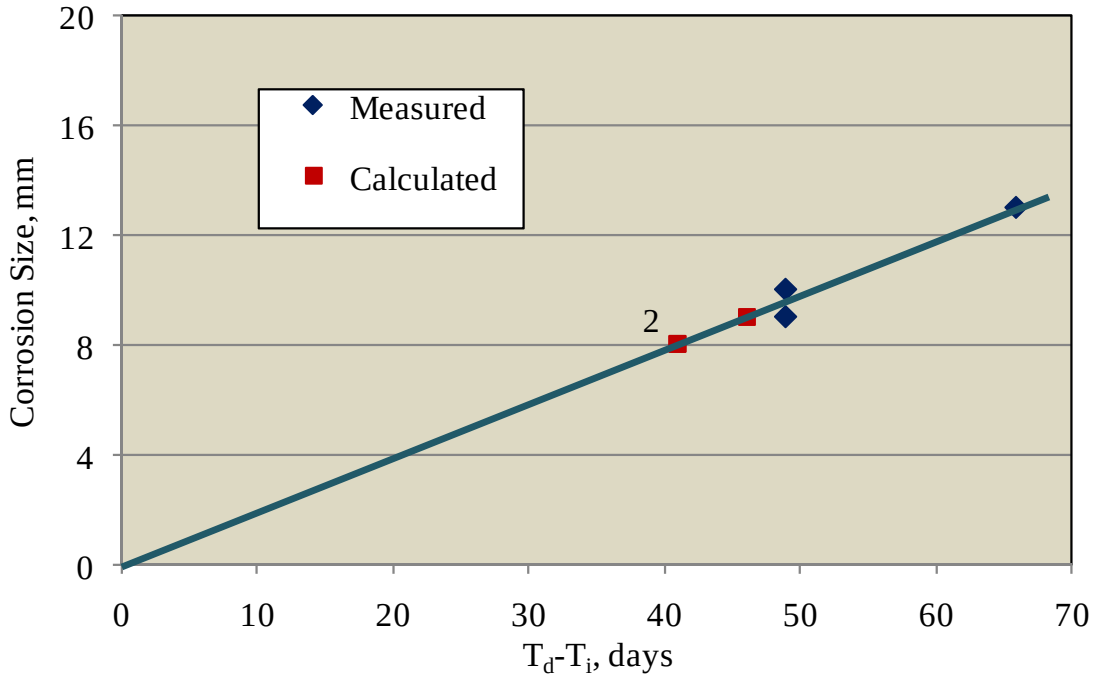

Figure 31: Plot of corrosion size versus both measured and calculated propagation time (T_d-T_i) for polarized MD2 specimens.

Table 12: Listing of corrosion size and other measured and calculated parameters for polarized MD2 specimens.

Specimen Number	Bar	T_i	T_d	T_d-T_i	Corrosion Size, mm
6A	L	104	153	49	10
	R	112	153	41	8
7A	L	101	147	46	9
	R	106	147	41	8
10A	L	104	153	49	9
	R	87	153	66	13

the various potential regimes for bars that exhibited this second plateau. Observations from these data include the following:

1. Initial current for all bars was approximately the same.

For three of the bars (left bar of Specimen 6A and both bars of Specimen 10A), current was constant for a period subsequent to connecting to the bare bar, the duration of which was essentially the same as that of the post-connection quasi-potential plateau. This is consistent with

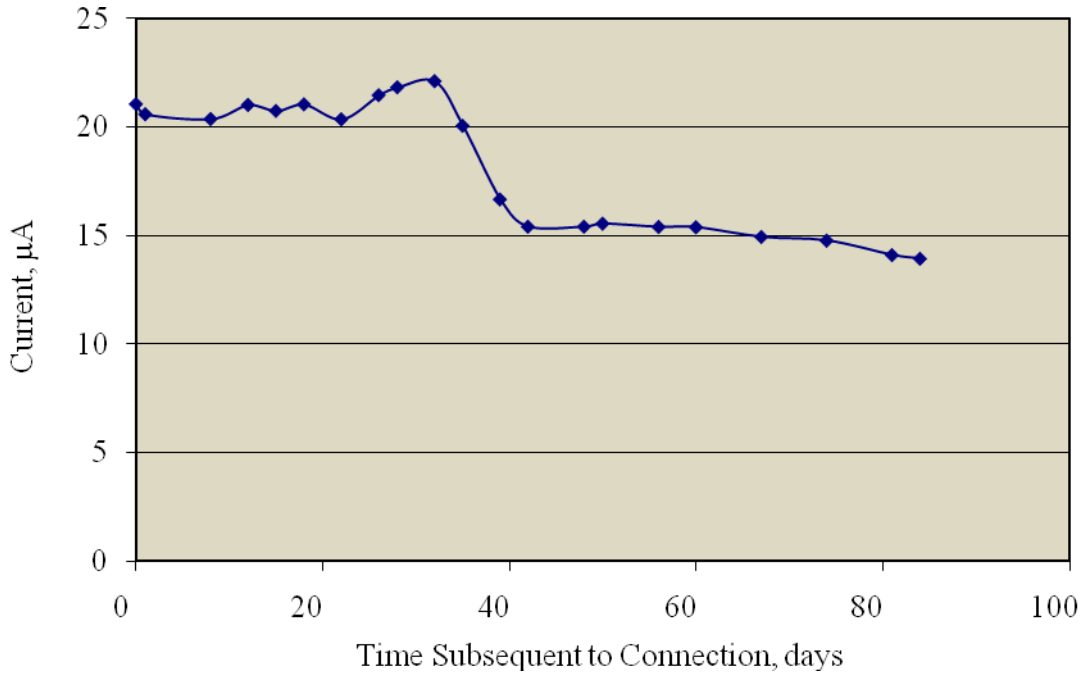

Figure 32: Current versus time history for the left bar of Specimen 6A.

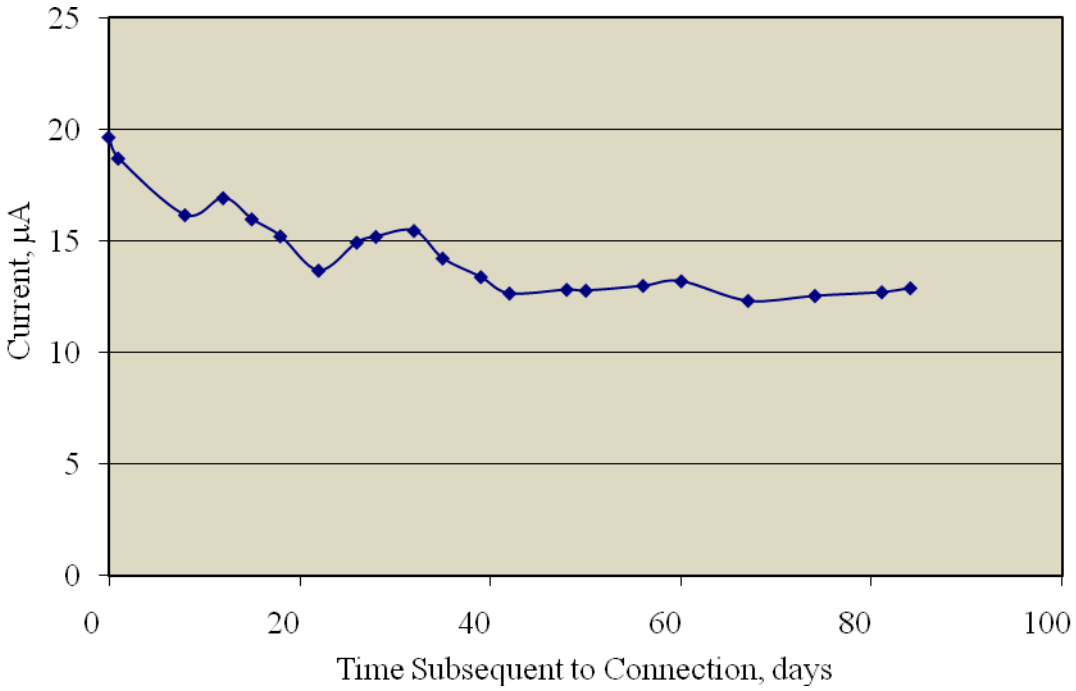

Figure 33: Current versus time history for the right bar of Specimen 6A.

2. these bars having a relatively high current demand until conclusion of the quasi-potential plateau but being more easily polarized thereafter. This supports the assumption that corrosion initiation was commensurate with termination of the quasi-potential plateau. It is unclear, however, why three bars retained a relatively high current demand and exhibited a quasi-potential plateau until corrosion apparently initiated and another three did not.

Based upon the above considerations, Figure 35 provides a cumulative probability distribution plot of T_i for the polarized MD2 specimens. Data for the initial bar of each free corrosion MD2 specimen to become active is also shown for comparison. These results show that T_i for the polarized specimens was almost twice as great as for the free corrosion ones, indicating that polarization had a greater effect on prolonging initiation that it did on reducing subsequent corrosion rate. This difference may have been even greater had the polarized specimens been connected to the submerged bare bar earlier.

Polarized MD1 Mix Specimens

Table 3 indicates that there were five specimens in this category (1A, 1B, 2A, 2B, and 4B). The time after exposure at which the connection to bare submerged steel was made ranged from 75 to 95 days. Figure 36 shows the potential versus time data for Specimen 1A. Here, potential at lower elevations was

Table 13: Current and related potential data for polarized MD2 specimens.

Specimen Number	Bar	Initial Current, μA	Duration of Upper Current Plateau, days	Steady-State Current, μA	Duration of Post-Connection Potential Plateau, days	Final Polarized Potential (Lowest Elevation), mV_{SCE}
6A	L	21	35	15	32	-422
	R	20	NA	13	NA	-426
7A	L	21	NA	9	NA	-477
	R	21	NA	11	NA	-455
10A	L	22	33	13	38	-438
	R	21	19	13	21	-434

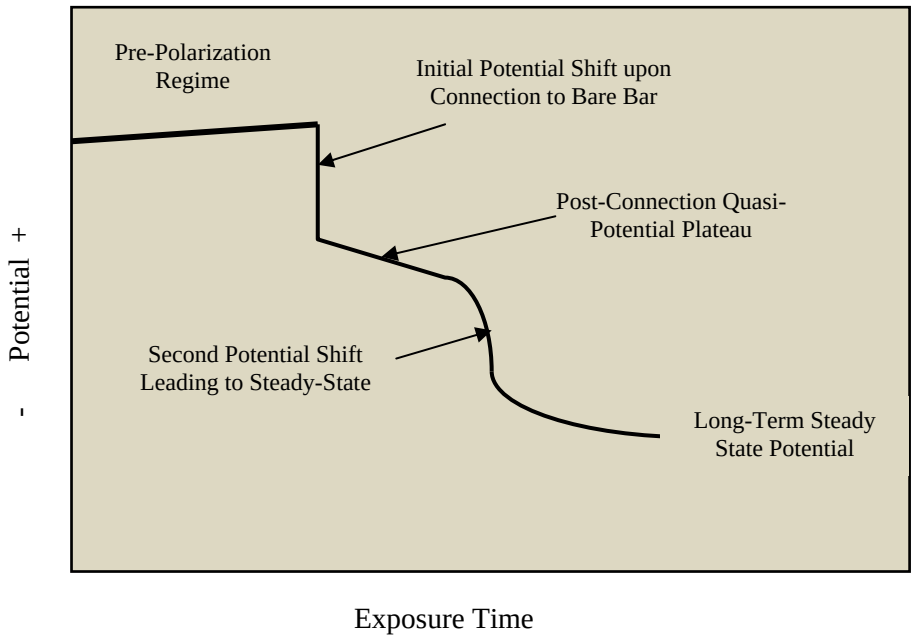

Figure 34: Schematic illustration of the multiple stages of the potential versus time response of some polarized MD2 bars.

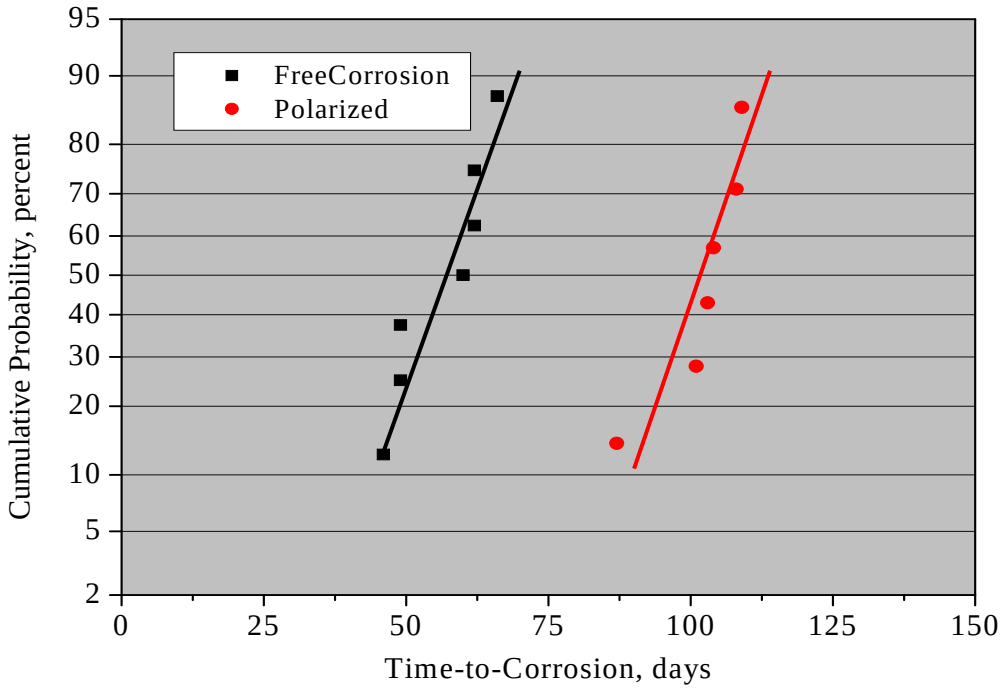

Figure 35: Cumulative distribution function plot of T_i for polarized MD2 specimens in comparison to results for freely corroding bars (Figure 15).

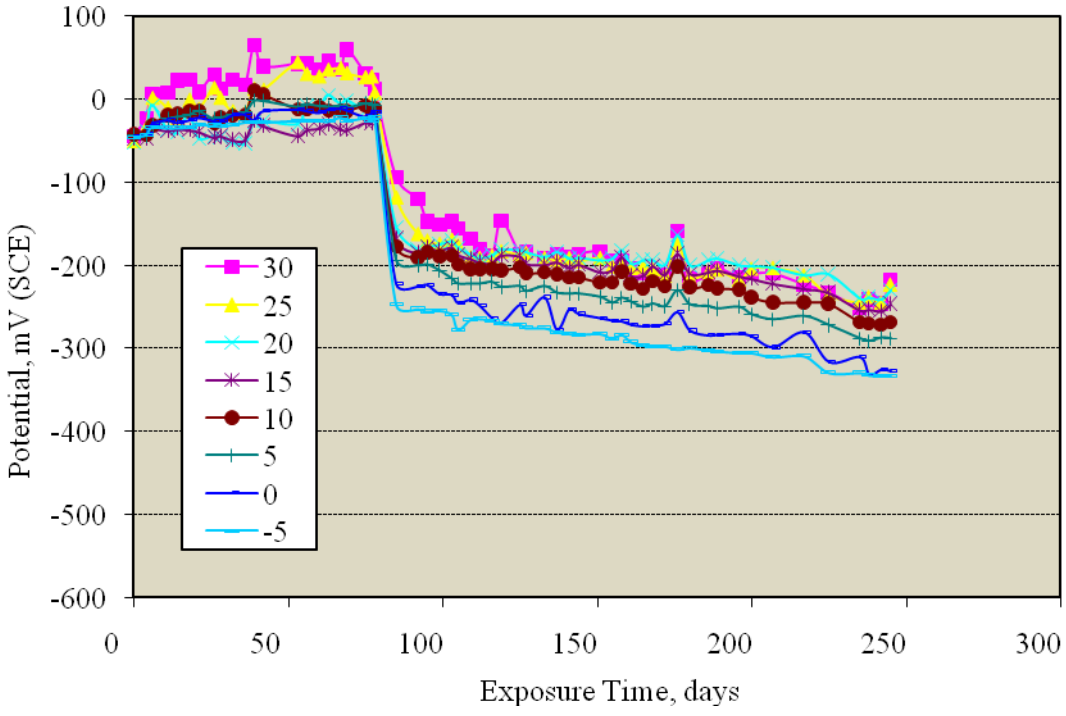

(a)

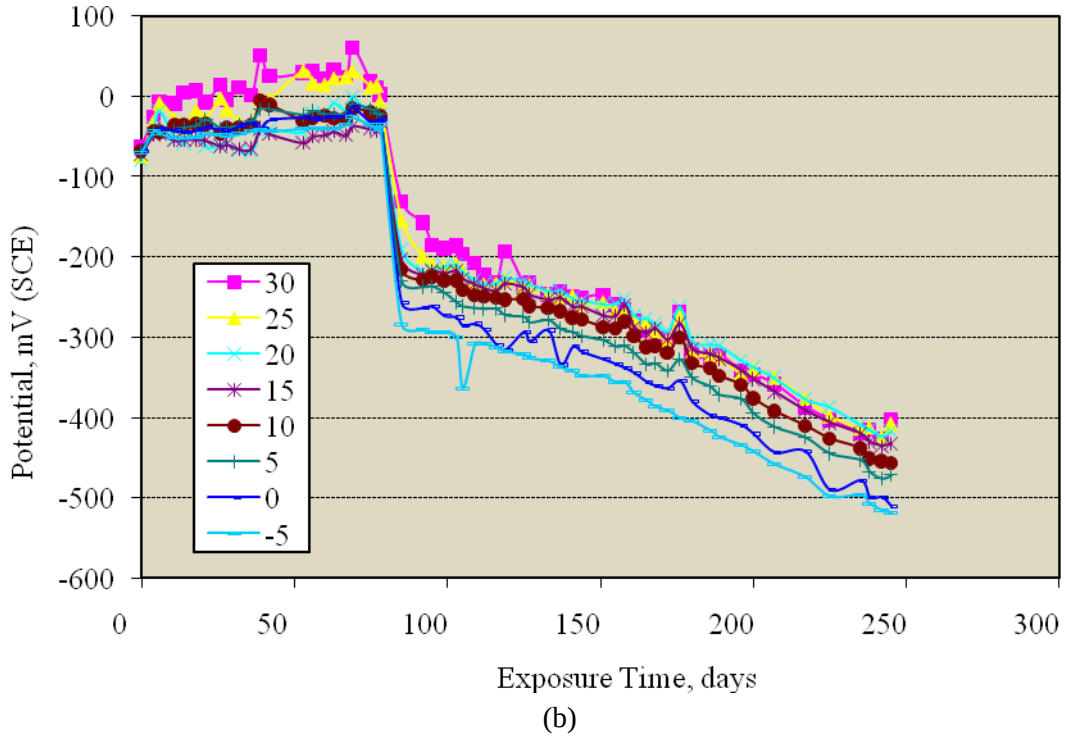

(b)

Figure 36: Potential of the left (a) and right (b) bars of Specimen 1A at different elevations as a function of exposure time (key shows measurement elevations in cm relative to the waterline).

approximately constant prior to connection; and an abrupt negative potential shift to more negative values occurred upon affecting the connection to submerged bare bar after 78 days. Potential decreased linearly with time after the connection was made. Figure 37 shows a photograph of each of rebar subsequent to dissection and reveals that no corrosion was apparent on the left bar but two rust spots about 20-21 cm from the specimen base were present on the right. No feature of the potential-time record that indicates initiation of this corrosion is apparent; however, final potential at the elevation of corrosion for the right bar was -402 mV_{SCE} and for the left at this same elevation -217 mV_{SCE}. The finding that the bar of a given specimen with the more negative potential was the one that initiated corrosion may have resulted from an added negative shift upon activation. Because bar pairs were connected through the submerged bare bar, once one bar initiated corrosion and its potential became more negative, it tended to cathodically polarized the still passive bar and possibly elevate C_T for that bar. On the other hand, from the outset subsequent to connection to the bare bar, the rate of potential decrease of the right bar (the one that activated) was more rapid than for the left.

As a second example, Figure 38 provides the potential versus time record for Specimen 1B. Different trends are apparent for the two bars, each of which differs from that of Specimen 1A bars. Thus, potential of the left bar became distinctly more positive with time prior to connection and was essentially constant subsequent to undergoing a negative shift upon connection. A more moderate initial

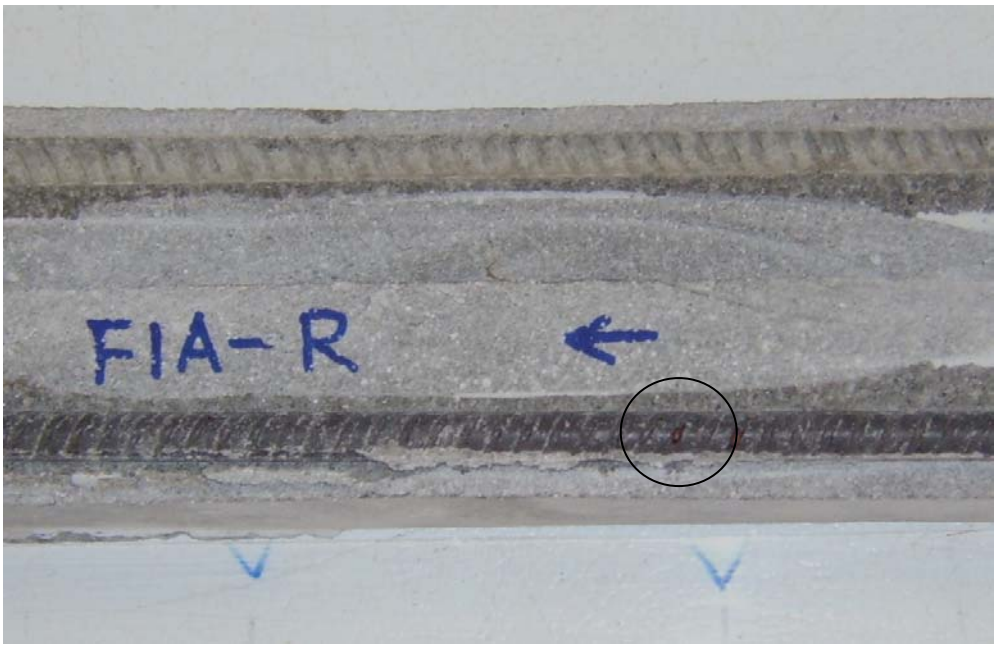

Figure 37: Photograph of the right bar from Specimen 1A subsequent to dissection showing two corrosion spots (circled area).

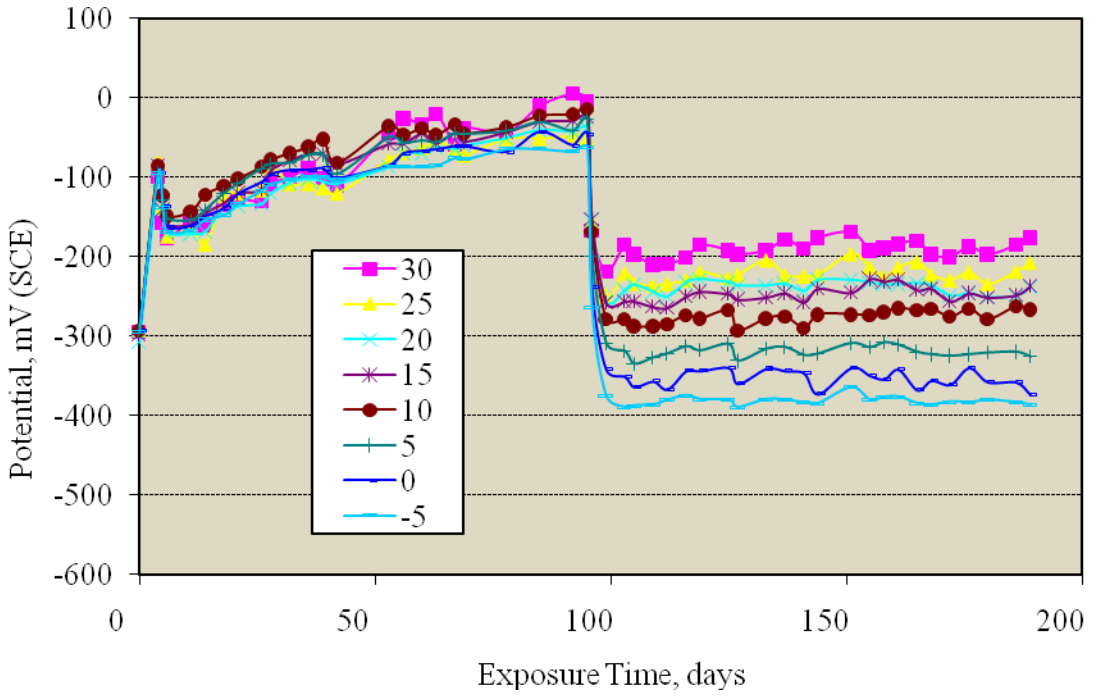

(a)

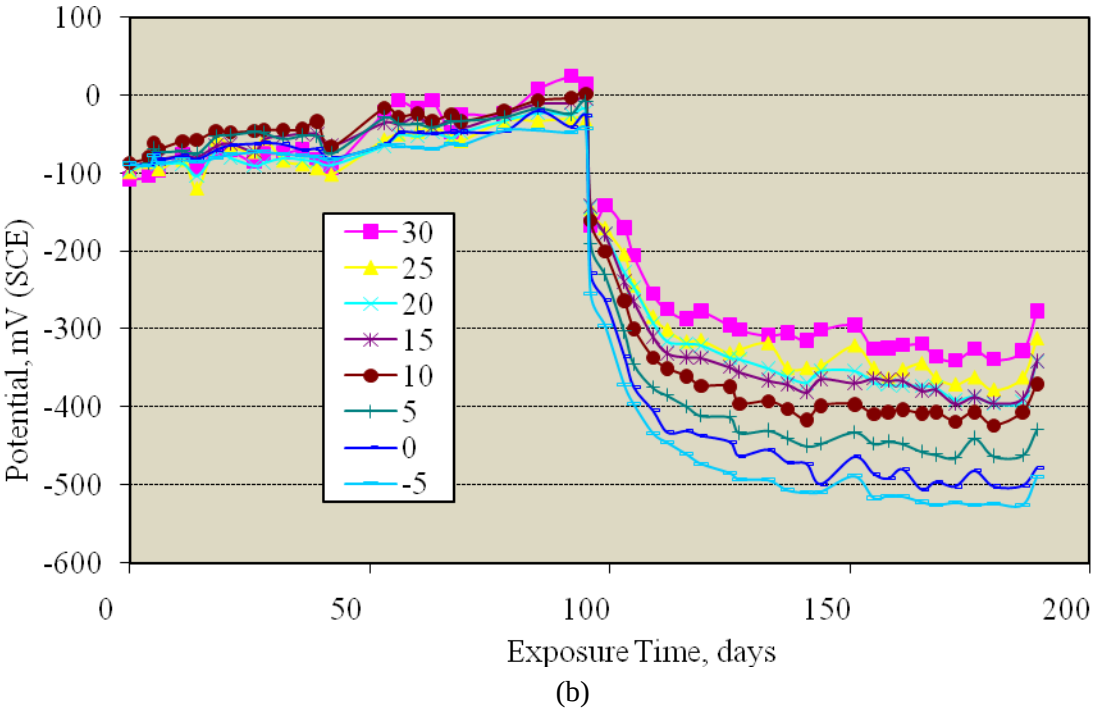

(b)

Figure 38: Potential of the left (a) and right (b) bars of Specimen 1B at different elevations as a function of exposure time (key shows measurement elevations in cm relative to the waterline).

potential increase occurred for the right bar, and potential decreased with time to an apparent steady-state after connection to the submerged bare bar and undergoing a negative potential shift. The latter difference is in spite of each bar being connected to a common submerged bare bar thus indicating distinct current demands in the two cases. Dissection revealed that the right bar had a corrosion spot at an entrapped air void approximately 30 cm above the specimen base, as shown in Figure 39. No corrosion was apparent on the left bar. The latter finding suggests that the constant potential for this bar subsequent to dissection may constitute a quasi plateau, as discussed above for polarized MD2 specimens.

Figure 39: Photograph showing corrosion (circled area) at an air void 26 cm above the specimen base on the right bar of specimen 1B.

Figure 40 provides the potential versus time results for Specimen 2A. Here, potential was relatively constant initially except for an unexplained momentary positive excursion of the left bar just prior to connecting to the bare bar. Subsequent to the negative shift as a consequence of connection, potential decreased gradually with time for both bars to an apparent steady-state. The last readings at the lowest elevation were -634 mV_{SCE} for the left bar and -644 mV_{SCE} for the right. Figure 41 shows a photograph of both bars upon dissection and reveals modest corrosion at locations above the waterline (28.5 cm from the specimen bottom for the left bar and 37 cm for the right).

Potential is plotted versus time for Specimen 2B in Figure 42. For both bars, the pre-connection potential was approximately constant with time. Subsequent to the negative potential shift upon

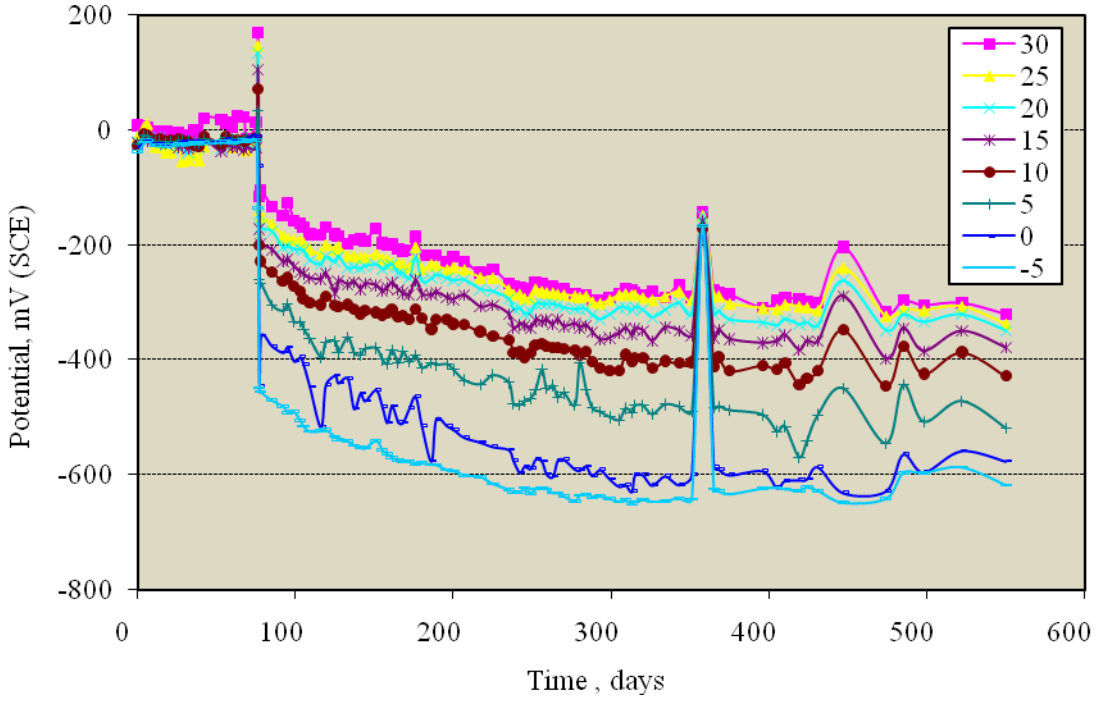

(a)

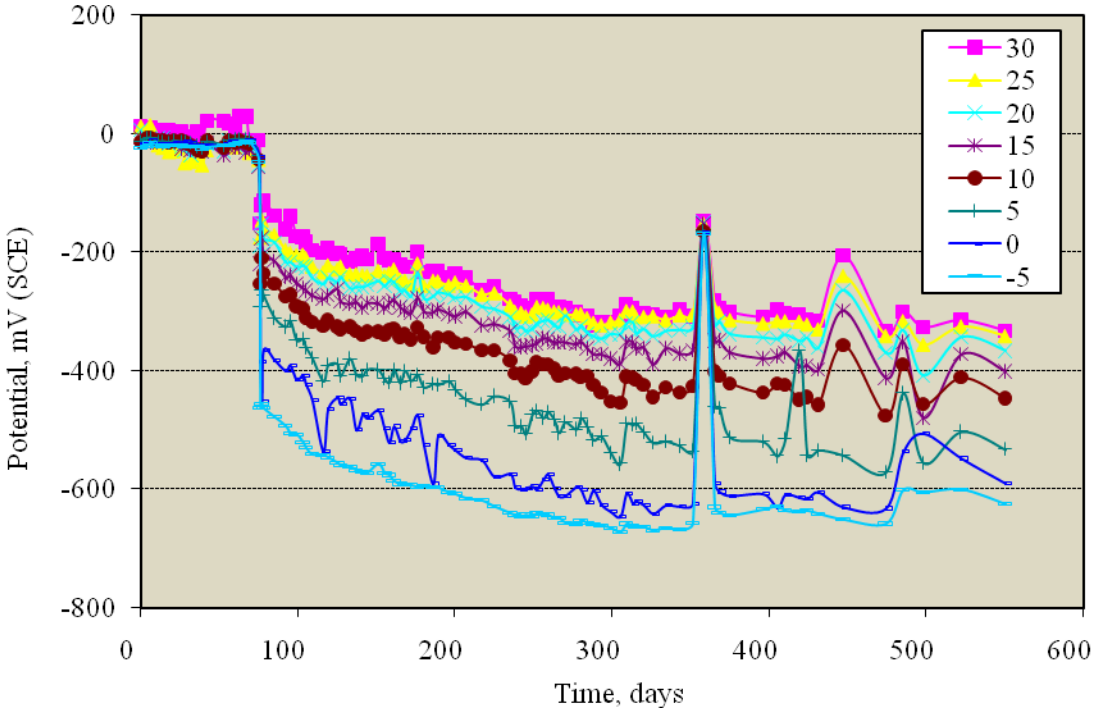

(b)

Figure 40: Potential of the left (a) and right (b) bars of Specimen 2A at different elevations as a function of exposure time (key shows measurement elevations in cm relative to the waterline).

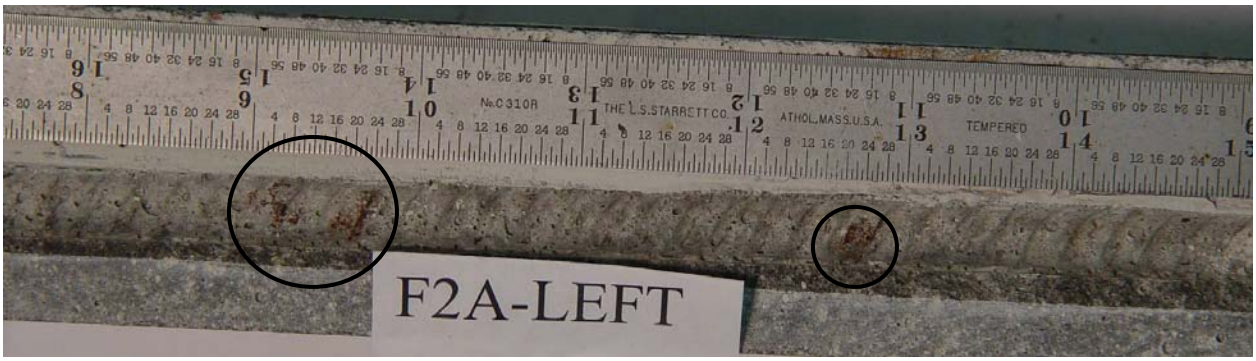

(a)

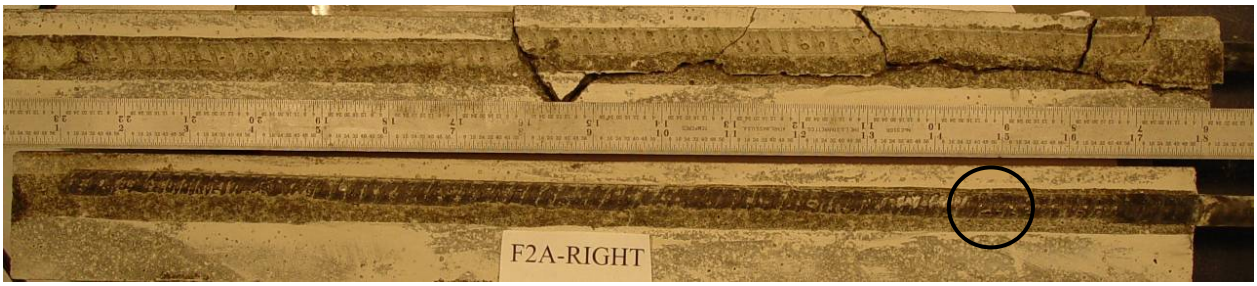

(b)

Figure 41: Photograph of corrosion on the left (a) and right (b) bars of Specimen 2A subsequent to dissection (mortar cracks resulted from the dissection process).

connecting to the bare bar, potential decreased with time at a progressively decreasing rate, although it is unclear that a steady-state was reached. Figure 43 shows a faint indication of what may be corrosion initiation near the waterline on the left bar. No corrosion was apparent on the right.

Lastly, Figure 44 shows the potential versus time record for Specimen 4B. For both bars, this is characterized by a relatively large positive potential increase with time in the pre-connection regime; and a gradual, near linear potential decrease with time subsequent to connection and the accompanying negative potential shift. Figure 45 is a photograph of the left bar and reveals light corrosion products near the bar end. There was no indication that corrosion had initiated on the right bar.

As for the polarized MD2 specimens, current subsequent to connection to bare submerged steel was monitored for MD1 counterparts also. Two general current versus time trends were apparent, one of which involved an initial plateau followed by a current decrease to a steady-state value similar to that reported above for MD2 specimens. Figure 46 shows an example of this for the right bar of Specimen 1A, although in this specific case (the only one of its kind) it is unclear that a steady-state was reached.

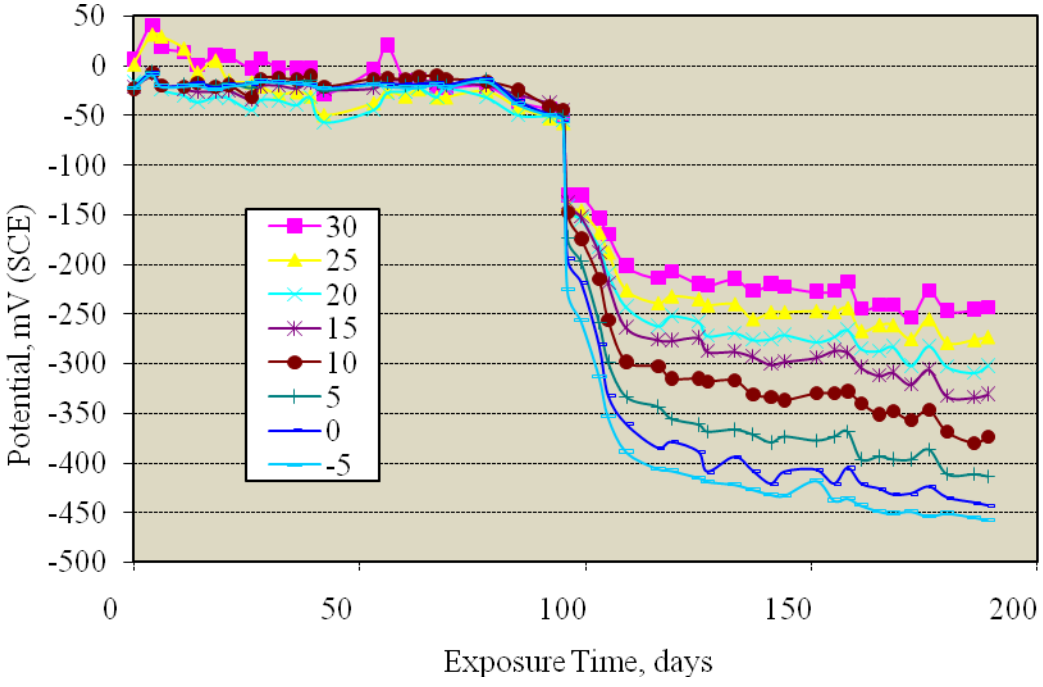

(a)

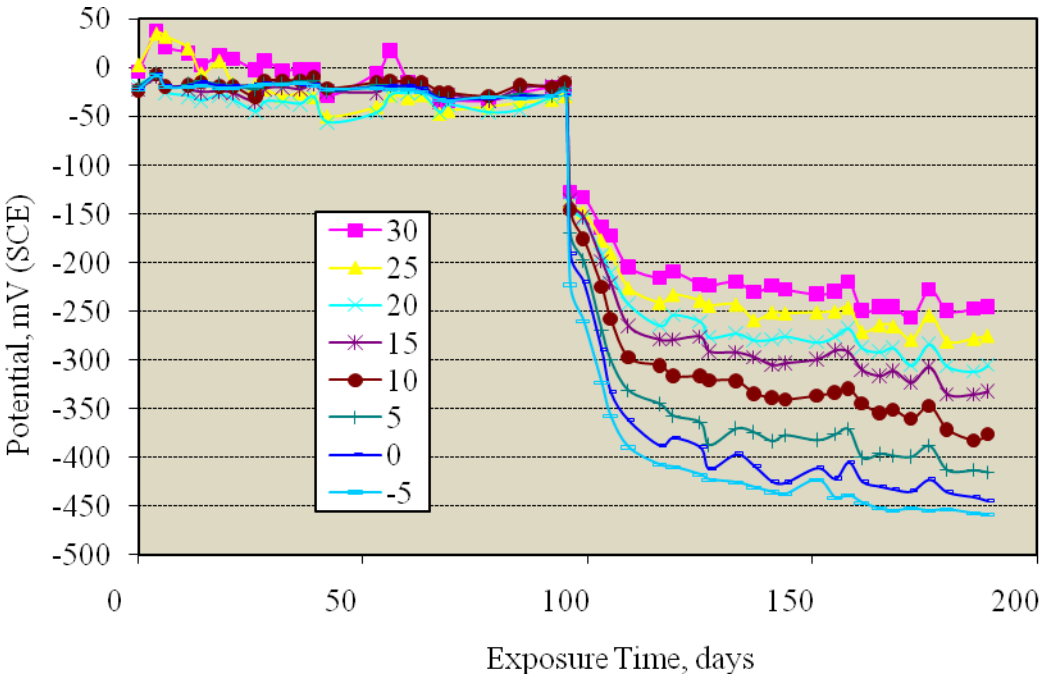

(b)

Figure 42: Potential of the left (a) and right (b) bars of Specimen 2B at different elevations as a function of exposure time (key shows measurement elevations in cm relative to the waterline).

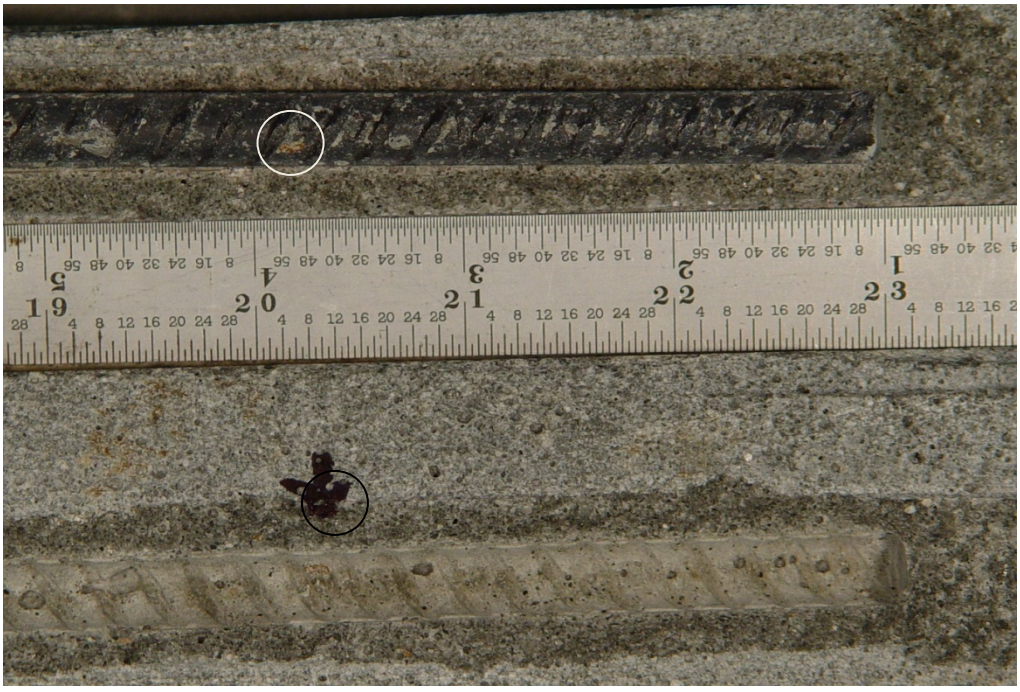

Figure 43: Corrosion spot (circled area) on the left bar of specimen 2B.

The other trend was one where current remained generally constant with time. Figure 47 plots current versus time for the left bar of the above specimen and exemplifies this behavior. Table 14 summarized these results. No explanation is apparent for why current was constant (C) in some cases and decreased with time (D) in others, even for bars in the same specimen. Also, it is unclear why current for Specimen 2A was so much greater than for the others (this specimen remains under test). With the possible exception of Specimen 2B, for which corrosion initiation is uncertain, it was the bar with the most negative final potential that exhibited corrosion.

In summary, corrosion occurred on four of the eight MD1 specimen bars that have been dissected, and the extent of this was modest in all cases. Table 15 lists T_i data for these, assuming that initiation occurred just prior to test termination in the case of specimens that showed corrosion activity; that is, $T_i = T_d$. Likewise, Figure 48 shows a Weibull cumulative distribution function plot of these T_i in comparison to results for polarized MD2 specimens (Figure 35). Only four data points are shown for the MD1 data corresponding to specimens that initiated corrosion. The software (Winsmith™) does not plot runouts but does take these into account in generating the best fit line. The data indicate that the mean T_i for the polarized MD1 specimens exceeded that of the MD2 by a factor of 1.9.

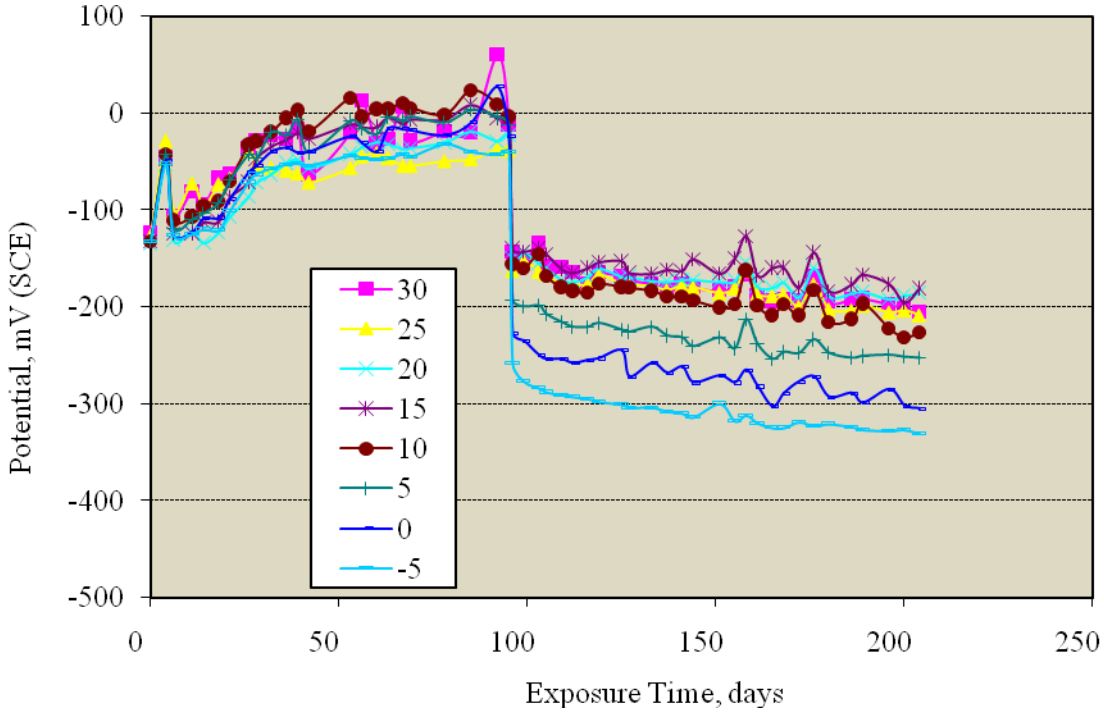

(a)

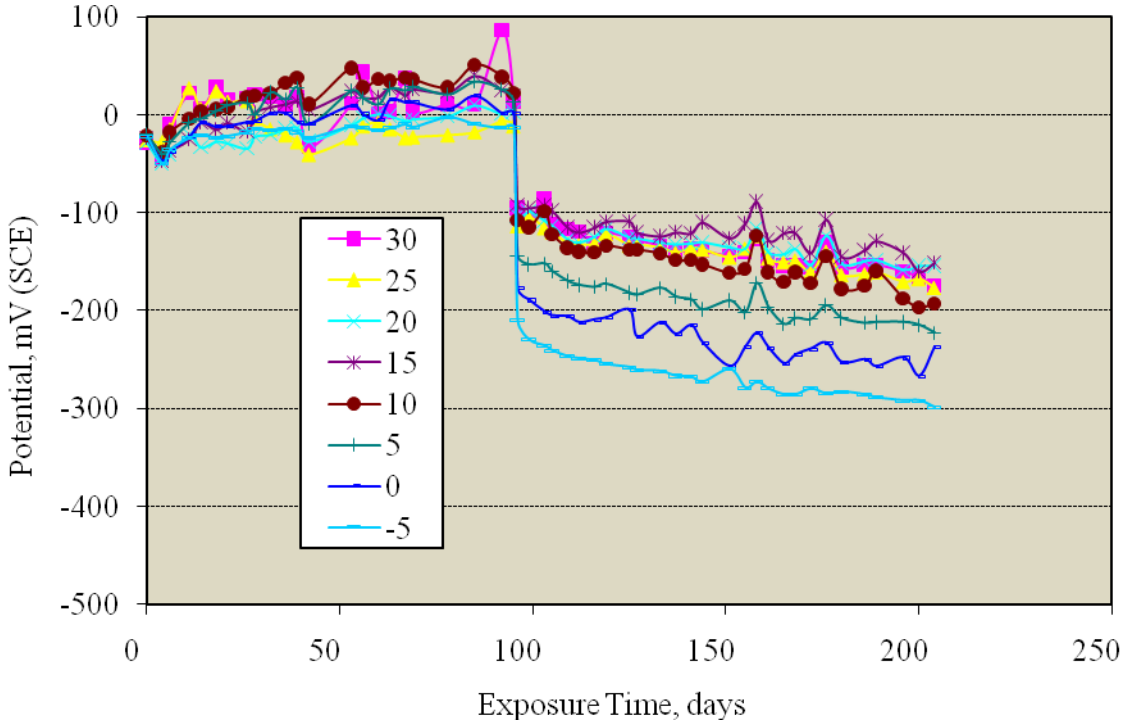

(b)

Figure 44: Potential of the left (a) and right (b) bars of Specimen 4B at different elevations as a function of exposure time (key shows measurement elevations in cm relative to the waterline).

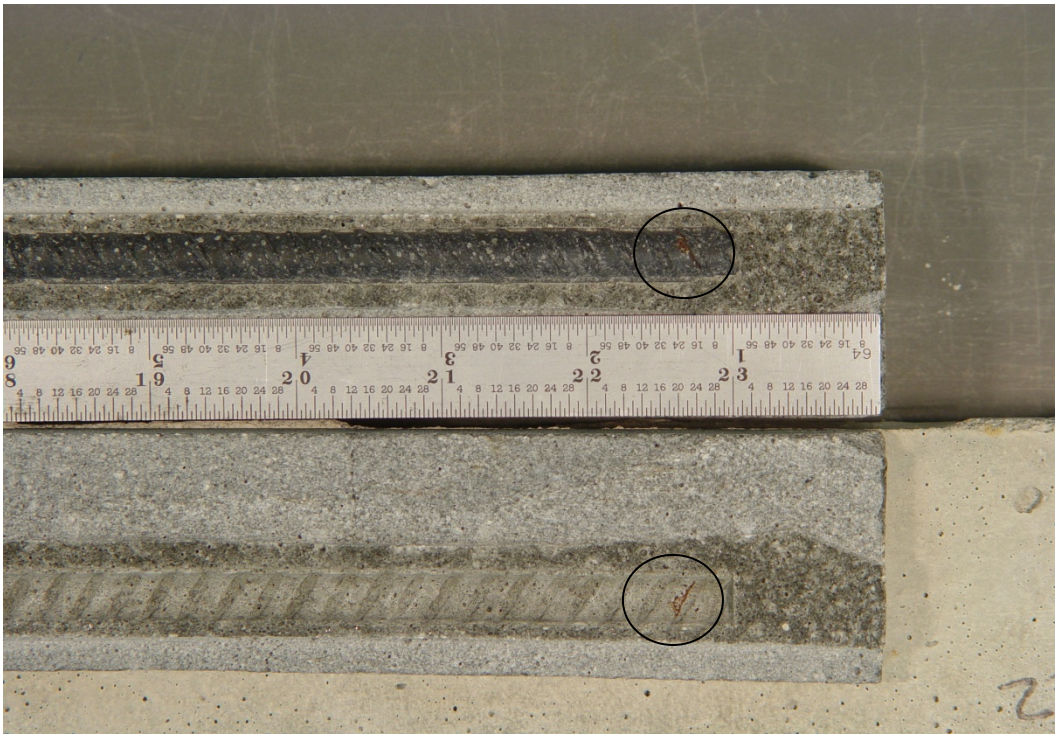

Figure 45: Corrosion spot (circled area) on the left bar of specimen 4B.

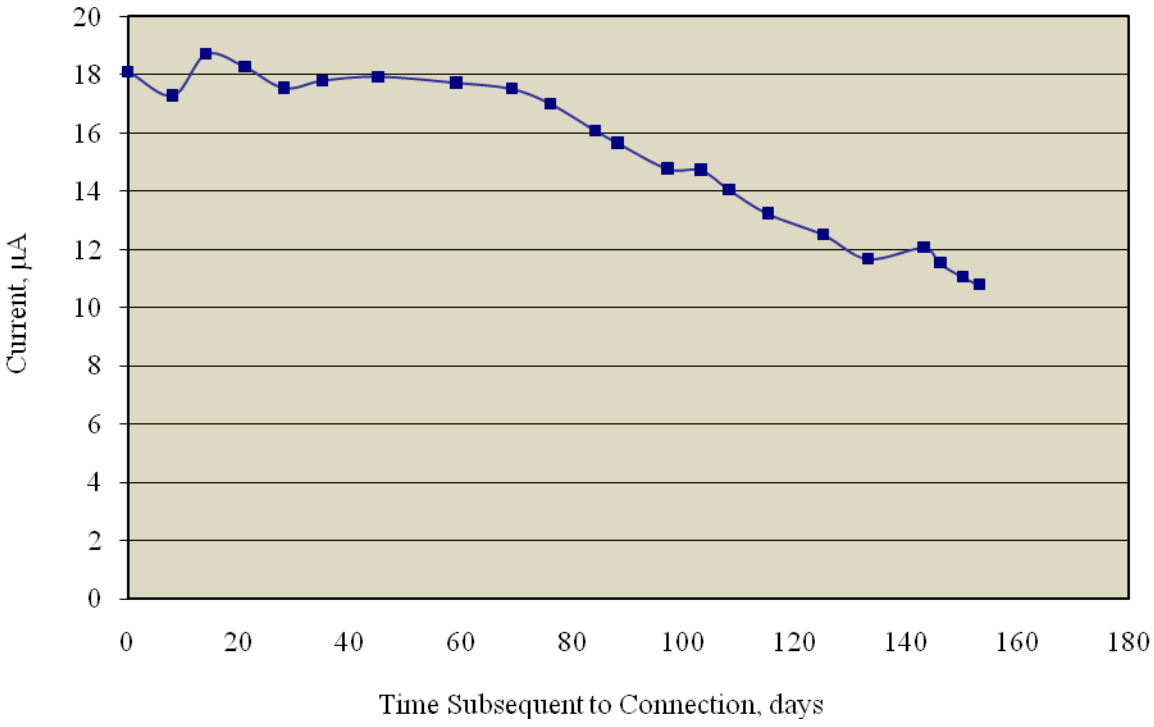

Figure 46: Plot of current versus time subsequent to connection for the right bar of Specimen 1A.

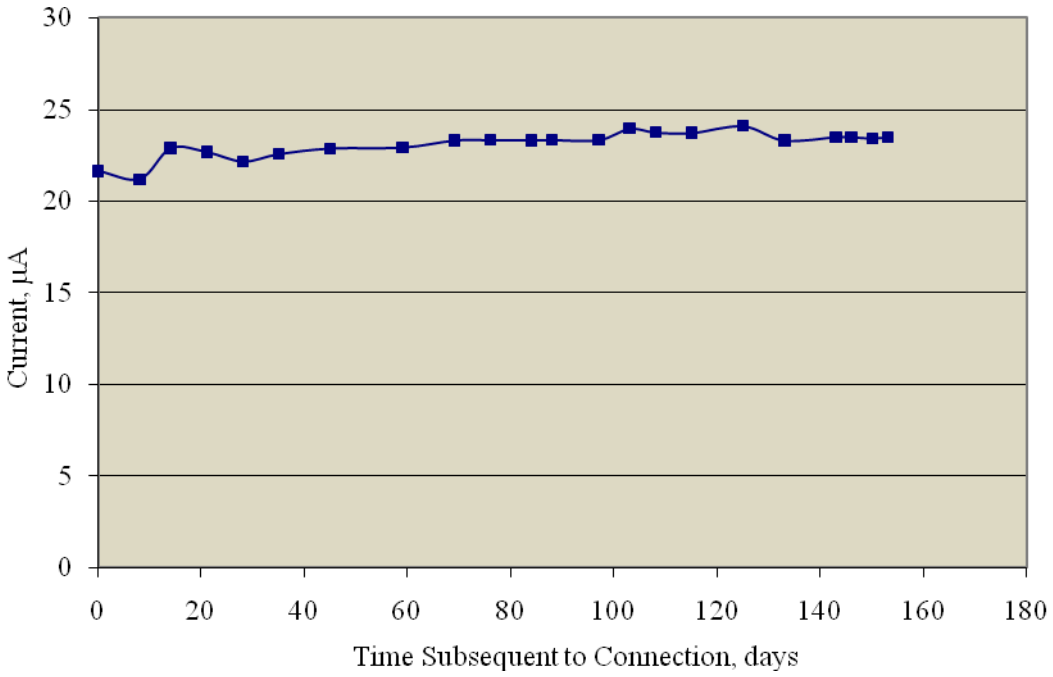

Figure 47: Plot of current versus time subsequent to connection for the left bar of Specimen 1A.

Table 14: Current and related potential data for polarized MD1 specimens.

Specimen Number	Bar	Initial Current, µA	Post-Connection Current Trend*	Steady-State Current, µA	Final Polarized Potential (Lowest Elevation), mV_{SCE}	Corrosion
1A	L	22	C	23	-334	No
	R	18	D	11	-518	Yes
1B	L	18	C	17	-386	No
	R	19	D	9	-525	Yes
2A	L	74	D	42	-625	Yes
	R	75	D	36	-618	Yes
2B	L	21	D	12	-458	Yes(?)
	R	24	D	13	-459	No
4B	L	19	C	22	-331	Yes
	R	22	C	24	-299	No

*C: Current was constant with time initially.
D: Current decreased with time subsequent to connection to the bare bar.

Table 15: Time-to-corrosion of polarized MD1 specimens.

Specimen Number	Bar	Time-to-Corrosion, days
1A	L	>252
	R	245
1B	L	>185
	R	185
2A	L	550
	R	550
2B	L	190
	R	>190
4B	L	204
	R	>204

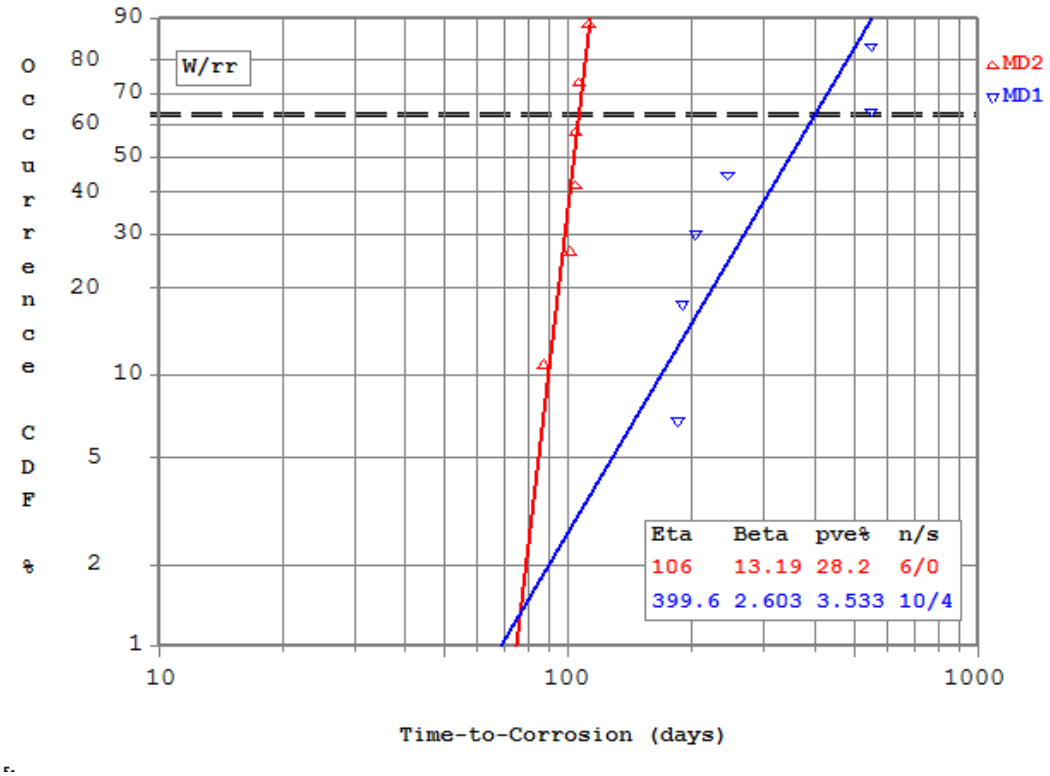

Figure 48: Weibull cumulative distribution function plot of T_i for polarized MD1 specimens compared to MD2.

Influence of Potential on Time-to-Corrosion

Figure 49 provides a plot of T_i for all specimens, as recorded in the respective tables above, versus

potential at the activation site just prior to corrosion initiation. Data for the MD2 mix specimens (solid points) conform to a trend where polarization from coupling to the submerged bare bar extended T_i; however, such a correlation is obscure for the MD1 case due, at least in part, to data scatter for the unsprayed specimens. Arrows just beneath some of the polarized MD1 specimen data points are intended to indicate that a second bar of each specimen had not activated at the indicated T_i. If testing of these specimens had been continued until the second bar initiated corrosion, this would increase the average T_i for the polarized specimens.

A possible source of error in the above data, in addition to uncertainty in determination of T_i, is that mortar cover may have varied from one bar to the next. To determine if this was the case, cover measurements were made on 11 MD1 and three MD2 specimens subsequent to dissection. Table 16 shows the results of this and indicates an average cover for MD1 specimens as 7.8 mm and for MD2 11.2 mm with standard deviations of 1.2 and 0.7 mm, respectively. The larger ratio of standard deviation to average cover for the MD1 compared to MD2 specimens is consistent with the greater scatter in T_i data for the former (Figure 48).

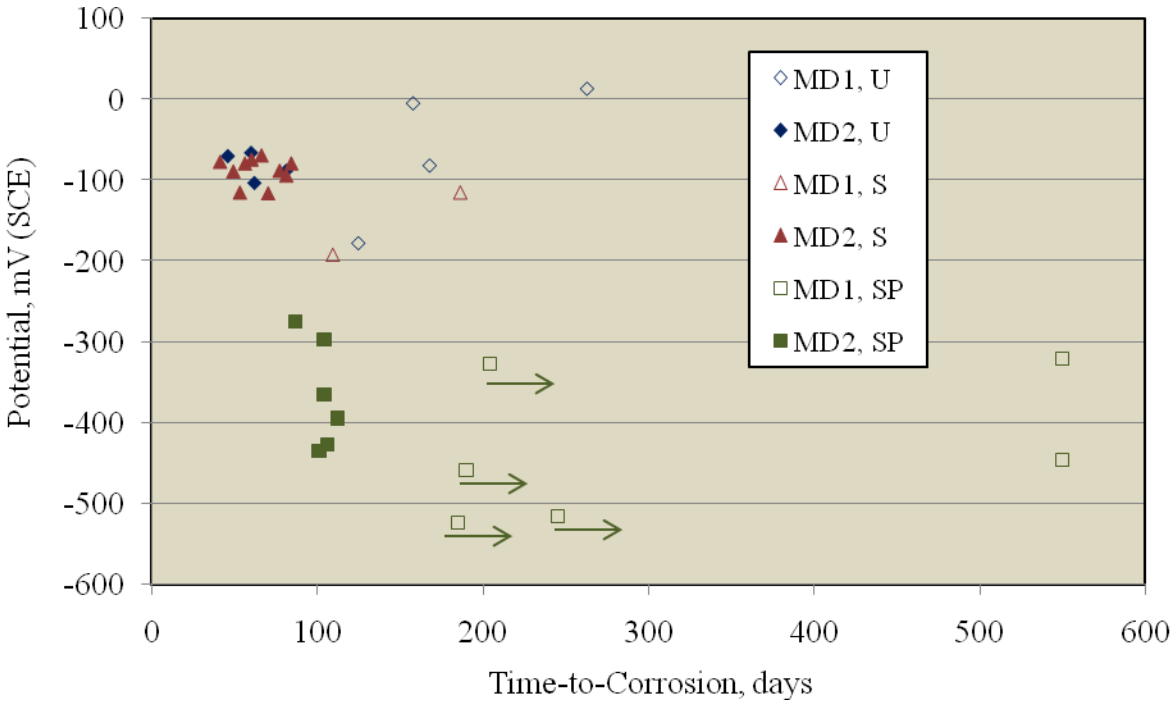

Figure 49: Plot of time-to-corrosion as a function of potential just prior to activation (U – unsprayed, S – sprayed, SP – sprayed and polarized).

Table 16: Listing of cover measurements for various bars.

	Specimen Number/Bar	Cover, mm
MD1	1A/L	8.9
	1A/R	8.4
	1B/R	6.5
	2B/L	7.1
	2B/R	9.8
	4B/L	8.2
	4B/R	7.7
	5A/L	8.7
	5A/R	7.1
	5B/L	5.3
	5B/R	8.3
	Average/Standard Deviation	7.8/1.2
MD2	9A/L	11.2
	10B/L	10.4
	10B/R	11.8
	Average/Standard Deviation	11.2/0.7

Specimen Design Commentary and Depolarization Testing

On the basis of the above, it was reasoned that corrosion behavior of the presently configured, polarized and sprayed specimens provides an improved simulation of actual marine pilings compared to previously employed unsprayed, unpolarized designs. In the future, it is recommended that connection of specimen bars to bare submerged steel be affected upon first exposure or shortly thereafter, as this should enhance the likelihood that corrosion initiates in the splash zone. However, a shortcoming of this approach arises with regard to defining the time at which corrosion initiates since, unlike unpolarized specimens, onset of active corrosion is not necessarily accompanied by a distinctive potential shift. On the other hand, the potential-time data for freely corroding (unpolarized) MD1 specimens often failed to provide a clear indication of T_i. Development of a larger corrosion size versus $T_d - T_i$ database and refinement of the approach to determining corrosion size may overcome this, as noted above. As an alternate possibility, a complementary approach was considered where specimens were individually disconnected from the submerged bare steel bar during exposure for up to 24 hours; and the magnitude of potential increase (specimen depolarization) was measured. The rationale behind this is that potential decay should occur to a greater extent for passive compared to active steel, since corrosion potential for the former is expected to be more positive than for the latter. Figure 50 shows a typical example of depolarization at various elevations and times subsequent to disconnection from the submerged bare bar.

Likewise, Figure 51 plots the magnitude of depolarization after one hour of disconnection as a function of elevation. In all cases, depolarization was conducted shortly before dissection. Data for rebars that were determined upon dissection to still be passive are shown in blue and ones that exhibited corrosion in red.

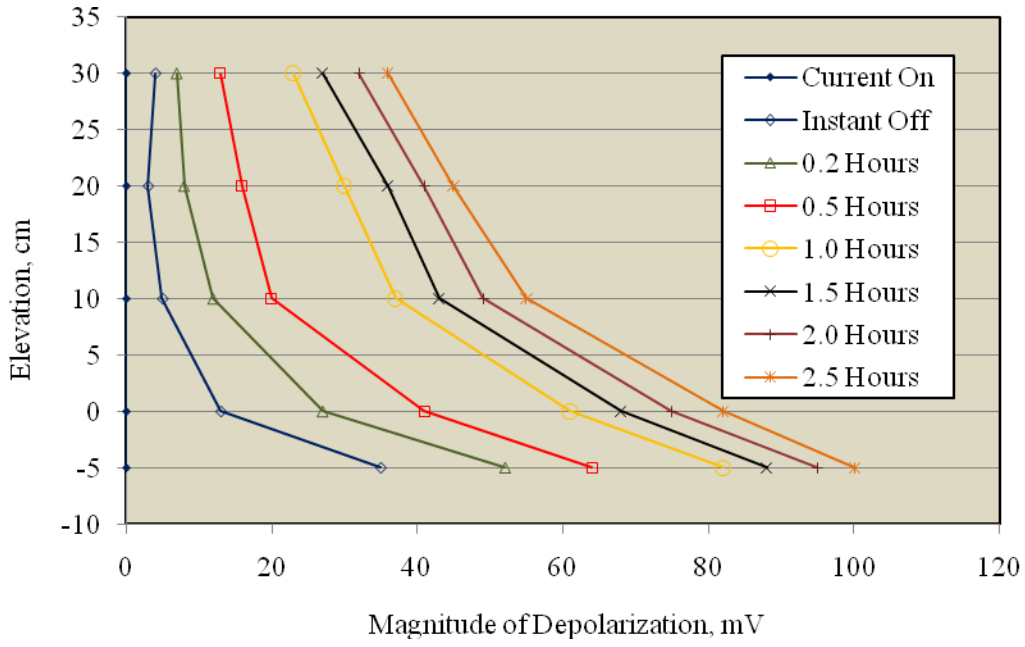

Figure 50: Example of potential versus time depolarized for a typical specimen (left bar Specimen 1A).

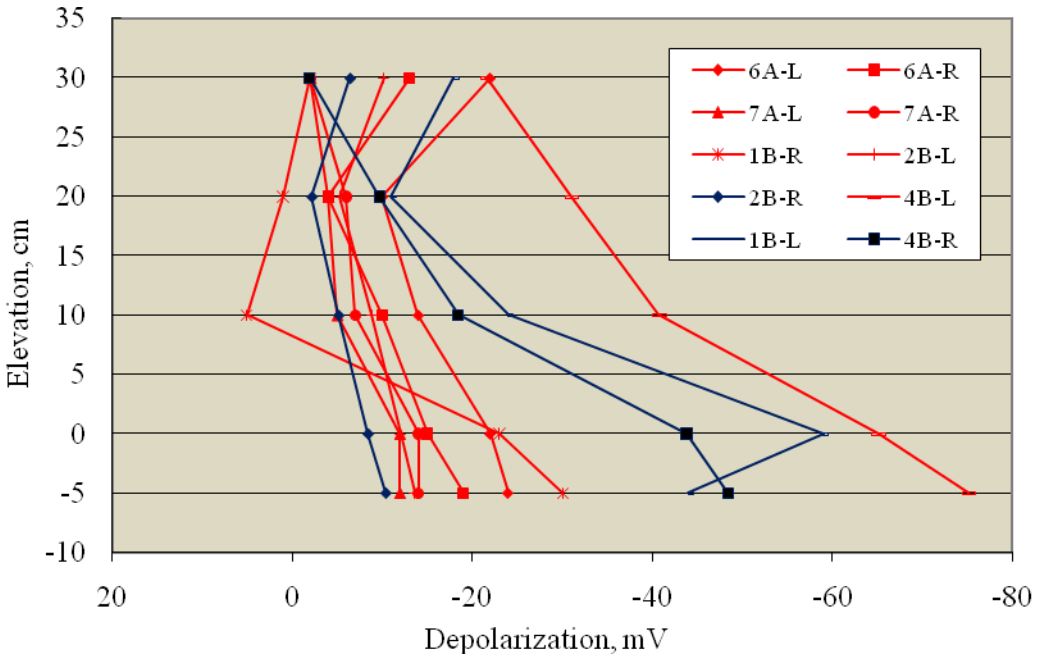

Figure 51: One hour depolarization data as a function of elevation for polarized specimens that were so tested and dissected.

With two exceptions, the depolarization data for the ten specimens correspond to the above projected trend (greater depolarization for still passive bars than active ones). For the active bar exception (left bar of Specimen 4B), the amount of corrosion was small (see Figure 45). For the other exception (right bar of Specimen 2B), it is questionable that corrosion had initiated, as noted above. In this regard, both exceptions are MD1 specimens for which the magnitude of corrosion was small compared to that of the MD2. Possibly, C_T for these was reached; but the incubation period for active corrosion had not yet been realized.

[18] Additional study is needed to clarify the utility of the depolarization method for identifying corrosion initiation in sprayed, polarized specimens.

Comparison with Field Results

Figure 52 shows potential versus elevation data for a typical piling of the Hurricane Pass Bridge near Ft. Myers, FL, as collected at different times.[19] While no polarization resistance measurements were made, the fact that, first, the data were acquired at a relatively early bridge age (commissioning was in 1991) and, second, high performance concrete with silica fume was used, is consistent with bars having been passive and corrosion rate very low. The data indicate that potential at a given elevation was generally similar from one measurement time to the next and was relatively negative at the lower

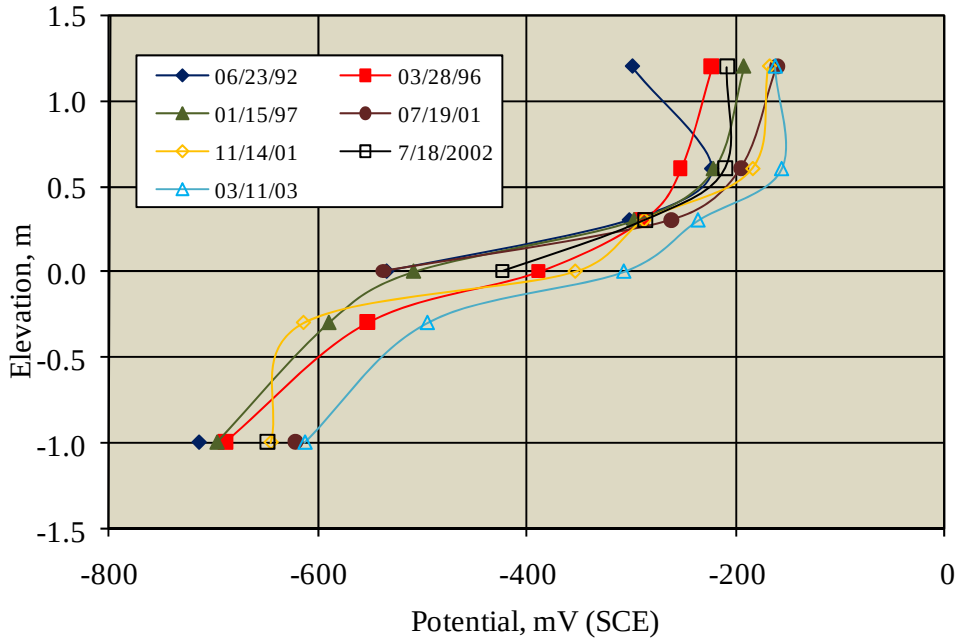

Figure 52: Potential versus elevation data for piling C of bent 4 of the Hurricane Pass Bridge (elevation referenced to mean high tide with data at -1.0 m for reference electrode in the water).

elevations but transitioned to more positive values in the elevation range 0-0.5 m. As such, the potential profiles for the present polarized, simulated piling specimens were generally similar to those for an actual piling (see Figure 23). A distinction, however, is that the potential profile for the present specimens resulted from cathodic polarization via an external source, whereas O_2 depletion in the submerged zone concrete was responsible for the relatively negative potentials at lower elevations in the case of the Hurricane Pass Bridge piling. However, in both cases, cathodic polarization of the splash/spray zone steel, which is the region of interest, resulted; and the source of this polarization should not be relevant.

Chloride Analyses

Chloride concentration determinations were made as a function of elevation on a total of eight bar traces. An additional three specimens were analyzed for $[Cl^-]$ at the corrosion site elevation alone. Figure 53 shows a typical $[Cl^-]$ versus elevation plot, in this case for the right bar of Specimen 6A. Figure 54 provides a photograph of this bar and bar trace after dissection and reveals that corrosion had initiated near the bottom of the bar in the submerged zone 2.5-3.0 cm above the base. This is the same elevation at which the maximum $[Cl^-]$ was measured. Similar plots and companion photographs for the other specimens for which $[Cl^-]$ elevation profiles were made are provided in Appendix F. In all of these cases, corrosion initiated in the submerged zone; and $[Cl^-]$ was greatest on the bar trace at the activation site

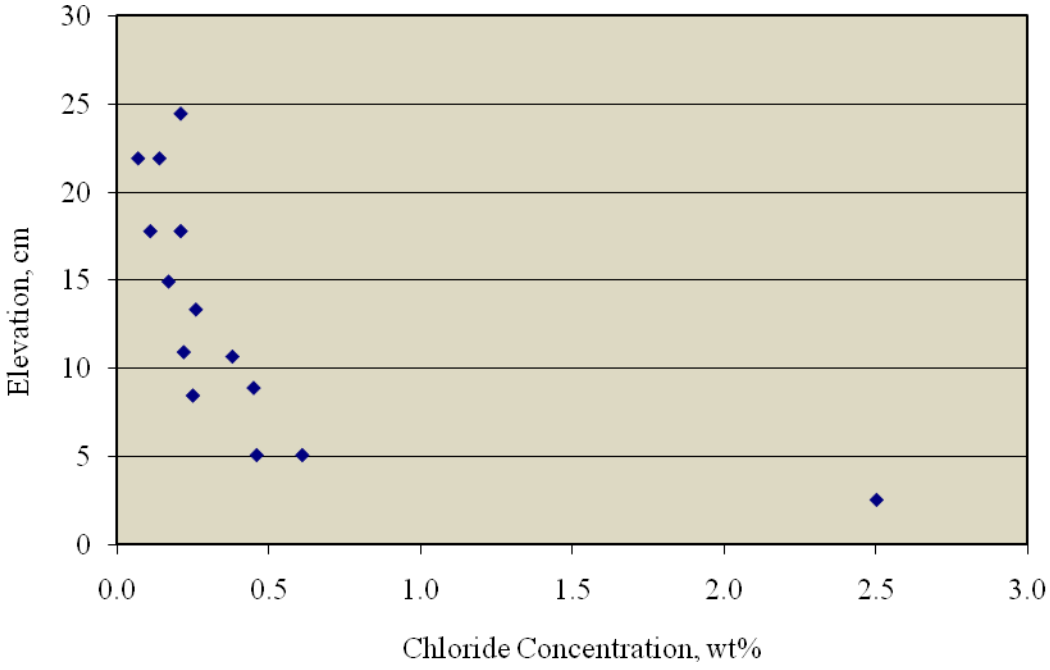

Figure 53: Plot of [Cl^-] versus elevation for the right bar of Specimen 6A.

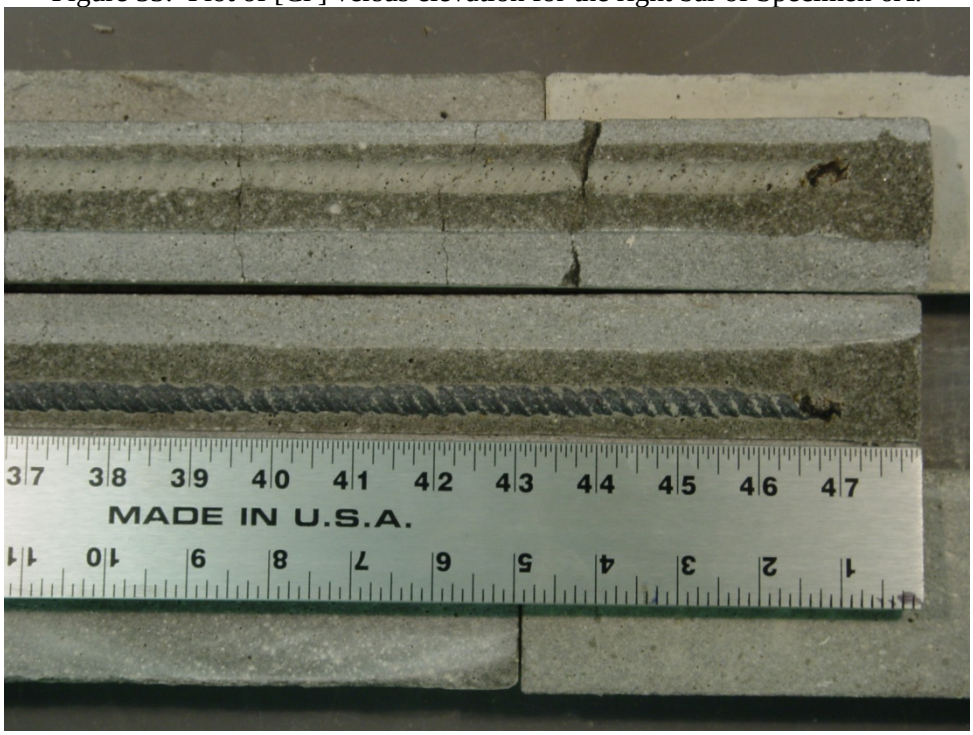

Figure 54: Photograph of the right bar of Specimen 6A.

elevation. Table 17 lists specimen bars and [Cl^-] on the bar trace at the corrosion site elevation, not only for the above specimens but also for ones for which [Cl^-] was measured only at the active site. As an

additional consideration, the major dimension of corrosion on a given bar was measured and plotted versus [Cl^-] at the active site with results being as shown in Figure 55. Irrespective of mix design and

Table 17: Listing of [Cl^-] measurement results at corrosion sites.

Specimen Number/Bar	Exposure*	T_i, days	[Cl^-], wt%
2B/L	SP	190	0.8
3B/L	S	109	5.6
3B/R	S	**	1.9
6A/R	SP	112	2.5
6B/R	S	70	1.9
7A/L	SP	101	6.0
8A/L	U	81	1.5
8B/R	S	81	2.3
9A/R	U	65	1.5
9B/R	S	87	1.1
10A/L	SP	104	3.3

* S-sprayed, SP-sprayed and polarized, U-neither sprayed or polarized.
** Corrosion initiated at an air void.

type of exposure, the data conform to a linear trend of increasing [Cl^-] with increasing size of the corrosion with a vertical intercept, which represents C_T, of 0.71 wt% Cl^- (R^2 for the best fit line is 0.92). This implies that, first, electromigration of chlorides to the active site occurred subsequent to initiation and, second, C_T was either approximately the same irrespective of type of mix or exposure or that data scatter exceeded the difference between these. Electromigration of chlorides may also have contributed to the relatively high C_T for simulated piling specimens reported by Spellman and Stratfull et al.[10] as discussed earlier. Unlike the calculation of T_i which utilized the spread dimension of corrosion, the major dimension was employed for the Figure 54 data considering that the extent of Cl^- electromigration should be proportional to this irrespective of whether or not multiple initiation sites were involved.

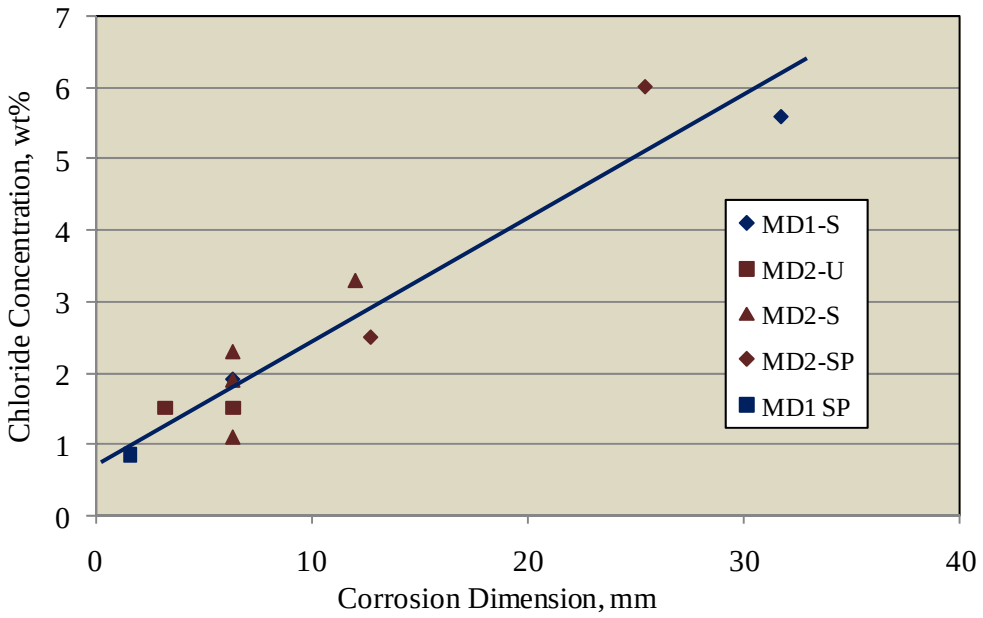

Figure 55: Plot of [Cl^-] at locations of corrosion versus major dimension of the corrosion.

It is now recognized that [Cl^-] at activation sites is normally higher than elsewhere along the reinforcement at the same time.[2] This was confirmed in the present cases, as noted by the data in Figure 53 and Appendix F. For this reason, [Cl^-] data other than at the active site were also analyzed, since these values should be more typically found upon random sampling. Table 18 lists the submerged zone data for the eight bars for which [Cl^-] profiles were determined. Based upon T_i for each bar and the time at which testing of individual specimens was terminated, T_d, [Cl^-] at T_i was back calculated using the one dimensional solution to Fick's second law assuming a constant surface [Cl^-] of 2.80 wt%. The procedure involved inputting the average measured [Cl^-] in the submerged zone at T_d and calculating the effective Cl^- diffusion coefficient, D_{eff} for each specimen. A source of error in this approach is that the bar obstruction effect is ignored;[20] and because of this phenomenon, diffusion is actually in two, rather than one, dimensions. A second calculation then utilized this D_{eff} and T_i to calculate [Cl^-] at the time of corrosion initiation for each bar. Table 19 presents results of these calculations. The average D_{eff} and C_T are $4.29 \cdot 10^{-12}$ m^2/s and 0.34 wt%, respectively, for MD2 specimens and for MD1 $2.70 \cdot 10^{-12}$ m^2/s and >0.28 wt%. The C_T for MD2 specimens (0.34 wt%) determined from these calculations is 52 percent below that determined from the active site extrapolation (0.71 wt%, Figure 55). This higher C_T determined from data acquired at the active site compared to the average value elsewhere along bars could have resulted from a relatively low local aggregate amount along the Cl^- diffusion path.[9] X-ray penetration depth into the mortar bar trace was estimated to be about 3 μm; and consequently, the above concentrations are considered to be on a cement weight basis.

Table 18: Submerged zone [Cl^-] other than at the active site.

	Specimen/Bar							
	3B/L	3B/R*	6A/R	6B/R	8A/L	8B/R	9A/R	9B/R
Chloride Concentration, wt%	0.30	0.20	0.46	0.36	0.22	0.53	0.52	0.32
	1.00	0.13	0.61	0.52	0.49	0.36	0.38	0.61
	0.30	0.24	0.25	0.38	0.48	0.34	-	0.19
	0.53	0.17	0.45	0.23	0.45	0.40	-	-
	-	0.28	-	-	0.29	-	-	-
	-	0.19	-	-	0.30	-	-	-
	-	0.19	-	-		-	-	-
	-	0.18	-	-	-	-	-	-

* Initiation occurred at an air void 30 cm above the specimen base.
No corrosion in the submerged zone.

Table 19: Data related to calculation of C_T in the submerged zone from the measured [Cl^-] other than at the active site.

Specimen/Bar	Measured [Cl^-], wt%	Calculated C_T, wt%	D_{eff}, m^2/s	T_i, days	T_d, days
3B/L	0.53	-	3.53E-12	-	137
	-	0.35	3.53E-12	109	-
3B/R*	0.20	>0.20	1.87E-12	>137	137
6A/R	0.44	-	2.73E-12	-	153
	-	0.29	2.73E-12	112	-
6B/R	0.37	-	4.55E-12	-	81
	-	0.34	4.55E-12	70	-
8A/L	0.37	-	3.91E-12	-	94
	-	0.32	3.91E-12	81	-
8B/R	0.41	-	4.20E-12	-	94
	-	0.33	4.20E-12	81	-
9A/R	0.45	-	6.42E-12	-	66
	-	0.45	6.42E-12	65	-
9B/R	0.37	-	3.91E-12	-	94
	-	0.33	3.91E-12	87	-

* Initiation occurred at an air void 30 cm above the specimen base.
No corrosion in the submerged zone.

Several specimens were found to have initiated corrosion above the waterline. Table 20 lists these and provides relevant information for each, including [Cl^-] at the corrosion site in cases where analyses were performed. All of these specimens are of the MD1 mix design. Equipment problems and staff illness resulted in [Cl^-] being measured on only two of these specimens, and these were ones for which

corrosion initiated at an entrapped air void. In view of this limitation, an attempt was made to relate the above waterline [Cl^-] data from specimens for which such analyses were performed to corrosion of the specimens listed in Table 20. Table 21 shows these data according to the elevation range 11-15 cm and Table 22 to 16-25 cm. These results were presented graphically in the [Cl^-] versus elevation plots in Figure 53 and Appendix F. The average [Cl^-] in the 11-15 cm elevation range for the two MD1 specimens is 0.25 wt% and for the four MD2 specimens that were sprayed 0.23 wt%. For the 16-25 cm range these averages are 0.21 and 0.17 wt%, respectively. As such, the average [Cl^-] at the lower elevation range exceeds that for the higher. This difference is thought to be real because of the systematic decrease in [Cl^-] with increasing elevation above the waterline as shown in Figure 53 and Appendix F. That the measured [Cl^-] for the two mix types are so close despite the difference in mix designs was

Table 20: Listing of specimens and information for which corrosion initiated above the waterline.

Specimen/ Bar	Exposure[+]	T_i, days	Elevation of Corrosion Relative to Specimen Base, cm	Photo of Corrosion	Measured [Cl^-] at Corrosion Site) , wt%
1A/R	SP	245	20	Figure 40	-
1B/R	SP	185	26*	Figure 42	5.2
2A/L	SP	550	9-15	Figure 41	-
2A/R	SP	550	26		-
3A/L	U	326	20	Figure 21	-
3B/R	S	137	26*	Figure 25	4.7
5A/L	U	168	7-23	Figure 23	-
5A/R	U	125	7.6, 19-21		-
5B/L	S	186	3.5-25.5	Figure 19	-
5B/R	S	186	3.8-23.8		-

[+] -S: Sprayed, P: Polarized, U: Neither sprayed or polarized.

* Corrosion initiated at an air void. For Specimen 3B/R corrosion products extended to the exposed concrete surface.

Table 21: Listing of individual [Cl^-] determinations in the elevation range 11-15 cm for the indicated specimens/bars.

	3B/L	3B/R	6A/R	6B/R	8A/L	8B/R	9A/R	9B/R
[Cl-], wt%	0.42	0.18	0.22	0.23	0.22	0.43	0.29	0.13
	0.18	0.29	0.38	0.29	0.15	0.12	0.29	0.31
	0.25	-	0.26	-	0.28	0.09	0.08	0.19
	0.17	-	0.17	-	-	0.19	-	0.08
	-	-		-	-	0.26	-	0.17
	Average							
	0.26	0.24	0.26	0.26	0.22	0.22	0.22	0.18

Table 22: Listing of individual [Cl^-] determinations in the elevation range 16-25 cm for the indicated specimens/bars.

	3B/L	3B/R	6A/R	6B/R	8A/L	8B/R	9A/R	9B/R
[Cl-], wt%	0.12	0.07	0.11	0.37	-	0.32	0.24	0.24
	0.13	0.18	0.21	0.13	-	0.16	0.15	0.12
	0.15	0.55	0.07	0.03	-	0.12	0.26	0.20
	0.22	0.18	0.14	0.34	-	-	-	0.12
	-	-	0.21	0.31	-	-	-	0.02
	-	-	-	0.11	-	-	-	-
	-	-	-	0.08	-	-	-	-
	Average							
	0.16	0.25	0.15	0.20	-	0.20	0.22	0.14

presumably a consequence of the cover distinction (8 mm for MD1 and 12 mm for MD2). Figures 56 and 57 plot the measured [Cl^-] (Tables 21 and 22) versus T_d for the 11-15 and 16-25 cm elevation ranges, respectively. Results for MD2 specimens are plotted as well. Also included is a curve based upon the one dimensional solution to Fick's second law that passes through the origin ([Cl^-] = 0 at T = 0) and the average [Cl^-] at T_d for the two MD1 specimens, although above waterline corrosion had not initiated for one of these (Specimen 3B/L). Next, [Cl^-] on the error function curve (solution to Fick's second law) corresponding to the respective T_i for the MD1 specimens that exhibited above waterline corrosion initiation (Table 20) was identified and assumed to represent C_T. These values for the respective specimens are listed in Table 23. Figure 58 provides a plot of the two error function curves from Figures 56 and 57 along with the C_T data from Table 23. This constitutes a graphical representation of these results and of the range of values likely to be encountered. In general, specimens that initiated corrosion at an entrapped air void tended to have lower C_T and T_i and polarized specimens tended to have higher. Figure 59 provides an alternative representation as a plot of these C_T as a function of potential just prior to activation. Here, the two lowest C_T data are for cases where corrosion initiated at an entrapped air void.

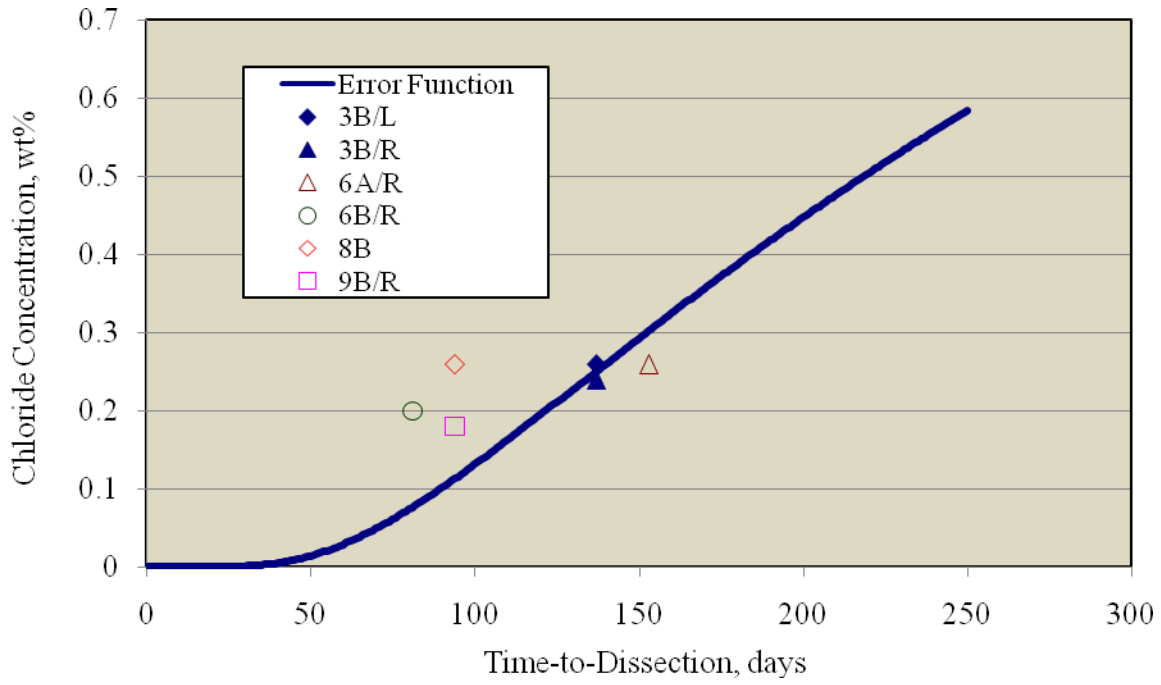

Figure 56: Plot of calculated [Cl^-] versus T_d for the elevation range 11-15 cm.

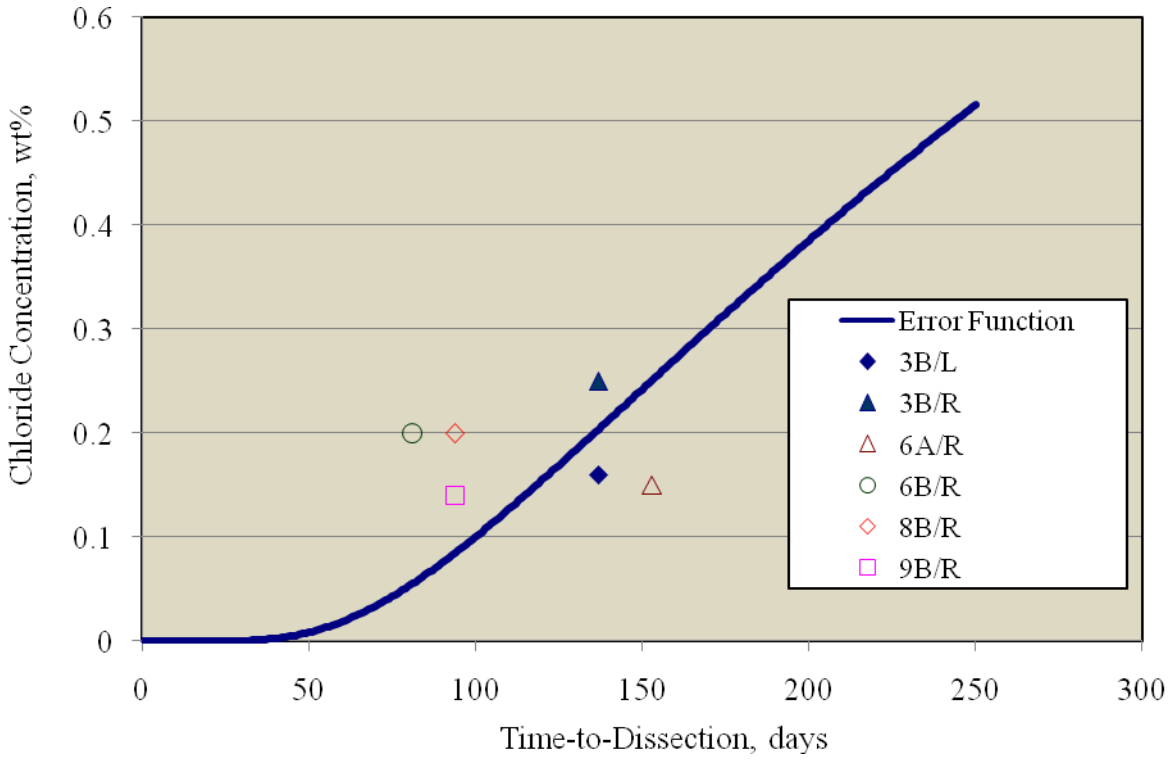

Figure 57: Plot of calculated [Cl^-] versus T_d for the elevation range 16-25 cm.

Table 23: Projected C_T for specimens that exhibited above waterline corrosion initiation.

Specimen/ Bar	Exposure*	Elevation of Corrosion Relative to Specimen Base, cm	T_i, days	C_T (projected), wt%	
				11-15 cm	16-25 cm
1A/R	SP	20	245	-	0.50
1B/R	SP	26^+	185	-	0.34
3B/R	S	26^+	137	-	0.20
5B/L	S	3.5-25.5	186	0.41	0.35
5B/R	S	3.8-23.8	186	0.42	0.35

* Corrosion initiation at an air void.

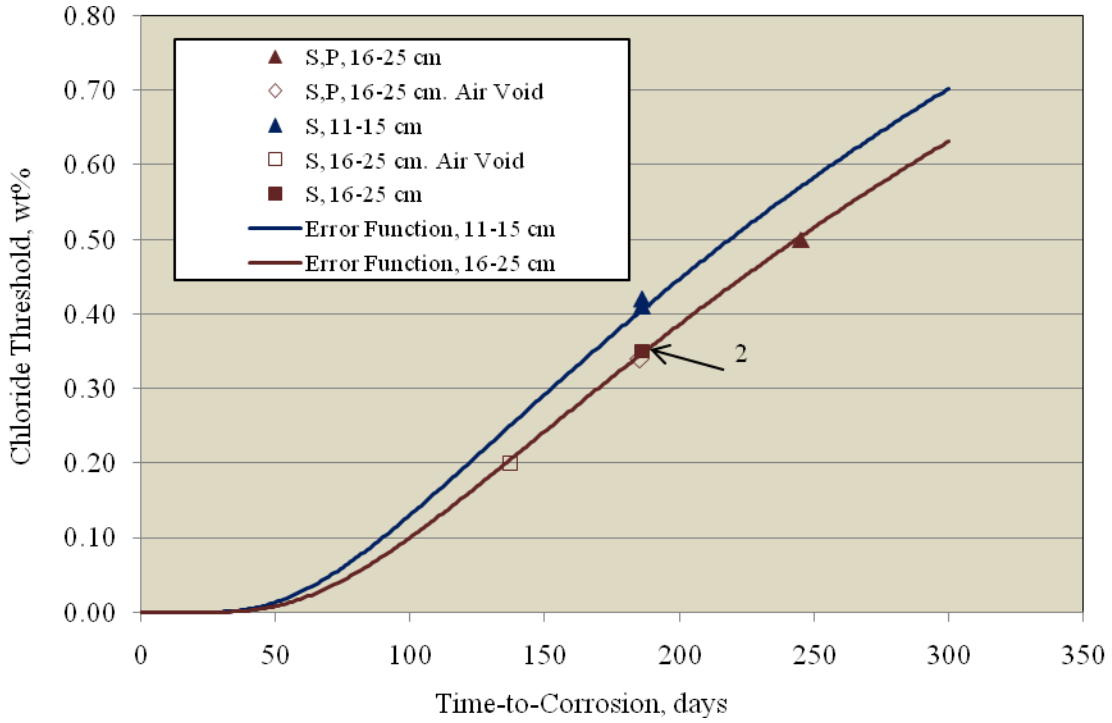

Figure 58: Plot of the error function curves from Figures 55 and 56 with the projected C_T at the respective T_i for MD1 specimens that exhibited above waterline corrosion.

Although the data are limited and considering that instances where corrosion initiated at an air void conform to a separate population, a trend of increasing C_T with decreasing potential is apparent as reported previously by others.[11,12,13]

The extent of polarization above the waterline by a submerged anode is controlled by concrete resistance, all other factors being maintained constant. As an approximation, resistance to current flow from a submerged source to the outward face of an above-waterline rebar should decrease linearly with

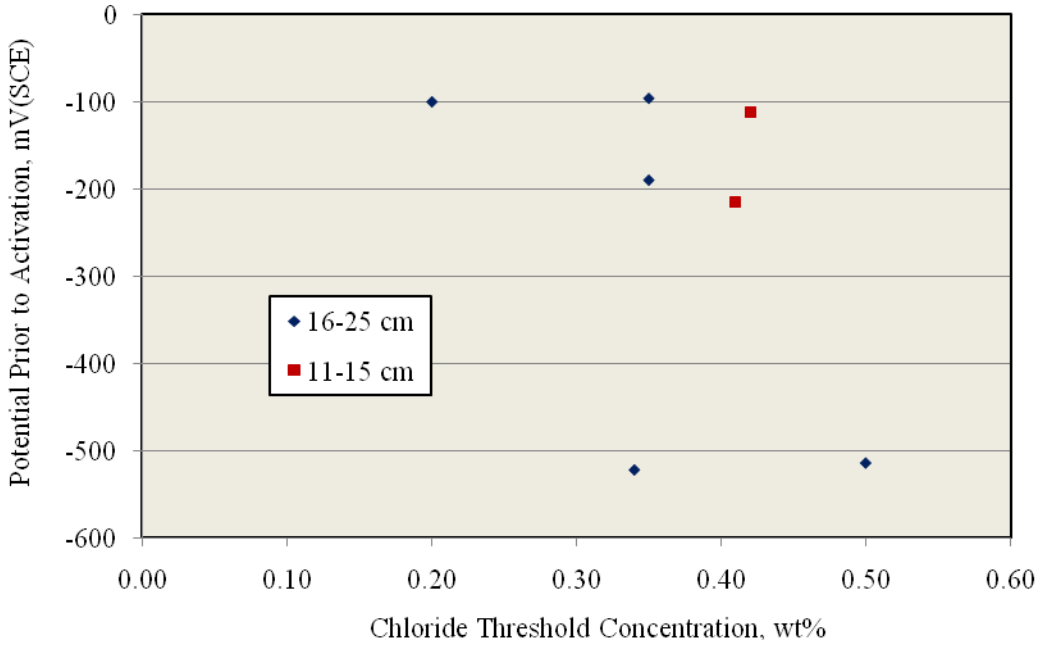

Figure 59: Plot of C_T versus potential of individual rebars just prior to corrosion activation.

increasing concrete cover. On this basis, the elevation on a structures with rebar covers in the range 25.4 to 10.16 cm (1.00 to 4.00 in.) which are estimated to polarize comparably to a present specimen with cover 8.0 mm was estimated from the expression,

$$HoP_{str} = Elev_{spec} \cdot (Cover_{str})/(Cover_{spec}), \quad (2$$

where HoP_{str} is the projected above-waterline elevation on a structure which polarizes the same as at specimen elevation $Elev_{spec}$ and $Cover_{str}$ and $Cover_{spec}$ are covers on the structure and specimen, respectively. Figure 60 provides a plot of the equivalent elevation above the waterline on an actual substructure element as a function of the concrete cover to which each of the two specimen elevation ranges should correspond. Such a representation may underestimate this correspondence since water saturation and, hence, a correspondingly low current demand for reinforcement is expected to extend to a higher elevation the greater the cover and member thickness.

In viewing the data in Table 23 it should be recognized that only three of a total of six bars in specimens that were sprayed and two of eight bars in ones that were sprayed and polarized and which were analyzed for $[Cl^-]$ initiated above waterline corrosion with the other bars having remained passive (runouts). Figure 61 presents a cumulative distribution function plot of these C_T based upon Weibayes statistics and a forced beta (slope of the best fit curve) of two, this method being necessitated by the small

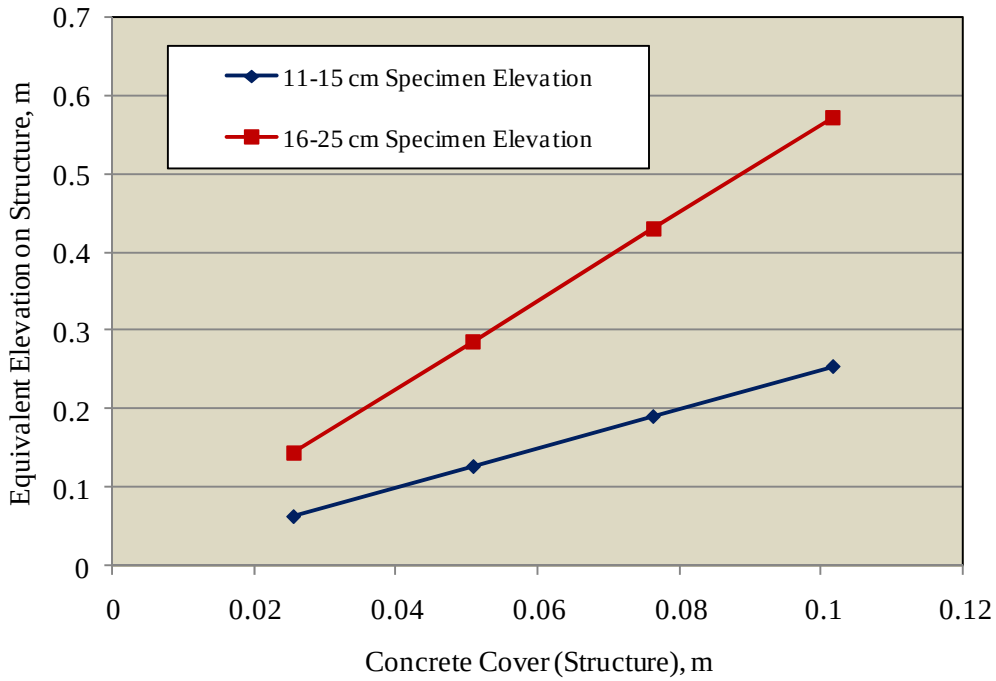

Figure 60: Plot of the elevation range above the waterline on an actual structure element to which the analyzed specimen elevation ranges are projected to represent.

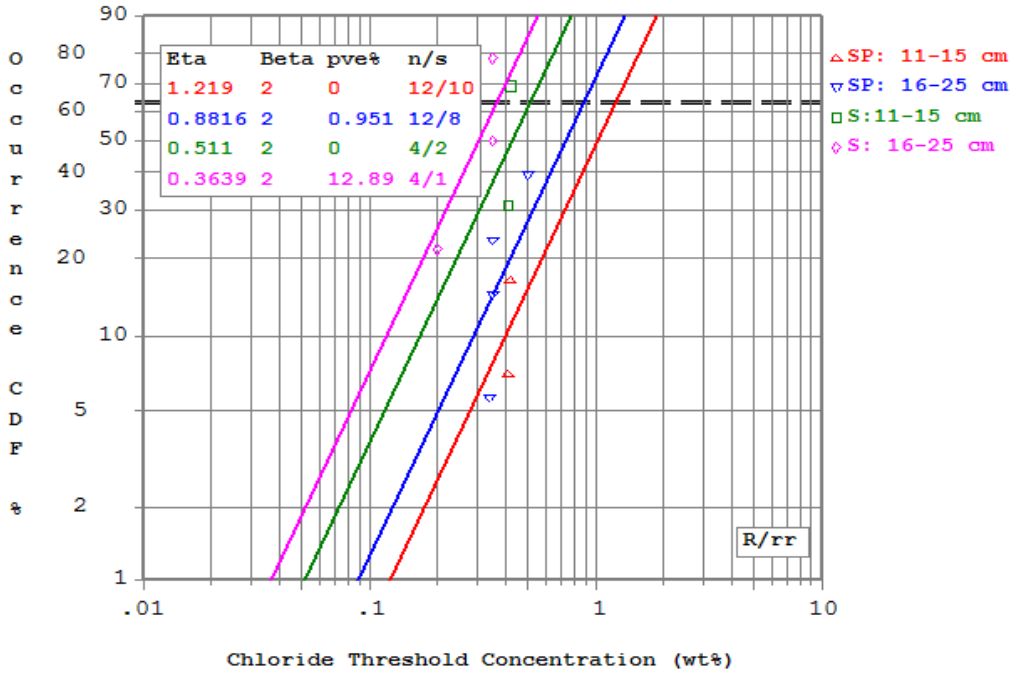

Figure 61: Weibayes cumulative distribution plot of C_T for above waterline corrosion initiation. Beta has been set as 2.00 for each of the four curves (S: sprayed, SP: sprayed and polarized).

sample number (corrosion active bars). As for the Weibull statistics plots above, the software takes runnouts into account in constructing the best fit line but does not plot these. Table 24 lists values for C_T for sprayed and polarized specimens corresponding to different probabilities of activation. The lower C_T for the higher elevation range at a given probability of corrosion initiation presumably resulted because the magnitude of cathodic polarization decreased with increasing elevation. While the limited C_T data raise concern regarding accuracy, still the experimental and analysis approach serve as a template for further study until a broader data base can be established.

Table 24: Listing of C_T for sprayed and polarized specimens in the two elevation ranges corresponding to a given probability of corrosion initiation.

Probability of Corrosion Initiation, percent	C_T, wt%	
	11-15 cm	16-25 cm
1	0.12	0.09
2	0.17	0.13
5	0.28	0.20
10	0.40	0.29
20	0.58	0.42
50	1.00	0.73

CONCLUSIONS

The following conclusions were reached based upon experiments performed upon simulated reinforced concrete piling specimens partially submerged in 15 wt% NaCl:

1. Connection of the embedded rebar to submerged bare steel resulted in a potential profile along the specimen height similar to that of actual bridge pilings. This, combined with intermittent spray of the concrete above the waterline, constitutes an improved procedure for simulating corrosion response of actual in-place pilings compared to those of existing experimental methods.

2. Design of mortar specimens with more shallow cover than is practical when concrete per se is employed facilitates evaluation of chloride threshold, C_T, and time-to-corrosion of service relevant mix designs in practical time frames.

3. Inclusion of more than one rebar in simulated piling specimens can result in stray current on the still passive bar(s) once one bar becomes active.

4. The C_T for specimens with fly ash that were sprayed and connected to bare steel was 0.9-5.2 wt% binder, whereas for similarly exposed ones without fly ash C_T was 3.3-6.0; however, these results are based upon relatively few specimens. Chloride threshold was lower for specimens not connected to bare steel.

5. The C_T of specimens connected to submerged bare steel increased with decreasing polarized potential of the embedded steel in or near the submerged zone.

ACKNOWLEDGMENTS

The authors appreciate financial support of this research provided by the Florida Department of Transportation. The opinions expressed represent those of the authors and not necessarily of the FDOT.

APPENDIX A
Relationship Between Specimen Configuration and Mix Design Variables

Time-to-corrosion calculations were made using the one dimensional solution to Fick's second law,

$$\frac{C_T}{C_S} - 1 - erf\left(\frac{x}{2\times(D_{eff}\times T_i)^{0.5}}\right), \qquad \text{(A1}$$

where C_S is the surface $[Cl^-]$ (assumed as 18 kg/m^3), x is concrete cover, and D_{eff} is the effective diffusion coefficient. Figure A1 shows the results of four calculations, where D_{eff} values were 10^{-11} and 10^{-12} m^2/s, which were assumed representative of the MD1 and MD2 mixes, respectively; and x = 0.008, 0.010, and 0.012 m. From these calculations, a design cover of 0.008 m was selected for specimens with the MD1 mix and 0.012 m for the MD2, since yielded a T_i of less than one year for C_T = 1-6 kg/m^3..

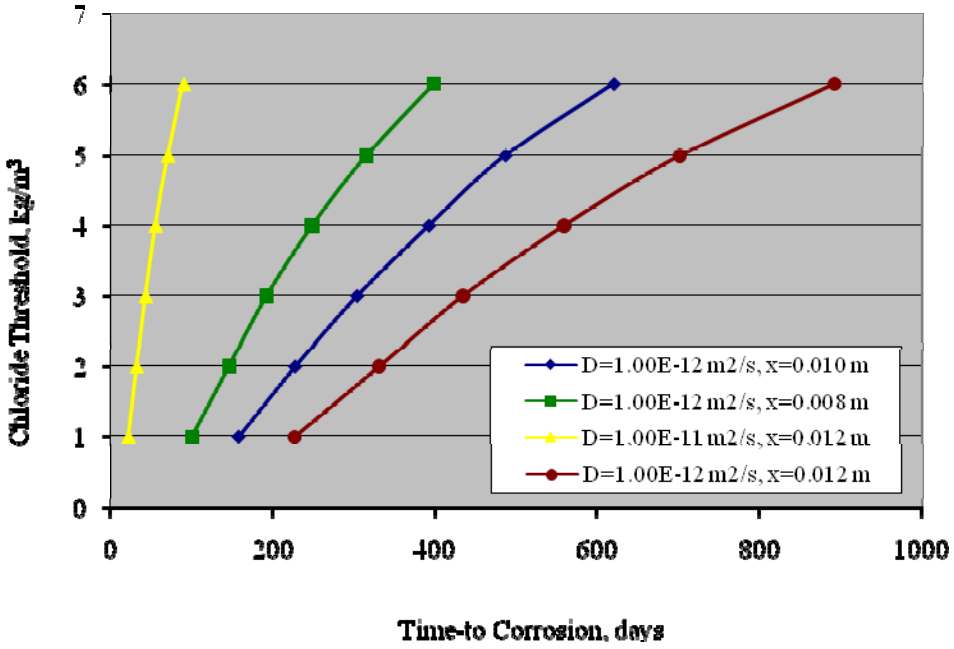

Figure A1: Time-to-corrosion as a function of C_T for the assumed D_{eff} and x values.

APPENDIX B
Potential Versus Time Plots for SP Specimens Not Coupled to Bare Steel

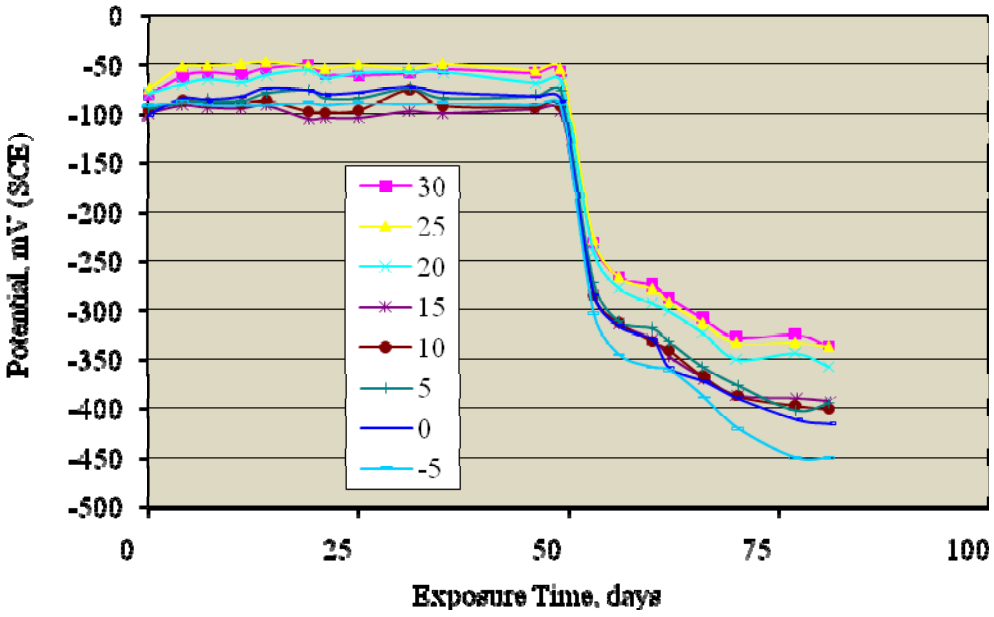

(a)

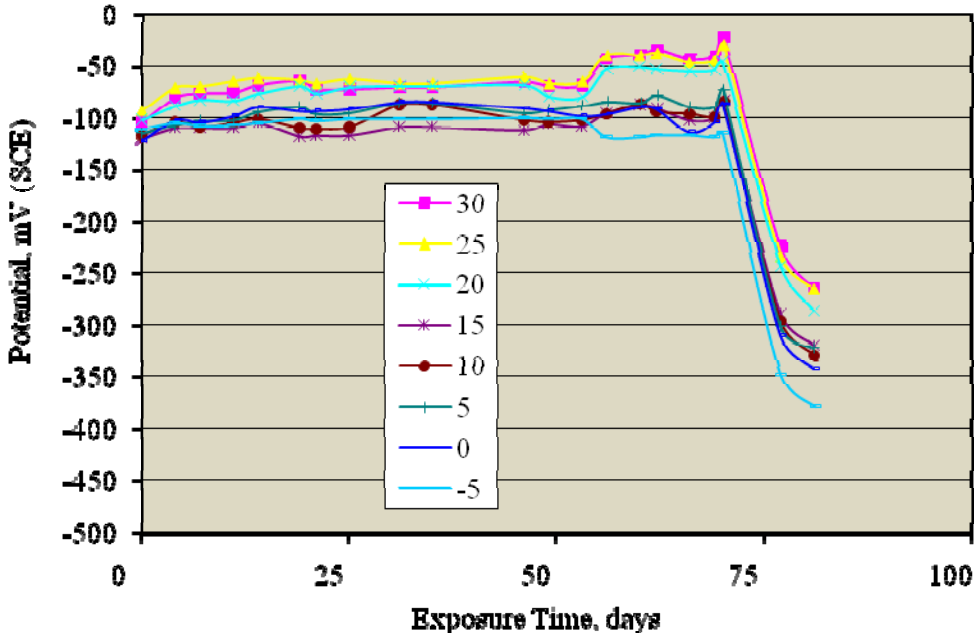

(b)

Figure B1: Potential versus time data for Specimen 6B: (a) left bar and (b) right bar.

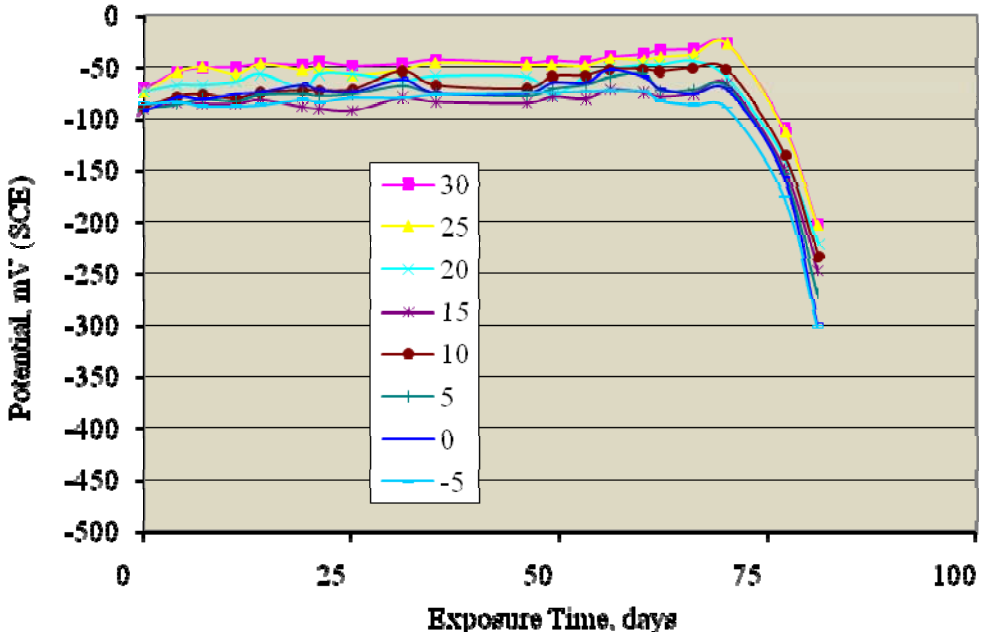

(a)

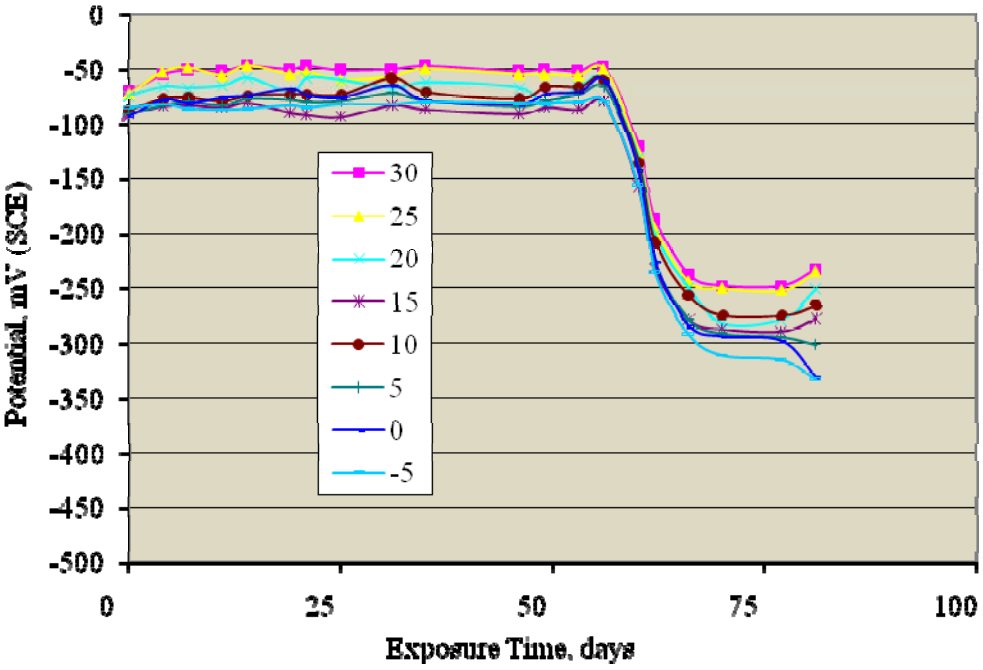

(b)

Figure B2: Potential versus time data for Specimen 7B: (a) left bar and (b) right bar.

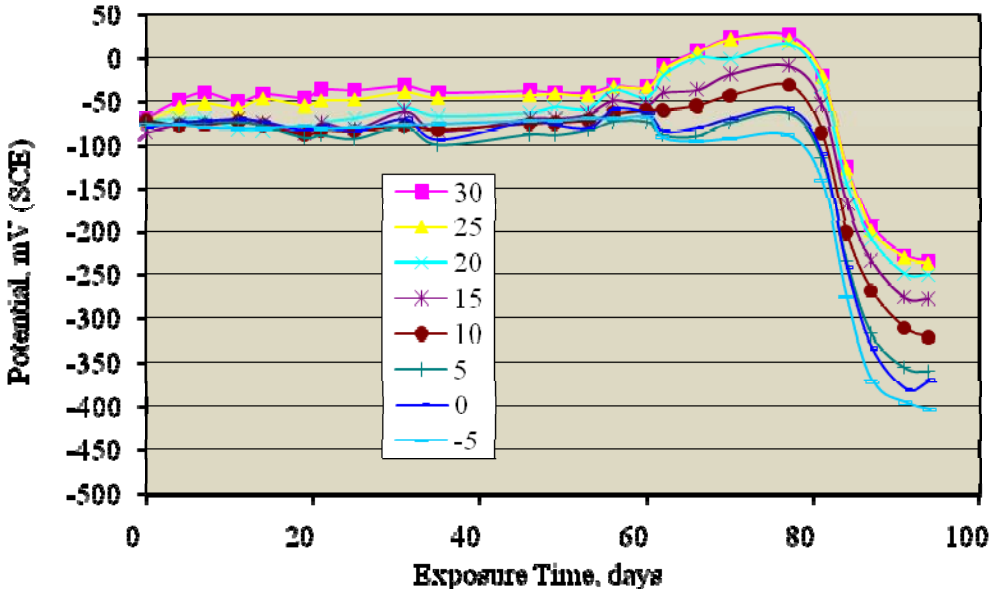

(a)

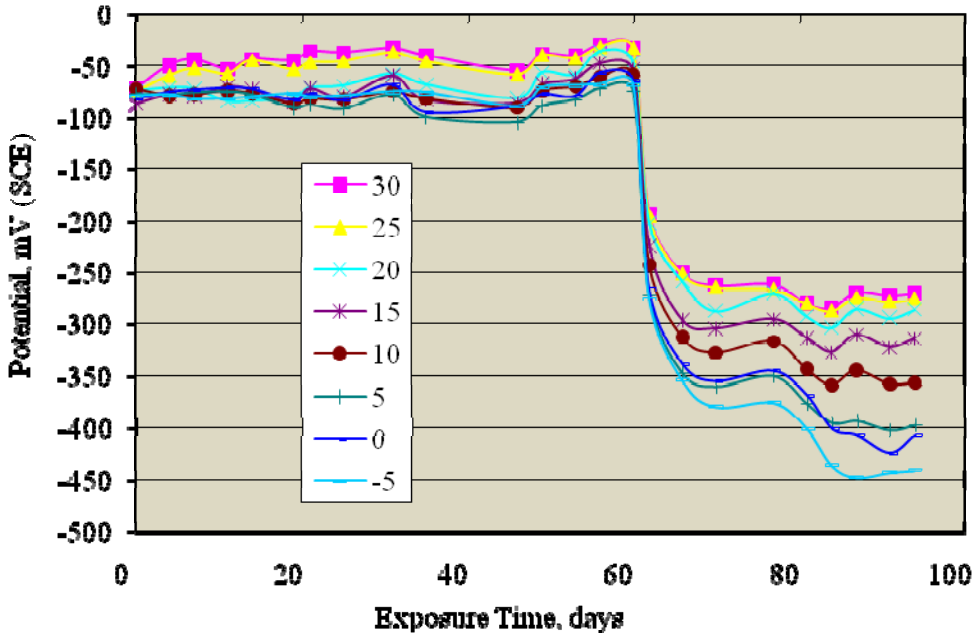

(b)

Figure B3: Potential versus time data for Specimen 8A: (a) left bar and (b) right bar.

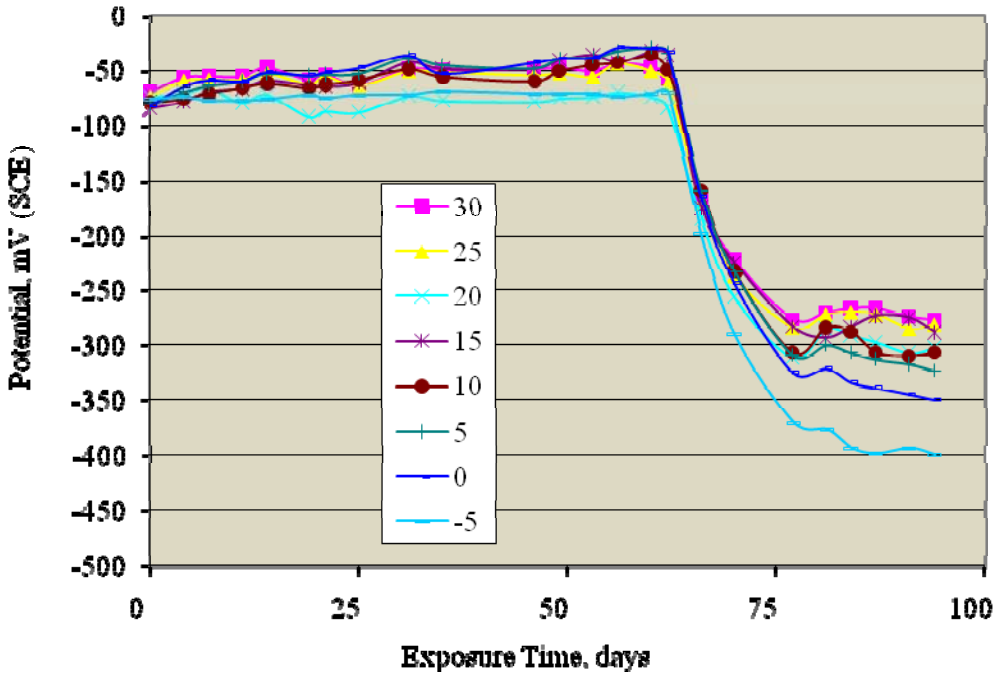

(a)

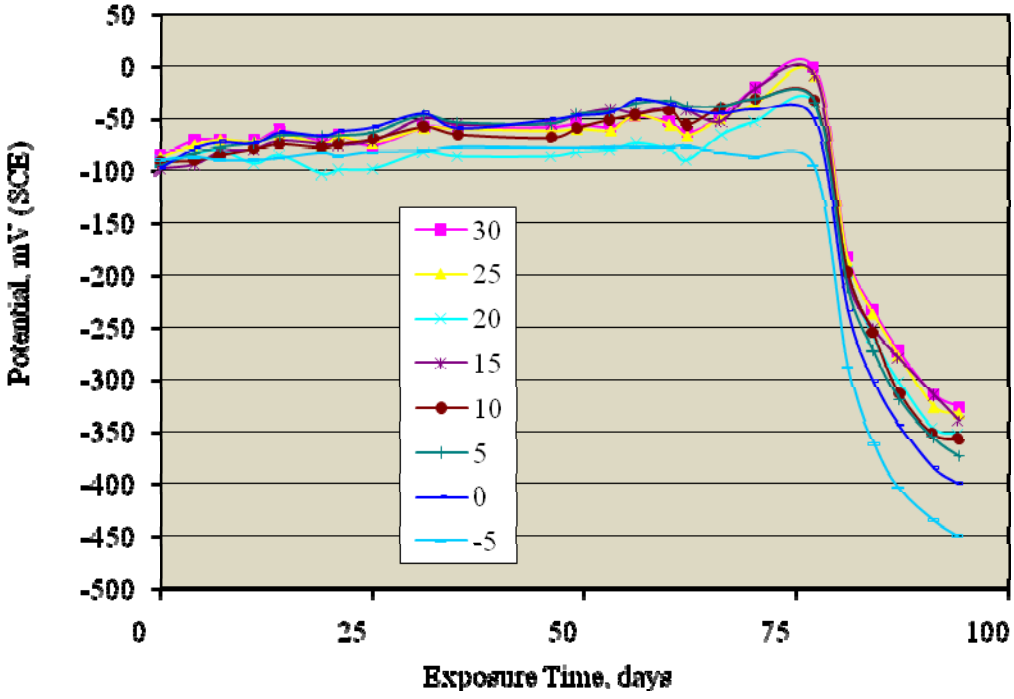

(b)

Figure B4: Potential versus time data for Specimen 8B: (a) left bar and (b) right bar.

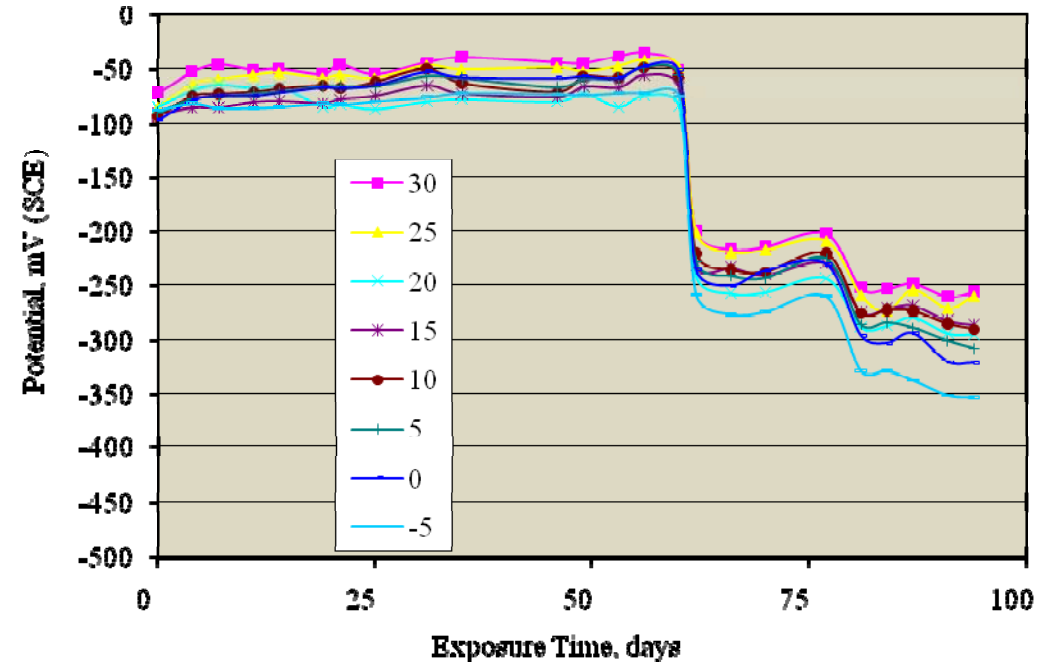

(a)

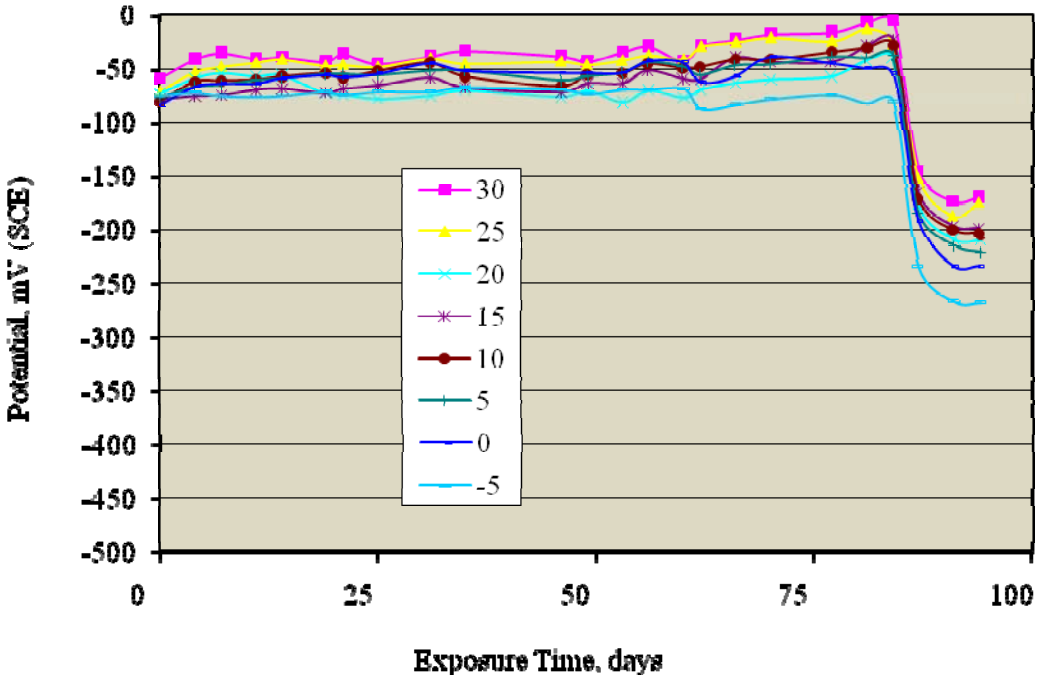

(b)

Figure B5: Potential versus time data for Specimen 9B: (a) left bar and (b) right bar.

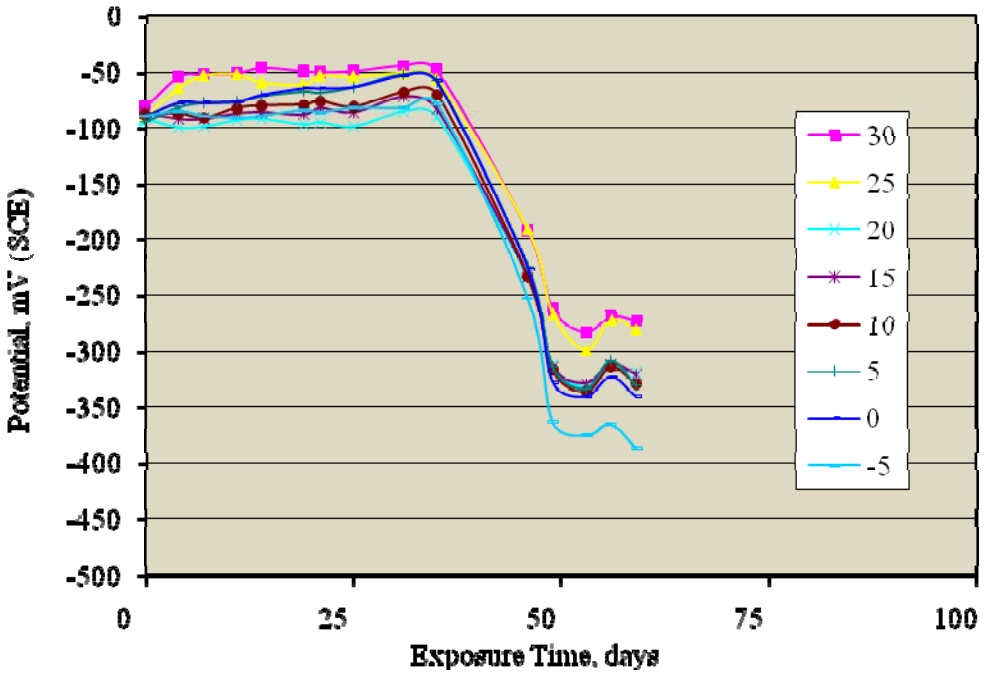

(a)

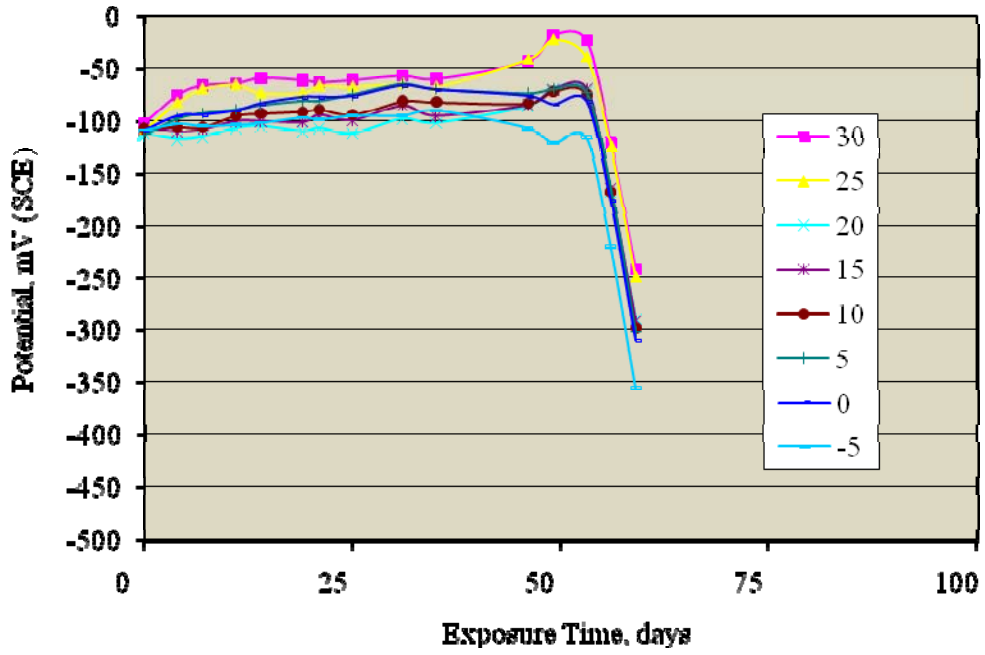

(b)

Figure B6: Potential versus time data for Specimen 10B: (a) left bar and (b) right bar.

APPENDIX C
Photographs of Free Corrosion MD2 Specimens Subsequent to Dissection

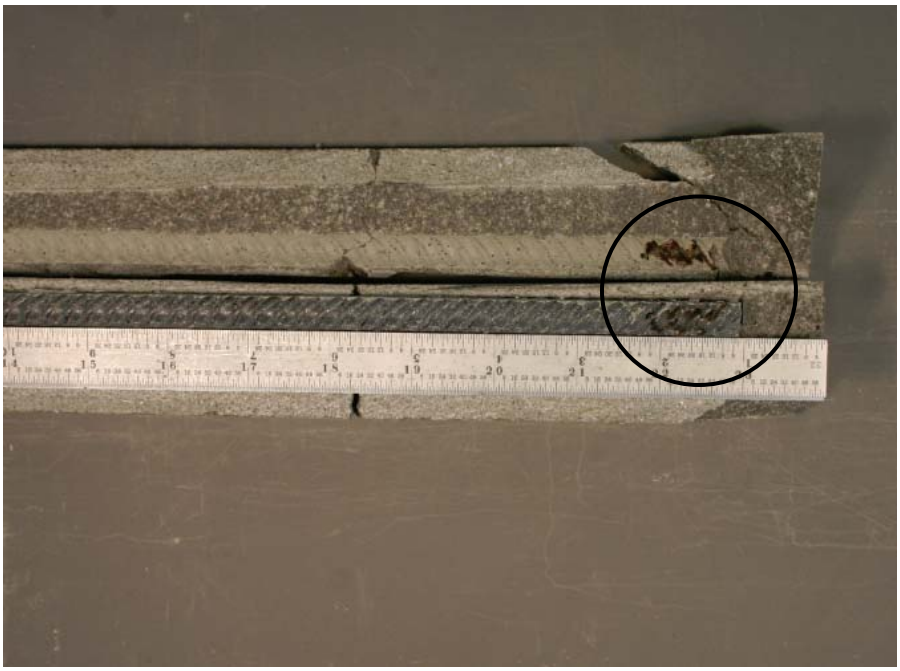

(a)

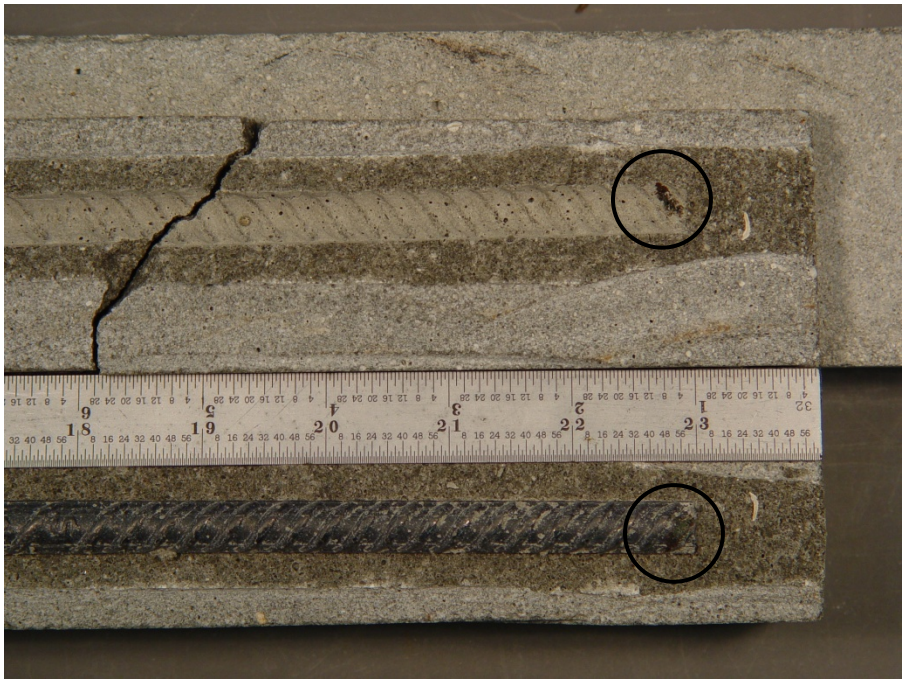

(b)

Figure C1: Photograph of the left (a) and right (b) rebar and mortar trace from Specimen 6B subsequent to dissection. Circled areas indicate corrosion or corrosion products (mortar cracks resulted from the dissection process and not from corrosion).

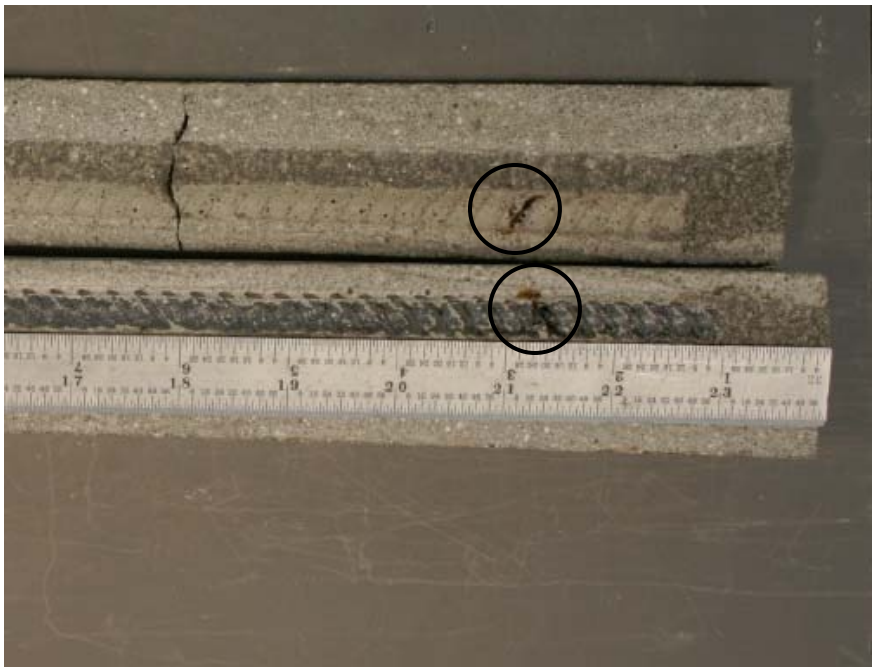

(a)

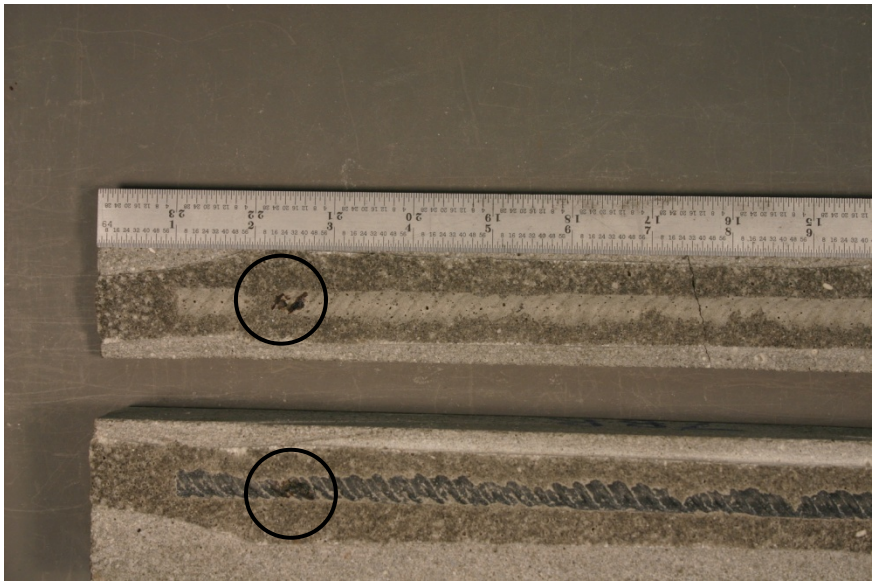

(b)

Figure C2: Photograph of the left (a) and right (b) rebar and mortar trace from Specimen 7B subsequent to dissection. Circled areas indicate corrosion or corrosion products (mortar cracks resulted from the dissection process and not from corrosion).

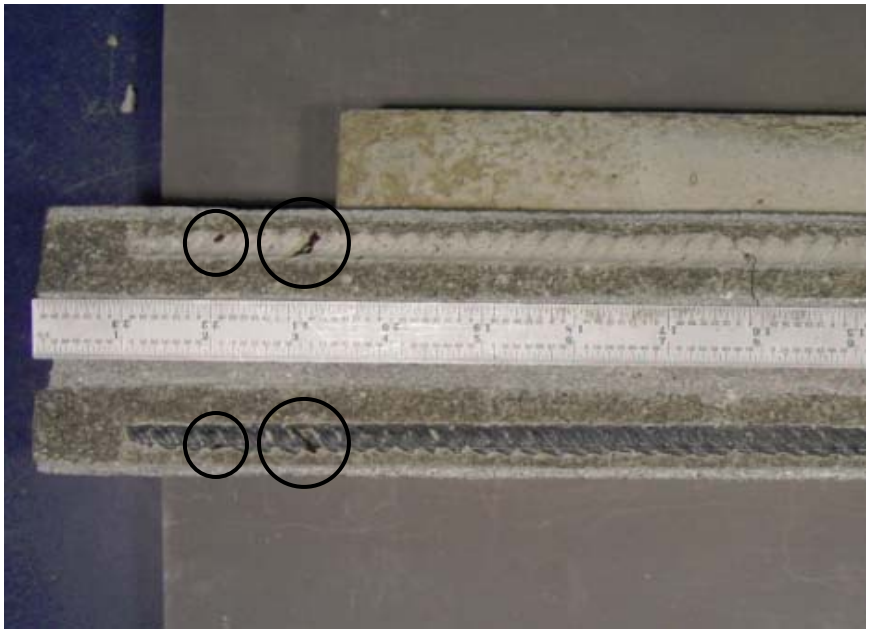

(a)

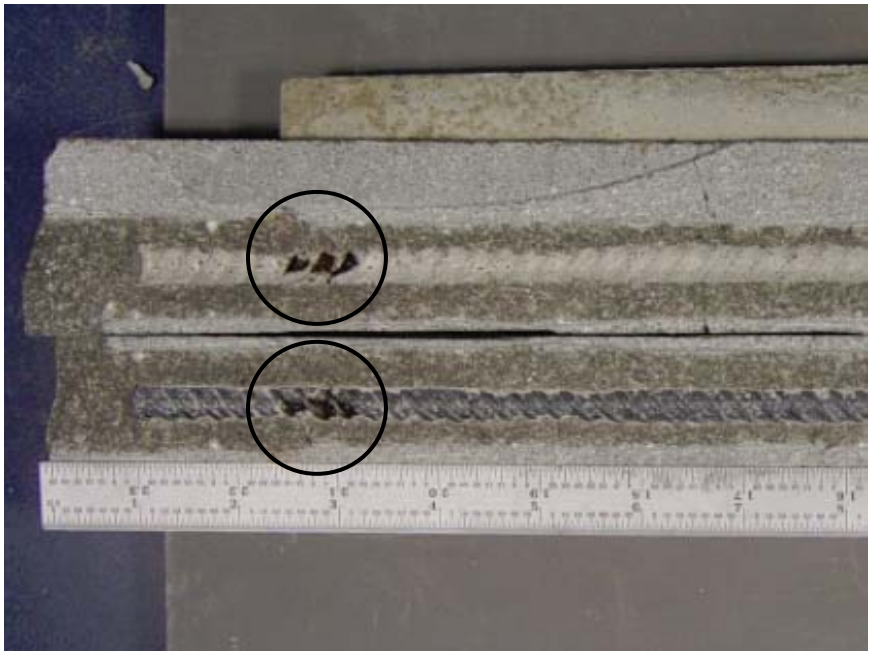

(b)

Figure C3: Photograph of the left (a) and right (b) rebar and mortar trace from Specimen 8A subsequent to dissection. Circled areas indicate corrosion or corrosion products.

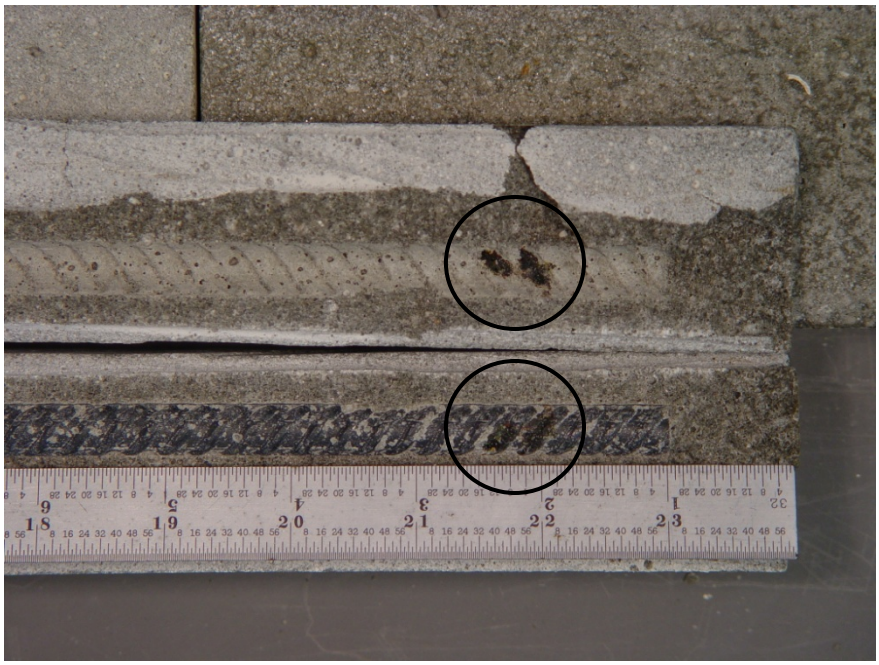

(a)

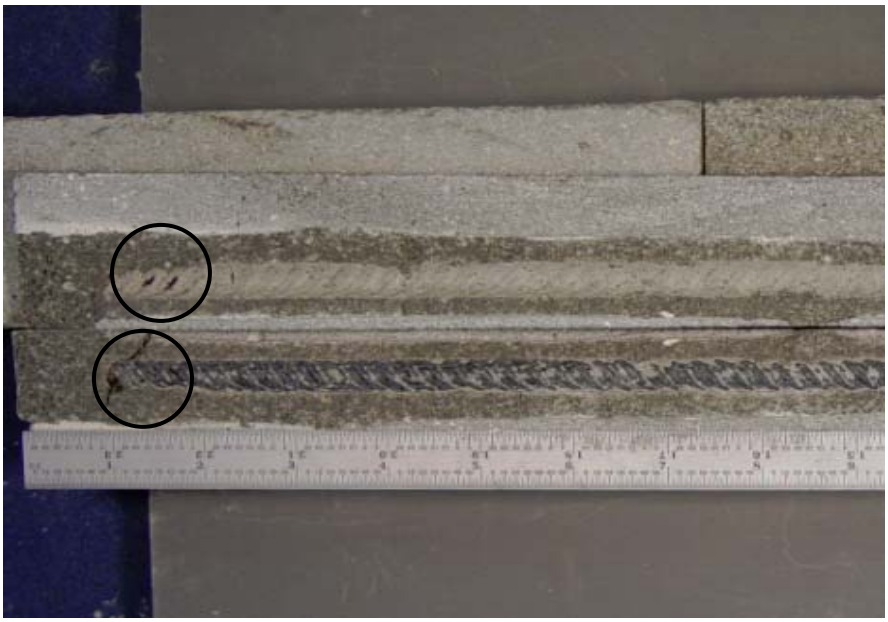

(b)

Figure C4: Photograph of the left (a) and right (b) rebar and mortar trace from Specimen 8B subsequent to dissection. Circled areas indicate corrosion or corrosion products.

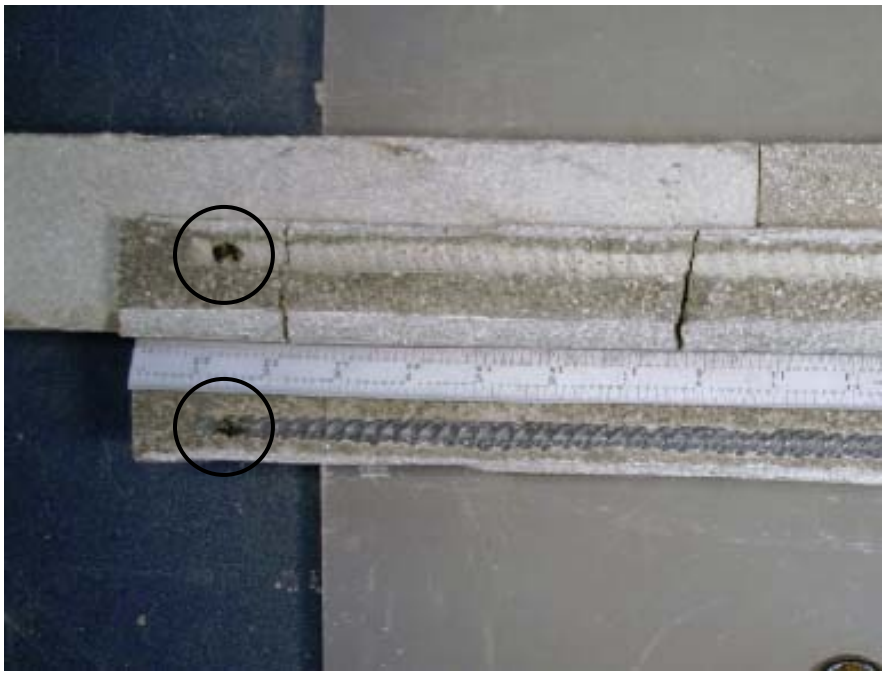

(a)

(b)

Figure C5: Photograph of the left (a) and right (b) rebar and mortar trace from Specimen 9B subsequent to dissection. Circled areas indicate corrosion or corrosion products (mortar cracks resulted from the dissection process and not from corrosion).

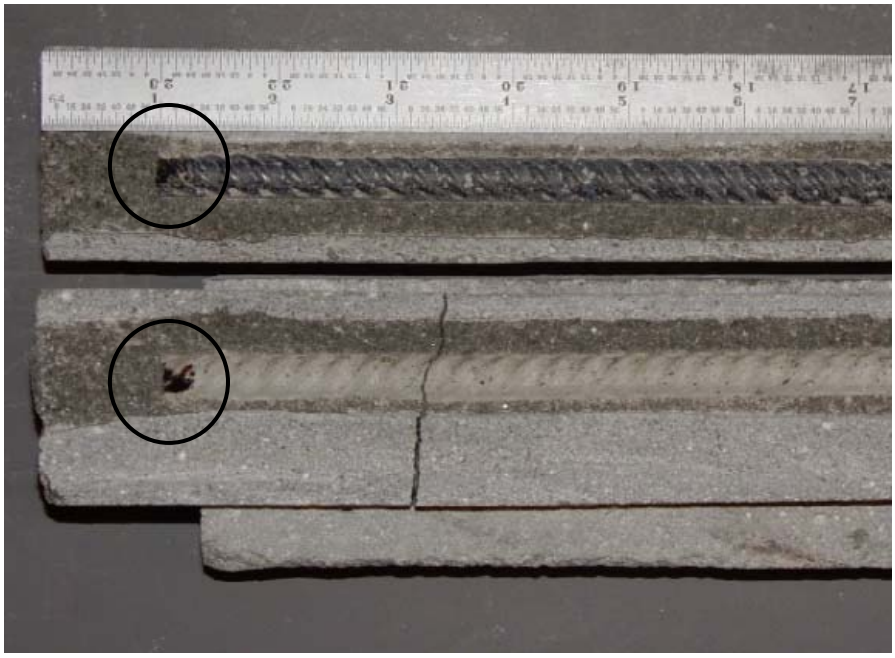

(a)

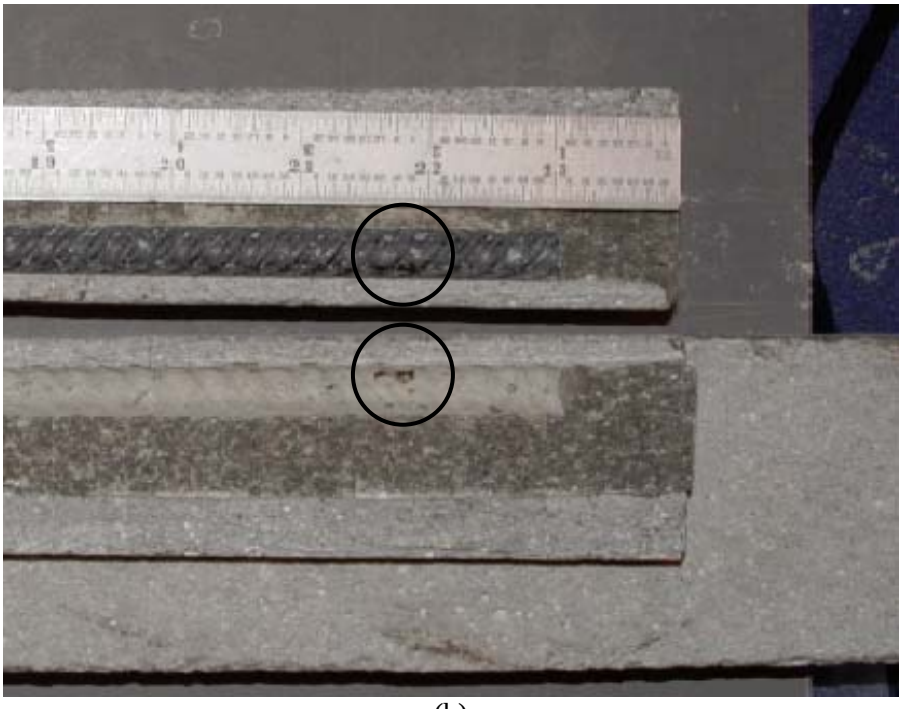

(b)

Figure C6: Photograph of the left (a) and right (b) rebar and mortar trace from Specimen 10B subsequent to dissection. Circled areas indicate corrosion or corrosion products (mortar cracks resulted from the dissection process and not from corrosion).

APPENDIX D
Summary of Data Relevant to Positive Potential Shift of Passive Reinforcement Subsequent to Activation of the Companion Bar

Table D1: Summary of data relevant to the positive potential trend near the bottom of the still passive bar subsequent to corrosion initiation of the companion bar (Specimen 6B).

Specimen 6B		
Left Bar	Time of Last Passive Reading, days	49
	Time of First Active Reading, days	53
Right Bar	Time of Last Passive Reading Prior to Activation, days	70
	Potential at 49 days, mV (SCE)	-67
	Potential at 53 days, mV (SCE)	-65
	Average potential 53-70 days, mV (SCE)	-44

Table D2: Summary of data relevant to the positive potential trend near the bottom of the still passive bar subsequent to corrosion initiation of the companion bar (Specimen 7B).

Specimen 7B		
Right Bar	Time of Last Passive Reading, days	56
	Time of First Active Reading, days	60
Left Bar	Time of Last Passive Reading Prior to Activation, days	70
	Potential at 56 days, mV (SCE)	-42
	Potential at 60 days, mV (SCE)	-43
	Average potential 60-70 days, mV (SCE)	-34

Table D3: Summary of data relevant to the positive potential trend near the bottom of the still passive bar subsequent to corrosion initiation of the companion bar (Specimen 8A).

Specimen 8A		
Right Bar	Time of Last Passive Reading, days	60
	Time of First Active Reading, days	62
Left Bar	Time of Last Passive Reading Prior to Activation, days	77
	Potential at 60 days, mV (SCE)	-33
	Potential at 62 days, mV (SCE)	-12
	Average potential 62-77 days, mV (SCE)	9

Table D4: Summary of data relevant to the positive potential trend near the bottom of the still passive bar subsequent to corrosion initiation of the companion bar (Specimen 8B).

Specimen 8B		
Left Bar	Time of Last Passive Reading, days	62
	Time of First Active Reading, days	66
Right Bar	Time of Last Passive Reading Prior to Activation, days	77
	Potential at 62 days, mV (SCE)	-56
	Potential at 66 days, mV (SCE)	-38
	Average potential 66-77 days, mV (SCE)	-20

Table D5: Summary of data relevant to the positive potential trend near the bottom of the still passive bar subsequent to corrosion initiation of the companion bar (Specimen 9B).

Specimen 9B		
Left Bar	Time of Last Passive Reading, days	60
	Time of First Active Reading, days	62
Right Bar	Time of Last Passive Reading Prior to Activation, days	84
	Potential at 60 days, mV (SCE)	-41
	Potential at 62 days, mV (SCE)	-28
	Average potential 62-84 days, mV (SCE)	-18

Table D6: Summary of data relevant to the positive potential trend near the bottom of the still passive bar subsequent to corrosion initiation of the companion bar (Specimen 10B).

Specimen 10B		
Left Bar	Time of Last Passive Reading, days	35
	Time of First Active Reading, days	46
Right Bar	Time of Last Passive Reading Prior to Activation, days	53
	Potential at 35 days, mV (SCE)	-60
	Potential at 53 days, mV (SCE)	-41
	Average potential 46-53 days, mV (SCE)	-27

APPENDIX E
Summary of Data Relevant to Negative Potential Shift of Passive Reinforcement Subsequent to Activation of the Companion Bar

Table E1: Summary of data relevant to the negative potential trend near the bottom of the still passive bar subsequent to corrosion initiation of the companion bar (Specimen 6B).

Specimen 6B		
Left Bar	Time of Last Passive Reading, days	49
	Time of First Active Reading, days	53
Right Bar	Time of Last Passive Reading Prior to Activation, days	70
	Potential at 49 days, mV (SCE)	-101
	Potential at 53 days, mV (SCE)	-102
	Average potential 53-70 days, mV (SCE)	-116

Table E2: Summary of data relevant to the negative potential trend near the bottom of the still passive bar subsequent to corrosion initiation of the companion bar (Specimen 7B).

Specimen 7B		
Right Bar	Time of Last Passive Reading, days	56
	Time of First Active Reading, days	60
Left Bar	Time of Last Passive Reading Prior to Activation, days	70
	Potential at 56 days, mV (SCE)	-72
	Potential at 60 days, mV (SCE)	-73
	Average potential 60-70 days, mV (SCE)	-84

Table E3: Summary of data relevant to the negative potential trend near the bottom of the still passive bar subsequent to corrosion initiation of the companion bar (Specimen 8A).

Specimen 8A		
Right Bar	Time of Last Passive Reading, days	60
	Time of First Active Reading, days	62
Left Bar	Time of Last Passive Reading Prior to Activation, days	77
	Potential at 60 days, mV (SCE)	-68
	Potential at 62 days, mV (SCE)	-92
	Average potential 62-77 days, mV (SCE)	-93

Table E4: Summary of data relevant to the negative potential trend near the bottom of the still passive bar subsequent to corrosion initiation of the companion bar (Specimen 8B).

Specimen 8B		
Left Bar	Time of Last Passive Reading, days	62
	Time of First Active Reading, days	66
Right Bar	Time of Last Passive Reading Prior to Activation, days	77
	Potential at 62 days, mV (SCE)	-76
	Potential at 66 days, mV (SCE)	-83
	Average potential 66-77 days, mV (SCE)	-88

Table E5: Summary of data relevant to the negative potential trend near the bottom of the still passive bar subsequent to corrosion initiation of the companion bar (Specimen 9B).

Specimen 9B		
Left Bar	Time of Last Passive Reading, days	60
	Time of First Active Reading, days	62
Right Bar	Time of Last Passive Reading Prior to Activation, days	84
	Potential at 60 days, mV (SCE)	-68
	Potential at 62 days, mV (SCE)	-87
	Average potential 62-84 days, mV (SCE)	-81

Table E6: Summary of data relevant to the negative potential trend near the bottom of the still passive bar subsequent to corrosion initiation of the companion bar (Specimen 10B).

Specimen 10B		
Left Bar	Time of Last Passive Reading, days	35
	Time of First Active Reading, days	46
Right Bar	Time of Last Passive Reading Prior to Activation, days	53
	Potential at 35 days, mV (SCE)	-90
	Potential at 53 days, mV (SCE)	-107
	Average potential 46-53 days, mV (SCE)	-112

Appendix F
Chloride Concentration versus Elevation Plots and Corresponding Photographs of the Bar and Bar Trace

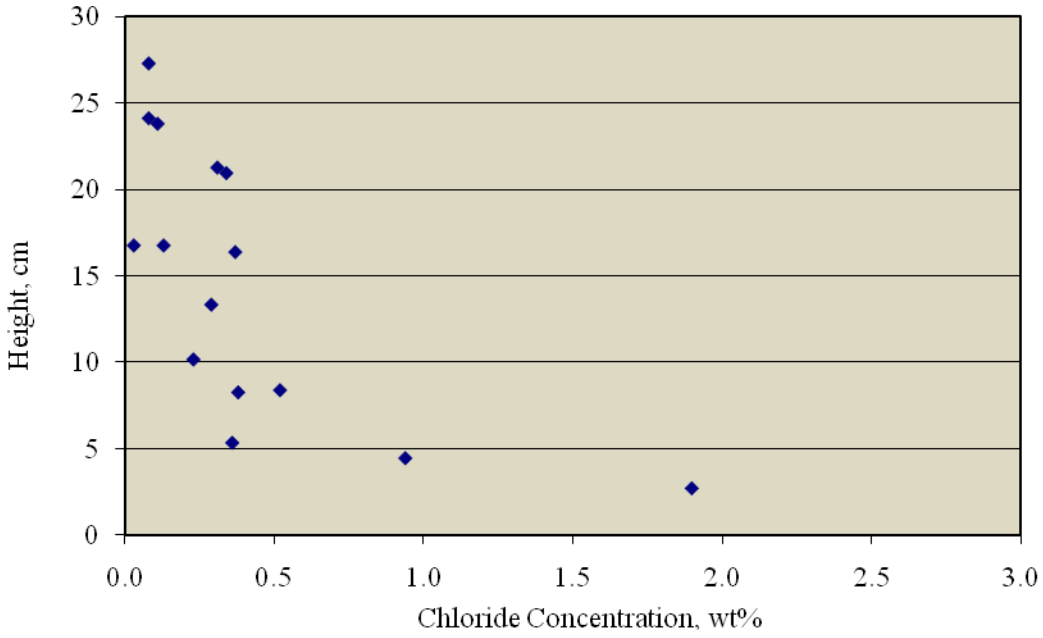

Figure F1: Chloride concentration on the right bar trace as a function of elevation for Specimen 6B.

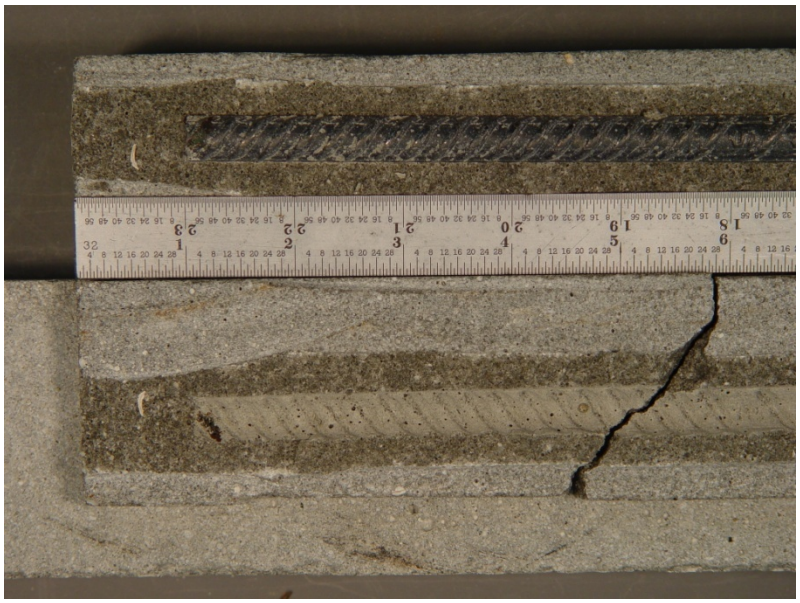

Figure F2: Photograph of the right bar and bar trace of Specimen 6B.

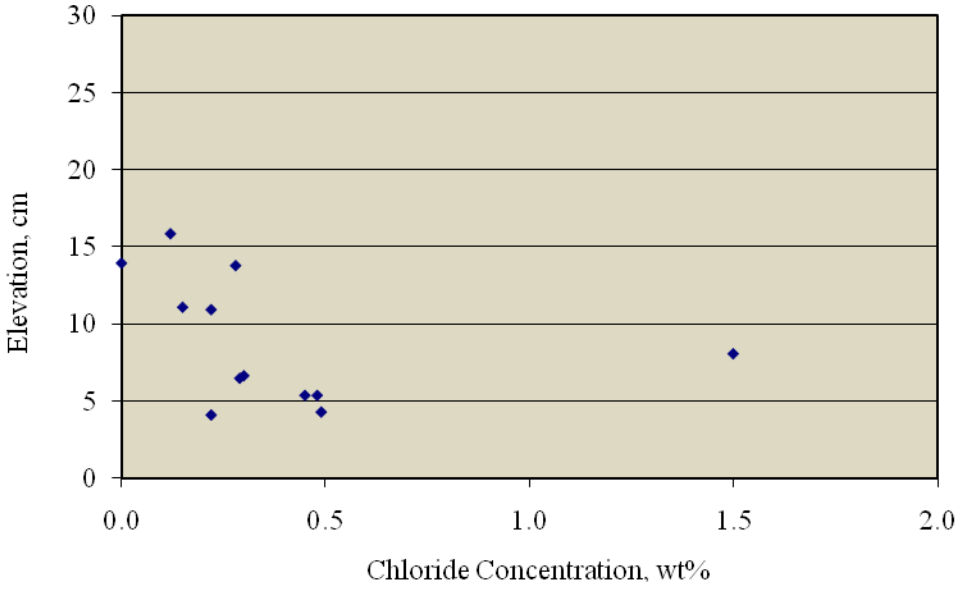

Figure F3: Chloride concentration on the left bar trace as a function of elevation for Specimen 8A.

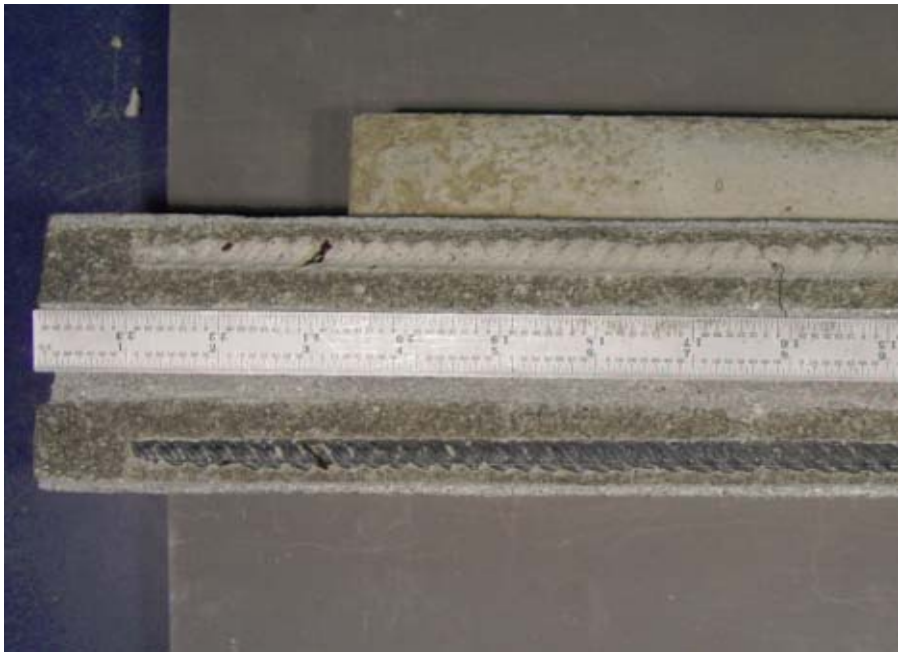

Figure F4: Photograph of the left bar and bar trace of Specimen 8A.

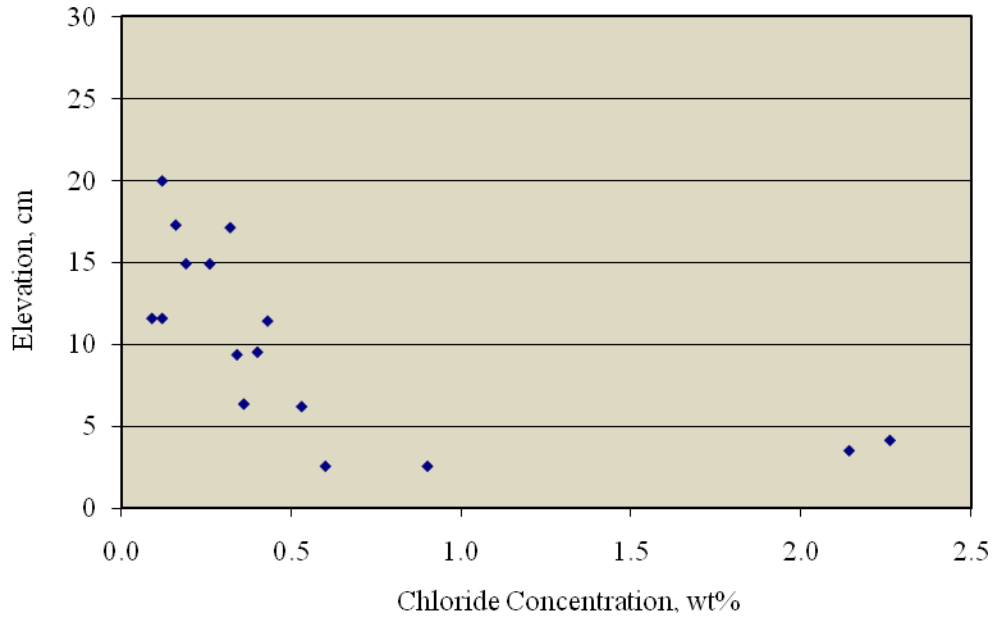

Figure F5: Chloride concentration on the right bar trace as a function of elevation for Specimen 8B.

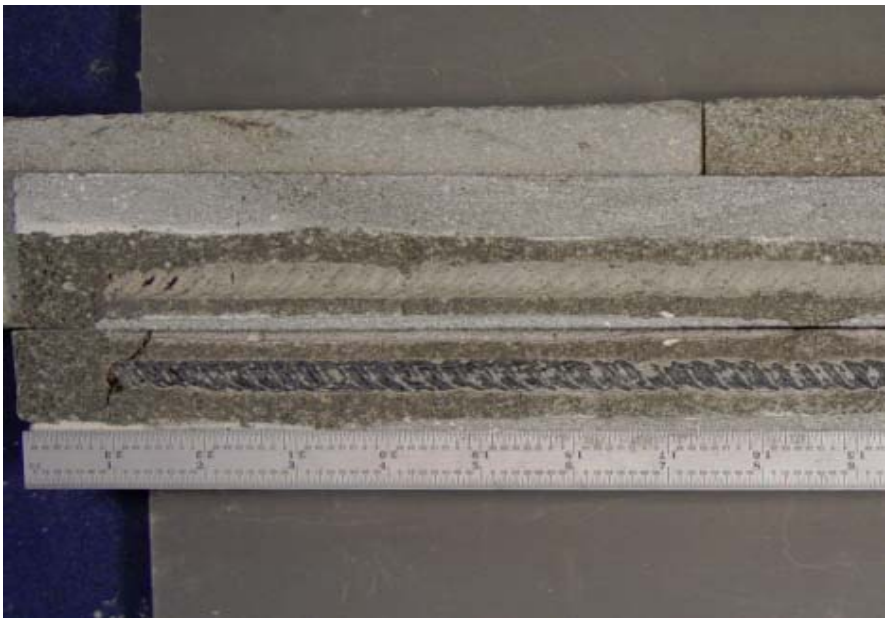

Figure F6: Photograph of the right bar and bar trace of Specimen 8B.

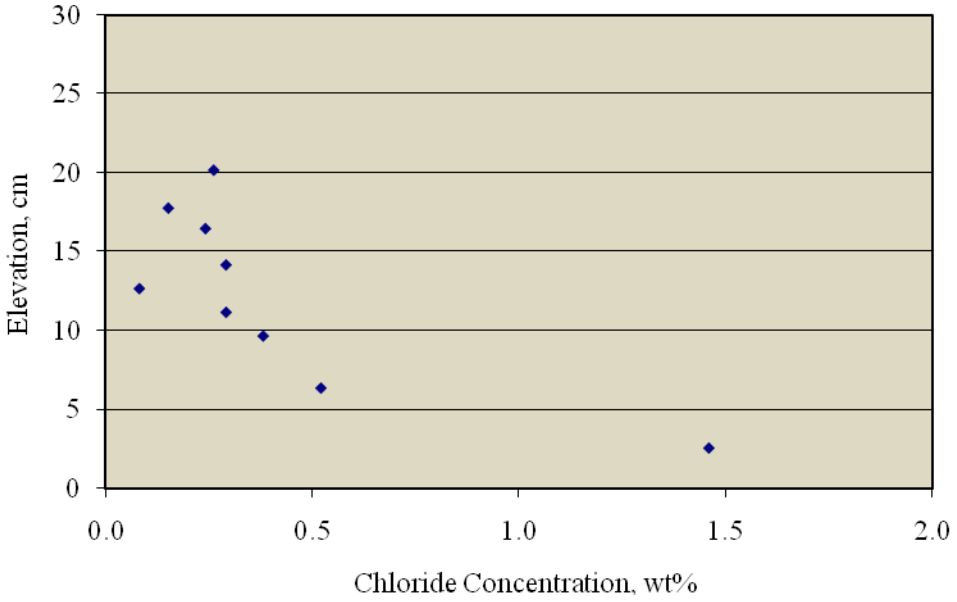

Figure F7: Chloride concentration on the right bar trace as a function of elevation for Specimen 9A.

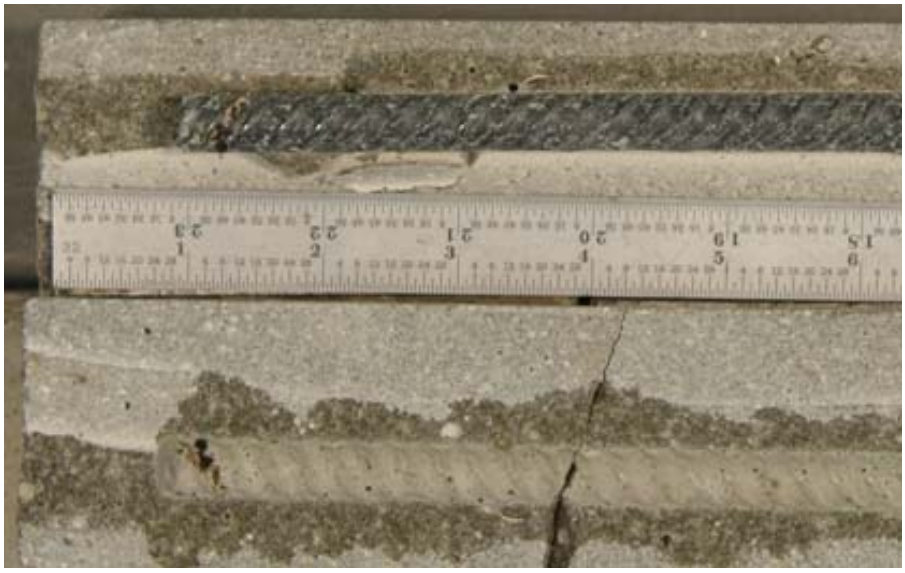

Figure F8: Photograph of the right bar and bar trace of Specimen 9A.

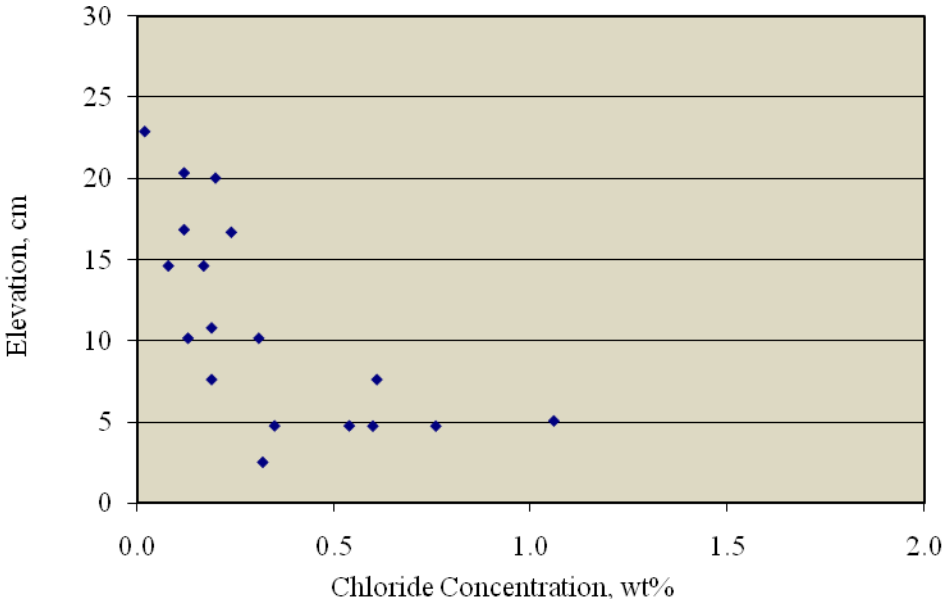

Figure F9: Chloride concentration on the right bar trace as a function of elevation for Specimen 9B.

Figure F10: Photograph of the right bar and bar trace of Specimen 9B.

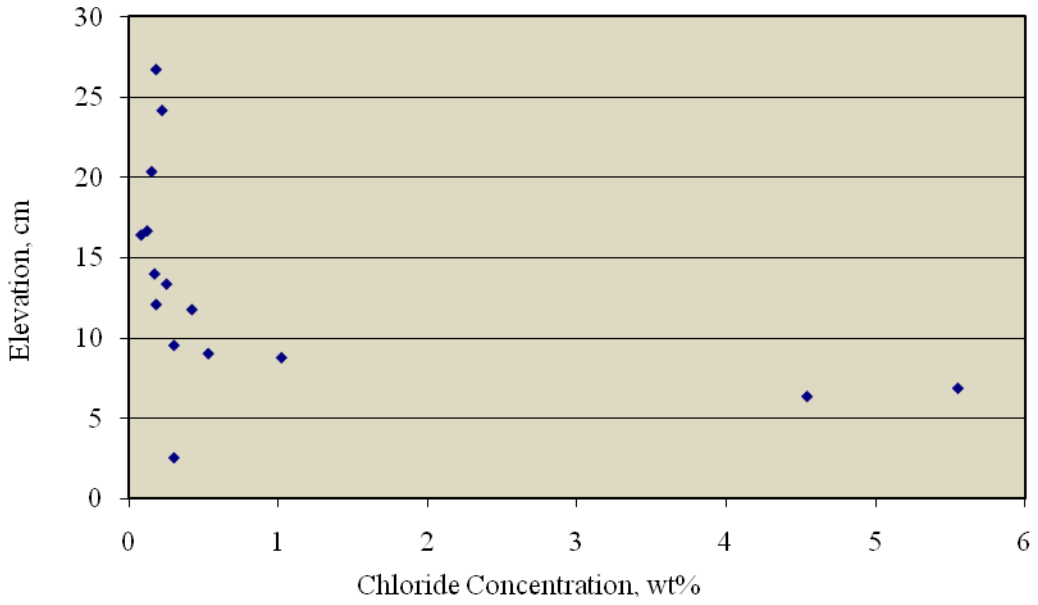

Figure F11: Chloride concentration on the left bar trace as a function of elevation for Specimen 3B.

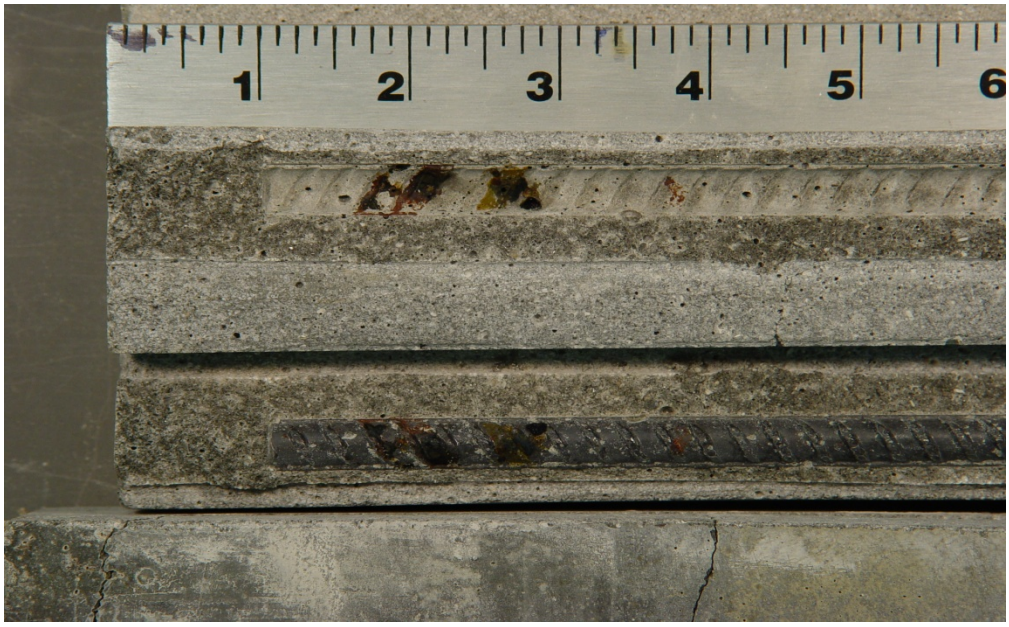

Figure F12: Photograph of the left bar and bar trace of Specimen 3B.

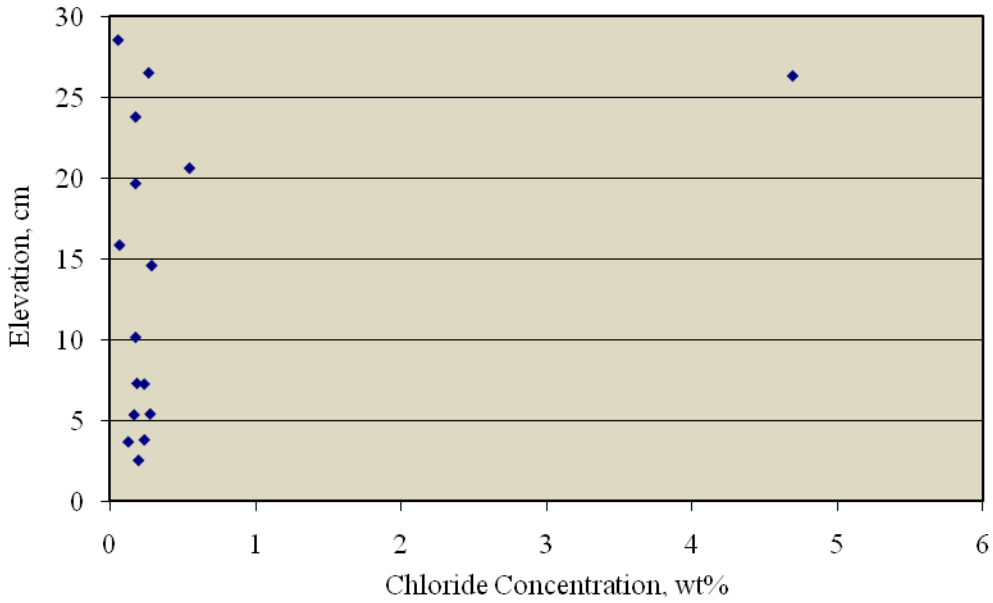

Figure F13: Chloride concentration on the right bar trace as a function of elevation for Specimen 3B.

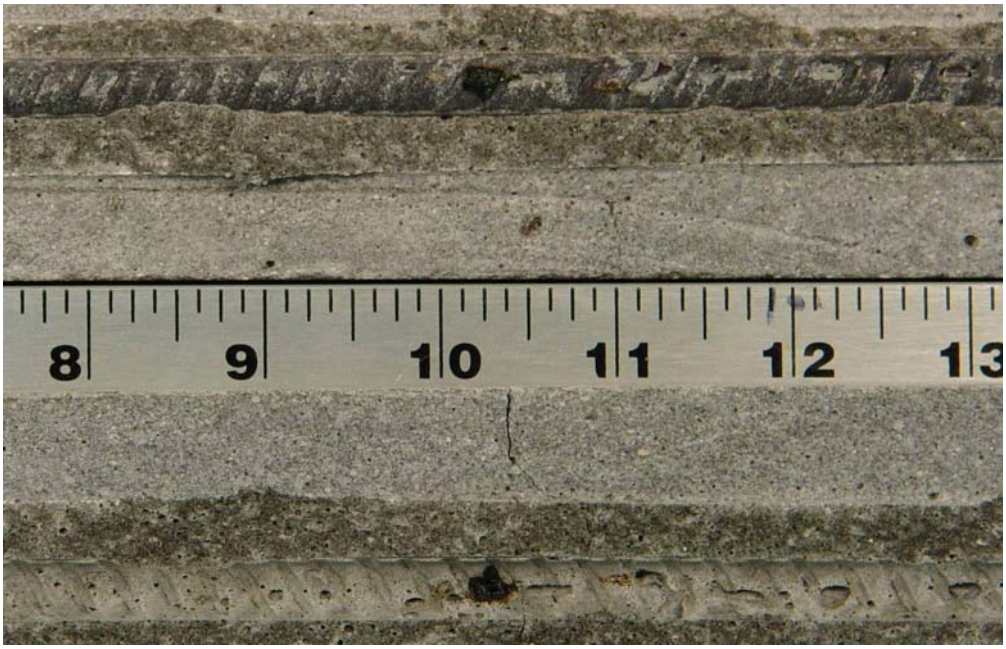

Figure F14: Photograph of the left bar and bar trace of Specimen 3B. Corrosion initiated at a void 26 cm above the specimen bottom.

BIBLIOGRAPHY

[1] Glass, G.K. and Buenfeld, N.R., "Chloride Threshold Levels for Corrosion Induced Deterioration of Steel in Concrete," paper no. 3 presented at RILEM International Workshop on Chloride penetration into Concrete, Oct. 15-18, 1995, Saint Rémy-les-Chevreuse.

[2] Yu, H., Himiob, R.J., and Hartt, W.H., Corrosion, Vol. 63, 2007, p. 924.

[3] ACI Committee 201, Guide to Durable Concrete, Chapter IV – Corrosion of Steel and Other Materials embedded in Concrete, Manual of Concrete Practice, Part I, American Concrete Institute, Detroit, 2001.

[4] Clear, K.C., "Evaluation of Portland Cement Concrete for permanent Bridge Deck Repair," Federal Highway Administration Report No. FHWA-RD-74-5, Washington, DC, 1974.

[5] Lewis, D.A., Some Aspects of the Corrosion of Steel in Concrete," Proc. First International Congress on Metallic Corrosion, London, 1962, pp. 547-555.

[6] Virmani, Y.P. and Clemena, G.G., "Corrosion Protection – Concrete Bridges," Federal Highway Administration Report No. FHWA-RD-98-088, p. 1, Washington, DC, 1974.

[7] Berman, H.A., "Determination of Chloride in Hardened Portland Cement Paste, Mortar, and Concrete," Federal Highway Administration Report No. FHWA-RD-72-12, Washington, DC, 1972.

[8] Stratfull, R.F., Jurkovich, W.J., and Spellman, D.L., Transportation Research Record, Vol. 539, 1975, p. 50.

[9] Yu, H. and Hartt, W.H., Corrosion, Vol. 63, 2007, p. 843.

[10] Spellman, D.L. and Stratfull, R.F., Highway Research Record, Vol. 423, 1973, p. 27.

[11] Bamforth, P.B. and Chapman-Andrews, J.F., "Long-Term Performance of RC Elements under UK Coastal Exposure Conditions," Proc. Intl. Conf. on Corrosion and Corrosion Protection of Steel in Concrete, Vol. 1, University of Sheffield, July, 1994, p. 139.

[12] Presuel-Moreno, F.J., Sagüés, A.A., and Kranc, S.C., Corrosion, Vol. 61, 2005, p. 428.

[13] Presuel-Moreno, F.J., Kranc, S.C., and Sagüés, A.A., Corrosion, Vol. 61, 2005, p. 548.

[14] Standard Specification for Road and Bridge Construction, Section 346: Portland Cement Concrete, Florida Department of Transportation, Tallahassee, FL, 2007.

[15] ASTM G109-07, "Standard Test Method for Determining Effects of Chemical Admixtures on Corrosion of Embedded Reinforcing Steel in Concrete Exposed to Chloride Environments," Annual Book of Standards, American Society for Testing and Materials, West Conshohocken, PA.

[16] ASTM C231-04, "Standard Test Method for Air Content of Freshly Mixed Concrete by the Pressure Method," Annual Book of Standards, American Society for Testing and Materials, West Conshohocken, PA.

[17] ASTM C192-07, "Standard Practice for making and Curing Concrete Specimens in the Laboratory," Annual Book of Standards, American Society for Testing and Materials, West Conshohocken, PA.

[18] Foley, R.T., Ind. Eng. Chem. Prod. Res. Dev., Vol. 17, 1978, p. 14.

[19] Unpublished data provided by Mr. Ivan Lasa, Florida Department of Transportation – State Materials Office, Gainesville, FL.

[20] Kranc, S.C., Sagüés, A.A., and Presuel-Moreno, F.J., "Decreased Corrosion Initiation Time of Steel in Concrete Due to Reinforcing Bar Obstruction of Diffusional Flow" , ACI Materials Journal, Vol.99, 2002, pp 51-53.